Simulations of steady and oscillating flow in diffusers

L. Schoenmaker

Delft University of Technology
MSc track: Sustainable Process & Energy Technology

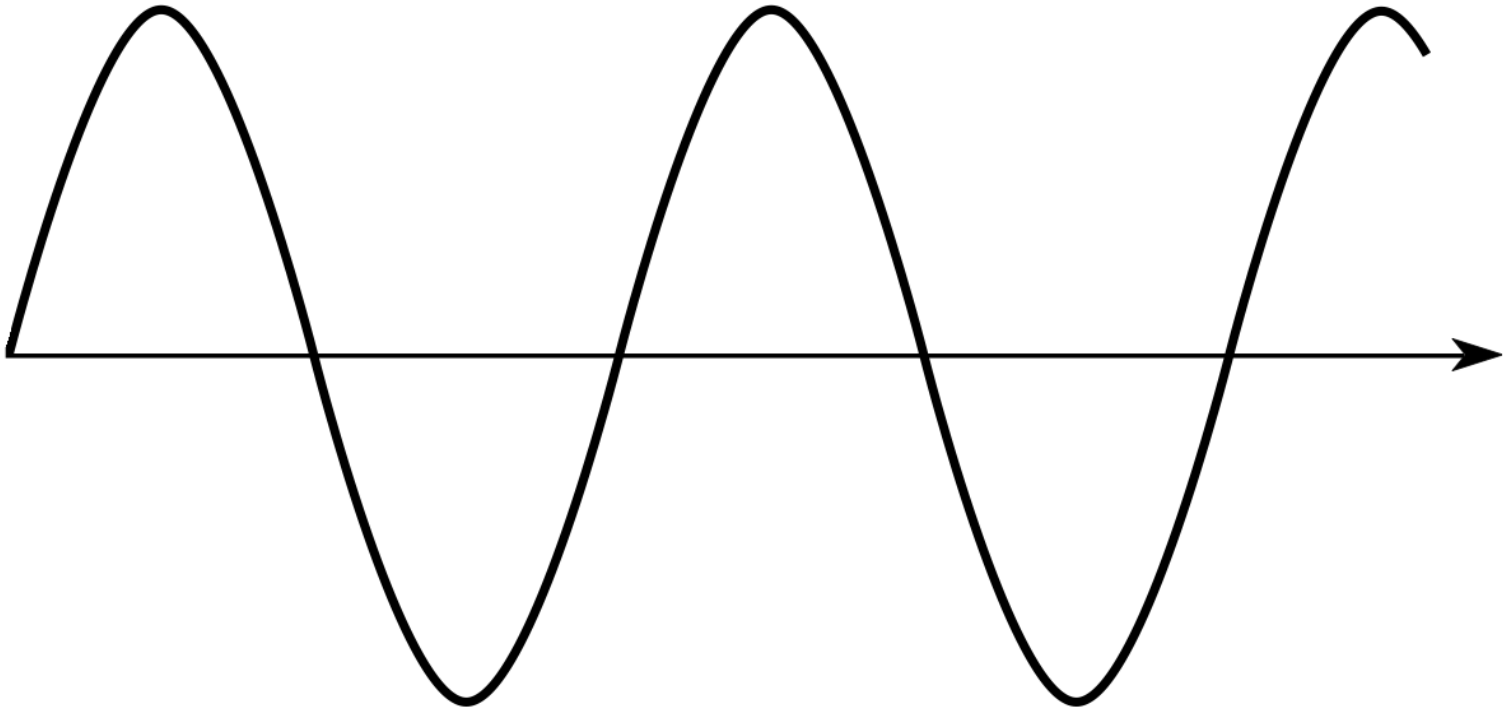

TU Delft

Simulations of steady and oscillating flow in diffusers

by

L. Schoenmaker

to obtain the degree of Master of Science
at the Delft University of Technology,
to be defended publicly on Thursday August 31, 2017 at 10:00 AM.

Student number:	1304577	
Date:	August 31, 2017	
Thesis committee:	Prof. dr. ir. B.J. Boersma,	TU Delft, supervisor
	Dr. ir. M.J.B.M Pourquie,	TU Delft
	Dr. ir. R. Pecnik,	TU Delft

An electronic version of this thesis is available at `http://repository.tudelft.nl/`.

TU Delft

Abstract

In this thesis diffuser performance will be simulated with computational fluid dynamics, which will be done with the program Ansys Fluent. The expanding geometry creates an adverse pressure gradient and under certain conditions there will also be separation.

At first a relative simple simulation will be done of a one-directional incompressible turbulent flow. It will show how different turbulence models perform at a Reynolds number of 15,000 in a conical diffuser with an angle of $2\theta = 8°$, no separation is expected in this geometry. The turbulence models investigated are the $k-\epsilon$, the $k-\omega$ and the RSM model. The mesh refinement is tested on produced accuracy of the results. The final results of the simulations are compared with both DNS (direct numerical simulation) and experimental results. All models produce different behavior, due to transport equations, algebraic models and empirical constants used. The deviations are dependent on geometry and flow conditions, where certain turbulence models are better for specific cases. The simulations showed different representations. The flow behavior of the $k-\omega$ model was the most realistic, due to the correct core velocity although it showed flow reversal at the wall. Various parameters are reviewed, such as velocity profile, flow reversal, pressure coefficient, friction coefficient and turbulent statistics.

The oscillating flow will represent a case which is more closely to the flow seen inside a thermoacoustic engine. The geometry is a rectangular diffuser and the flow is compressible. It is a much more complex flow with frequencies ranging from 6-21 Hz during the simulations. Laminar, transitional and turbulent cases are simulated by Re_δ numbers of 380, 580 and 740 with varying displacement amplitudes. The transitional $k-kl-\omega$ model is used, because of its ability to also simulate laminar and transitional cases besides only turbulent cases. Additional the $k-\omega$ SST model is tested. The velocity profiles are not simulated well with the $k-kl-\omega$ model, which was caused by the under estimation of simulated turbulence near the wall. It was found that for both models separation will induce early and low in the diffuser and expand downstream as the cycle passes. As a result the Reynolds shear stresses show higher values earlier in the cycle. It was also seen that the reattachment would differ in pattern. The trend is found that separation begins earlier with increasing Reynolds number and increasing displacement amplitude. The minor losses, or irreversibilities, vary in accuracy, the effect of the displacement amplitude is not always seen for variables which are dependent on the magnitude of the pressure. In addition turbulence would not show an increase at the point of transition compared to turbulent cases. Both models seem to deliver deviating results, but the $k-\omega$ SST models the cases better.

Acknowledgements

I have had a very hard time in finishing my thesis, because of psychological problems. However the support and trust I got from the TU Delft and the GGZ have made it possible for me to keep going on.

I want to thank Bendiks Jan Boersma as supervisor for his patience, kindness and many advice and corrections I got during my thesis, without it this was not possible for me. I also want to thank Mathieu Pourquie for the help and advice I got in getting the simulations started.

Jeroen Gijsberts has been there to motivate me and I am very thankful for all the coordination and appointments he has provided, they certainly did help. The internship he arranged at Hoogeheemraadschap Hollands Noorderkwartier has helped me in getting motivated and feeling better again. I therefor am also very thankful towards the organization of HHNK to realize this, because it didn't had much benefits for them. Johan Jonker, my coordinator at my internship, has always been very positive. He made the day go faster by using his sense of humor. I want to thank him for supporting me. I can also appreciate Lourdes Gallastegui Pujana always keeping contact, especially when I had problems. She wanted to make sure I would go in the right direction in many ways. I also want to make a quick thanks to my social workers Nynke Storm, Marcella Herour and Lia van Engelen.

Finally I want to thank my parents, family and friends. It was not possible to finish my thesis without them. I can move on now and close this chapter of my life.

L. Schoenmaker
Delft, August 2017

Contents

Nomenclature

Variables

δ	Viscous layer thickness (m)
$\dot{E}$	Acoustic power (W)
$\dot{V}$	Volume flow rate (m^3/s
ϵ	Turbulence dissipation rate (m^2/s^3)
ν	Kinematic viscosity (m^2/s)
ν_t	Turbulent viscosity($Pa \cdot s$)
ω	Specific turbulence dissipation rate ($1/s$)
ω_{osc}	Oscillating frequency in radians (rad/s)
ρ	Density (kg/m^3)
τ_w	Wall shear stress (Pa)
a	Oscillation amplitude (m/rad)
D	Pipe diameter (m)
f	Frequency (Hz)
H	Upper channel width (m)
h	Lower channel width (m)
k	Turbulent kinetic energy (m^2/s^2)
k_l	Laminar kinetic energy (m^2/s^2)
k_s	Small-scale kinetic energy (m^2/s^2)
l	Turbulence length scale (m)
L_0	Displacement amplitude (m)
p	Static pressure (Pa)
p_w	Pressure at the wall (Pa)
R	Radius (m)
r	Radial distance from axis (m)
T	Period of the cycle
u	Channel velocity (m/s)
u'	Fluctuating velocity (m/s)
u_τ	Friction velocity (m/s)
u_i	Velocity in a specified direction (m/s)
u_j	Velocity in a specified direction (m/s)
u_x	Velocity in x-direction (m/s)
u_y	Velocity in y-direction (m/s)
u_z	Velocity in z-direction (m/s)
$u_{m,in}$	Mean inlet velocity (m/s)
u_{max}	Highest velocity of the cycle (m/s)
x	Coordinate in x-direction (m)
y	Coordinate in y-direction (m)
t	Time (s)

Dimensionless parameters and numbers

α_B	Loss factor of minor losses blowing stroke (-)
α_S	Loss factor of minor losses suction stroke (-)
η	Area ratio between upper and lower channel (-)
C_f	Friction coefficient (-)
C_p	Pressure coefficient (-)
f_w^*	Normalized friction coefficient (-)
K	Minor loss coefficient (-)
K_B	Minor loss coefficient blowing stroke

(-)

K_S Minor loss coefficient suction stroke (-)

Re_δ Viscous penetration depth Reynolds number (-)

Re_ω Oscillating amplitude Reynolds number (-)

Re_h Channel width Reynolds number (-)

Re_{max} Maximum Reynolds number during the cycle (-)

TI Turbulence intensity (-)

u^+ Dimensionless velocity, law of the wall(-)

Wo Womersley number (-)

y^+ Dimensionless wall distance, law of the wall (-)

Other

δ_{ij} Kronecker delta (-)

1 Introduction

Background

Thermoacoustic heat engines are devices which can cool, heat and produce mechanical power in a sustainable and environmentally friendly way. In figure 1.1 an example of a thermoacoustic-Stirling engine is shown, this type of geometry is often used when high efficiencies are of importance [9] and are used to produce acoustic power. The devices can produce or absorb high intensity sound waves, where the first process will produce work and the second absorbs it to transfer heat from a cold to a hot heat reservoir, functioning respectively as a prime mover or a heat pump. This is possible without the use of a harmful cooling medium. The thermoacoustic heat engine functions with no moving parts, only an inert gas such as helium is needed to transfer heat between the heat exchangers. Therefore it is relative cheap to produce.

Thermoacoustic devices have had a rush in the past decennia. In 1999 Backhaus and Swift [9] developed a thermoacoustic-Stirling engine which reached a Carnot efficiency of 41%. The engine converts heat into acoustic power with an efficiency of 30% although this was with high temperatures (700-750°C) fluid, where it is easier to achieve higher efficiencies. A thermoacoustic-Stirling engine with a Carnot efficiency of 49% was developed in 2009 by Tijani [43]. The high efficiency makes it possible for the device to have commercial potential. ECN therefore started with other partners to invest in a model that can be produced on large scale. The first model would have a capacity of 10 kW and was ready to use in 2010, the second model would reach 100 kW in 2012. Finally working to a size where it is possible to deliver 1 MW. High capacities can be used by industries to heat waste water by the use of low frequent gasses and thereby making it reusable again. For homes the device can be used to ventilate a room.

In thermoacoustic heat engines diffusers are used to cancel out streaming. In figure 1.1(b) the diffusers are denoted by the term jet pumps. The amount of fluid that flows back from the hot to the cold heat exchanger will be reduced by the diffusers. Which is a problem in these type of engines, because it reduces the engines Carnot efficiency. The diffusing geometry introduces minor losses in the oscillating flow, which causes a suction effect on the flow below the diffusers.

Previous studies

Thermoacoustic heat engines are widely studied, which goes as far back into the 20th century. Swift [45] produced an article which gave an overview of different thermoacoustic engine's available at that moment and the theory behind it. Giving results about how each of them perform, for example by temperature and COP values. While for example Wheatley et al. [50] studied an intrinsically irreversible thermoacoustic heat engine, which consists of a simple tube with copper plates inside, also called the stack. Here especially the temperature behavior inside the stack was investigated. When looking for information about diffusers a different form of articles is found. The behavior is much more intuitive and this results in articles which are more about performance results than information, where often variables as pressure recovery coefficient or velocity profiles are showed to give an indication on performance. Also it must be noted that there are much more articles talking about compressible flow than incompressible. The article from McDonald and Fox [32] only handles pressure recovery for an incompressible flow through diffusers. From the article it follows that the point of first stall (separation of flow) at constant length/radius ratio occurs at a larger angle. Article's like these can be used to find trends. For this thesis an article about direct numerical simulation of turbulent

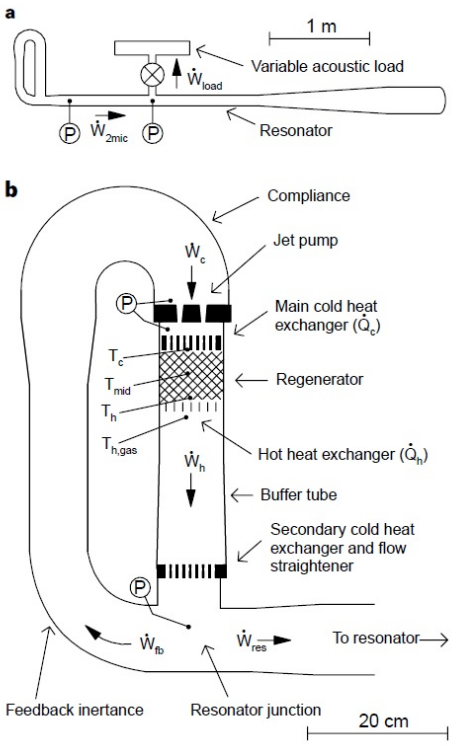

Figure 1.1: An overview of a thermoacoustic-Stirling engine, where (a) shows the entire engine and (b) zooms in on the regenerator part [9]

incompressible diffuser flow is used by Lee et al. [31]. In this article an in depth look is taken at performance versus diffuser angle including turbulence statistics. Oscillating flow inside a diffuser is a subject that is investigated little. Schachenmann and Rockwell [40] has done experiments in one type of diffuser by varying oscillation amplitude and frequency. The most important conclusion was that the time mean diffuser performance was almost not affected when applying oscillations to the flow. Smith and Swift [42] and Morris et al. [33] studied an oscillating flow through a sudden area change. The thesis by King [26] looks at the behavior of the flow inside a diffuser when the flow oscillates. Here it is found that a larger displacement amplitude causes earlier separation. Also a larger diffusing angle causes earlier separation.

Objectives

To have a better idea at how thermoacoustic engines work with diffusers installed, this device needs some research. In this thesis a better look is taken at this geometry. An investigation will be done with different kind of flows inside a diffuser, this will be done by Computational Fluid Dynamics. The theory is found inside fluid dynamic books and articles. The CFD simulations are done with the commercial package Ansys Fluent. There are results of experiments and numerical simulations available with different kind of flows through diffusing geometry. These articles are used to compare the simulation results. In this thesis a turbulent incompressible flow and a compressible oscillating flow will be studied. The oscillations will be in the laminar, transient and turbulent region with varying displacement amplitudes. The used flows will showcase the behavior of diffusing geometries. Also the oscillating flow will be an approximation of how the flow inside a thermoacoustic engine is influenced by it. The influence of the diffuser on the thermoacoustic engine will be described by its minor losses and acoustic power, which occur during the oscillating cycle. Exposing the diffuser to these flows will be a good test to see how Ansys Fluent performs. It is of importance that the correct boundary conditions, solution methods and turbulence model are chosen. The question to answer is if it is possible to simulate the cases well enough, will the flow behave in this structure as expected. Additionally it will be interesting to make a prediction whether it is possible to simulate a thermoacoustic engine.

Thesis structure

The thesis will be organized as follows. In chapter 2 there will be a review of the relevant literature. In chapter 3 modelling approaches and validation of the simulation model about the turbulent incompressible diffuser flow are done. In chapter 4 an oscillating flow in a diffuser will be modelled and validated with the experience from chapter 3. And finally the conclusion and recommendation can be found in chapter 5.

2

Literature study

In this chapter relevant literature for this research are presented. First of all an introduction to diffusing geometries will be given. An insight in how flow patterns and boundary layer develop inside a diffuser is given. Steady, unsteady, turbulent and oscillating flow are discussed. Additionally some numerical methods of how certain parameters of these flows can be calculated will be explained. The turbulence models of interest will be discussed. Finally a section presenting the thermoacoustic engine and its diffuser dependency is presented.

Steady flow in diffusers

The working principle of the diffuser is that it converts kinetic energy into potential energy i.e. converting speed into static pressure. When the fluid enters the expanding area it slows down, a part of the kinetic energy will be transformed into potential energy. An efficient diffuser will have small losses. In the diffuser an adverse pressure gradient causes the boundary layer to decelerate and thicken. Depending on geometry and fluid properties, the flow is able to show chaotic properties. Under these conditions low diffusion of momentum occurs (i.e. momentum is slowly transferred to other particles), although high convection of momentum is seen (where transfer is dependent on transport). Particles with momentum are spread throughout the fluid due to pressure gradients. Under turbulent conditions high velocity and pressure changes are seen, vorticity can also occur. All these phenomena can decrease pressure recovery and thus efficiency.

Four regions of flow patterns are defined for a steady flow inside a diffuser [25, 38]. The four regions are:

(1) No-stall
(2) Transitory stall
(3) Two-dimensional stall
(4) Jet flow

The no-stall region is identified by smooth flow and no separation, performance is moderate (fig. 2.1a). Separation is recognized when the speed of a flow relative to the object falls to zero. The flow becomes detached from the surface and will create vortices and more eddies (in case of turbulence). It is also known as an unsteady flow [44] and can be seen in fig. 2.1b. The next region is transitory stall, which is recognized by non-developed flow separation. The flow is unsteady with oscillation of pressure and overall flow pattern. Regions with reverse flow occurs near the diffusing wall and then wash out [13]. A big loss in pressure recovery is noticed when separation occurs. The best performance in pressure recovery is found in the transitory stall region. The two-dimensional stall is recognized when the flow starts to separate from one side to the other. The last region is jet flow. In this region the flow just skips the unsteady flow near the wall and flows directly to the exit. The flow in this region is separated from the walls, large eddies are seen on the diverging walls. The biggest losses will occur in this region. In figure 2.2 an overview of the different regions is shown, which occur dependent on used diffuser angle and length-to-width ratio.

In the region where stall occurs it is much harder to predict the characteristics of the flow and the accompanying losses although maps of flow losses are available by Eiffel [16], Karassik [25], White [52]. In figure 2.3 the performance of a flat diffuser is shown by its pressure coefficient as provided by Fox and Kline [18]. The

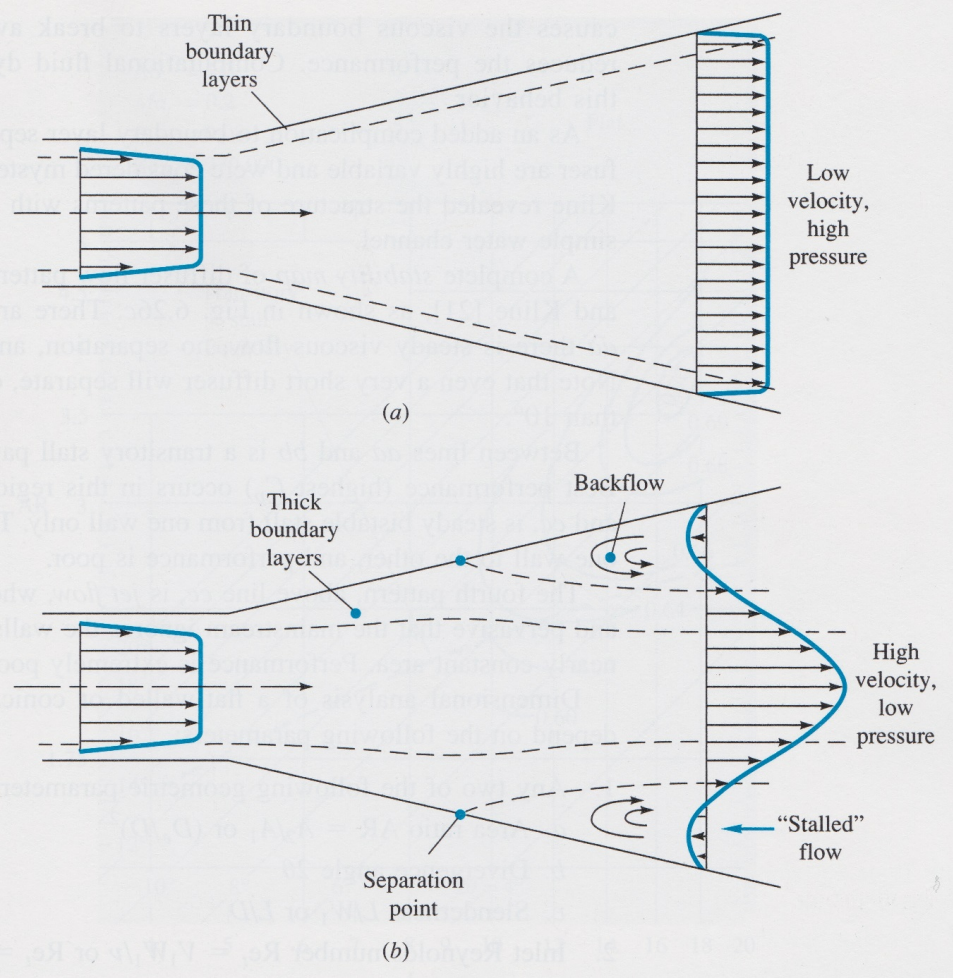

Figure 2.1: Flow patterns which can be found inside a diffuser [51].

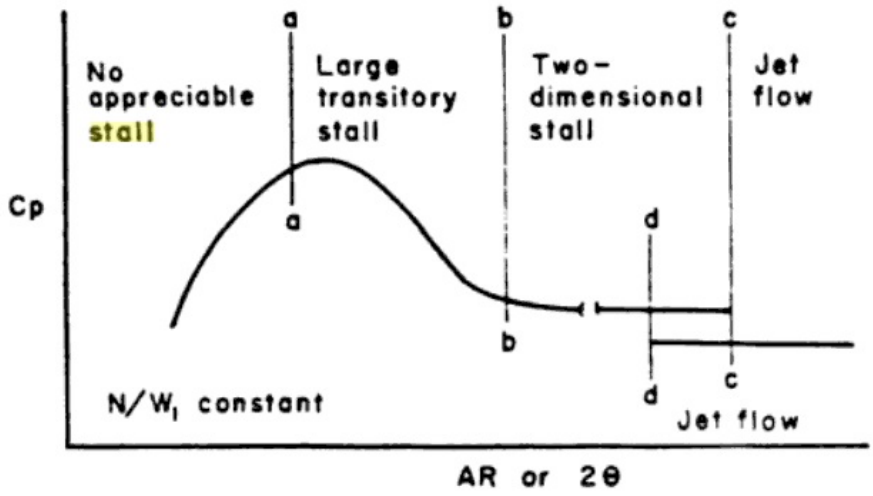

Figure 2.2: Flow patterns and there performance as function of the diffuser angle 2θ or area ratio inside a straight diffuser [38].

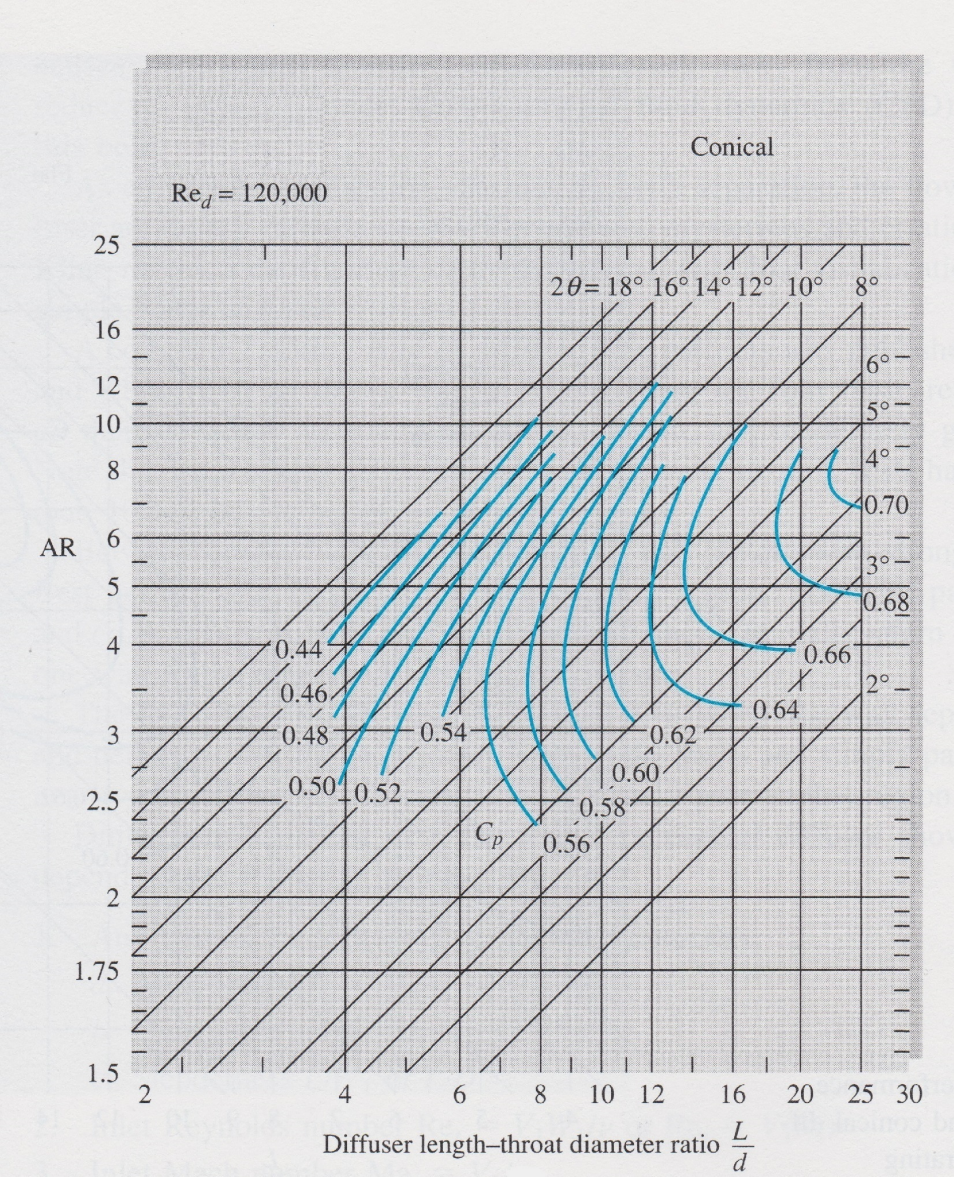

Figure 2.3: Performance map of a flat diffuser as function of area ratio, length to width ratio and diffuser angle [18].

loss coefficient can be evaluated and is based upon velocity head at inlet, diffuser angle, and length to width ratio. Increasing the length to diameter ratio will have beneficial effects on diffuser performance, because momentum is more gradually divided. Increasing the diffuser angle will, until separation appears, have beneficial effects on losses by resistance, because flow can easier flow through the section and this will decrease pressure losses [22]. When increasing the inlet velocity or the pipe diameter, there will be bigger inertial forces. An increase in inertial forces means the flow is less effected by viscous damping. In this case stall can develop in the expanding area, due to the bulk movement of the fluid. The flow will have a higher momentum, which makes it harder to correct for changes in direction. However it was discovered that the pressure recovery coefficient is only slightly dependent on Reynolds number, Mach number, velocity profile and turbulence level at inlet [23]. It is known that a thin boundary layer at the entrance of a pipe will cause a higher pressure drop compared to a fully developed flow, where the pressure drop will be linear, but will only slightly effect diffusing performance as was concluded. Separation causes the viscous boundary layer to be distorted and introduces big losses [51]. The flow separation is dependent on the sum of local velocity gradient, pressure gradient (in opposite direction), and viscous stresses. As turbulent energy introduces, the influence of the turbulent viscosity becomes bigger than the normal viscosity. Separation is independent on Reynolds number for laminar flow and separation resistance increases slightly with increasing Reynolds number.

Diffuser transitory stall occurs in the range of optimum pressure recovery. The transitory stall can be described as an unsteady flow, which causes noise oscillations. In the pipe section afterwards these oscillations are also seen. When this behavior can be predicted diffuser and accompanying pipe work can be designed such that the oscillations occurring are not causing any interference or resonance with the design. It was found that diffuser performance depends not only strongly on diffusing angle, but also on inlet blockage [29]. It followed that for a conical diffuser the power spectral density, the amount of squared pressure per frequency (Pa^2/Hz), increased with increasing inlet velocity and diffuser length.

Important non-dimensional numbers

For describing an oscillating flow inside a pipe or duct different Reynolds numbers are often used. In the case that there is not a steady component in the oscillating flow, it is in general dependent on two variables, i.e. the frequency and the amplitude [27]. The Reynolds numbers can be calculated using either of the following properties, the viscous penetration depth (Re_δ) , the (lower) channel width (Re_h), or the oscillation amplitude (Re_ω). All three forms of the Reynolds number are dependent on the maximum velocity. The Reynolds numbers are given by:

$$Re_\delta = \frac{u_{max}\delta}{\nu} \quad Re_\omega = \frac{a u_{max}}{\nu} = \frac{u_{max}^2}{\nu\omega_{osc}} \quad Re_h = \frac{h u_{max}}{\nu} \tag{2.1}$$

Here h is the channel width, u_{max} is the maximum velocity of the cycle, ω_{osc} is the radial frequency of the oscillations, $a = u_{max}/\omega_{osc}$ is the oscillation amplitude and ν is the kinematic viscosity. The viscous penetration depth is given by $\delta = \sqrt{\nu/\pi f}$, where f is the oscillation frequency. The frequency can be used to calculate $\omega_{osc} = 2\pi f$.

The Womersley number is another dimensionless number for describing oscillating flow. It describes the relation between transient inertial forces and viscous forces. The number is used to predict flow profiles.

$$Wo = h\sqrt{\omega_{osc}/\nu} \tag{2.2}$$

The frequency and stroke length are related to each other by:

$$L_0/h = \frac{u_{max}}{\pi f h} \tag{2.3}$$

Here $L0$ is the displacement amplitude.

The different Reynolds numbers and stroke length are also related to each other. In the following form:

$$Re_\omega = \frac{Re_\delta^2}{2} = \left(\frac{L_0}{h}\right)\frac{Re_h}{2} \tag{2.4}$$

Oscillating flow

There aren't much articles available on how oscillating flow behaves or performs in diffusers. For instance there is no performance map available, which shows under what conditions certain behavior will appear as described for steady flow. There is however a lot known about how it behaves in pipes and ducts.

The velocity shape profile for oscillating flow is dependent on the Womersley number. In figure 2.4 the different velocity profiles during one cycle for different Womersley numbers are shown, produced by Feldmann and Wagner [17]. The shape can be a parabola, a M-profile shape or a flat profile with increasing frequency. The M-profile shaped velocity profile is due to momentum of the fluid. Near the wall the fluid can react faster, because the flow is slowed down earlier due to the boundary layer and can then earlier react to the pressure gradient.

Furthermore the transition from laminar to turbulent, which will also be seen in a diffuser, is distinguished by four flow patterns.

(1) Laminar flow, where the flow is steady.
(2) Disturbed laminar flow, where small perturbations appear in the accelerating part of the cycle.
(3) Intermittently turbulent flow, here the flow is partly turbulent at the deceleration of the cycle and the acceleration part is laminar.
(4) Turbulent flow, where the whole cycle is existing of turbulent flow.

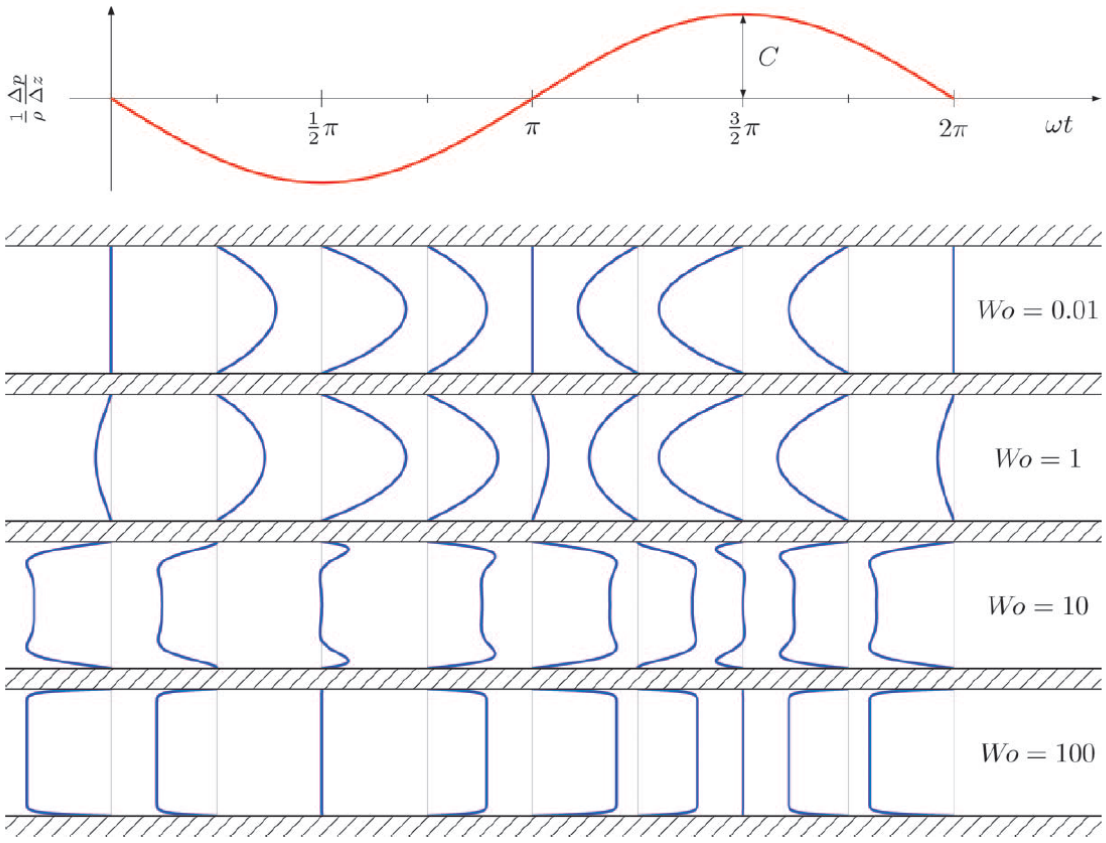

Figure 2.4: The axial velocity profiles (blue) at eight different phases of the cycle, normalized by u_{max}. The pressure gradient is shown at the top (red). It is based on the Sexl-Womersley solution of the incompressible Navier-Stokes for laminar oscillatory pipe flow [17].

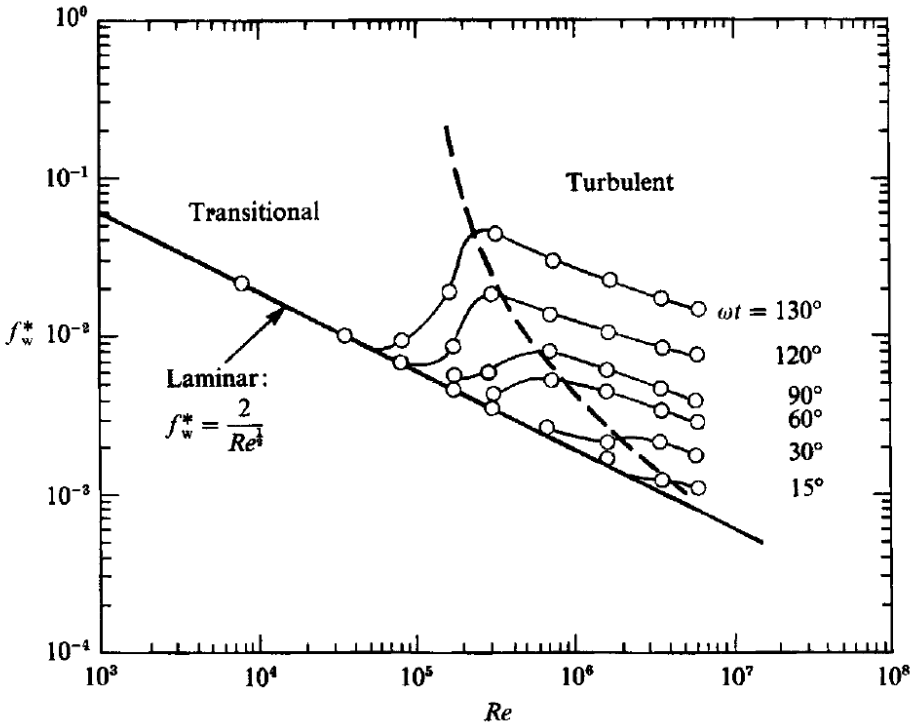

Figure 2.5: Normalized friction coefficient as function of $Re_\omega = 2 \cdot L0 \cdot u_{max}/\nu$ at different points of the cycle for a smooth bed [24]

It was observed by Kurzweg et al. [28] that in small diameter tubes the onset of turbulence would be delayed when the Womersley number was lower. A lower Womersley number would increase the stability of the flow. Therefore the used Reynolds numbers are often based on the frequency. The viscous penetration depth Reynolds number is used to clarify a number to find the four states the flow can be distinguished with. Although it is found that the transition from laminar flow to disturbed laminar flow can vary in Reynolds number. Akhavan et al. [4] found this transition to be dependent on experimental setup. Where Hino et al. [21] and Ohmi et al. [35] found transition at around $Re_\delta = 280$, but Poroseva and Girimaji [36] found the number of $Re_\delta = 400$ to be fully laminar.

The transition from disturbed laminar flow to intermittently turbulent flow is found to take place between $500 < Re_\delta < 550$ for $D/\delta > 2$ [27] and seems not to be dependent on experimental conditions, where D is the pipe diameter. The Reynolds number where transition occurs is dependent on D/δ [47]. By decreasing the number the transition to turbulent forms at a higher Reynolds number. If $D/\delta > 10$ the Reynolds number of transition will not increase any further. The boundary-layer thickness decreases with increasing frequency. By increasing the frequency and remaining the same Re_δ number, the speed will scale by the square root of the frequency. So the boundary layer decreases with decreasing stroke length.

When increasing the Re_δ number above 550 eventually a turbulent flow will start. The transition to a turbulent flow regime does not occur at once [24]. It was found that the normalized friction coefficient ($f_w^* = (2\frac{\tau_w}{\rho}/u_{max}^2)/\cos(\omega_{osc}t - \frac{1}{4}\pi)$, where τ_w is the wall shear stress, t is the time and ρ is the density) decreases with Reynolds number, but is also dependent on phase (fig. 2.5). The transition takes place between certain Reynolds numbers after which the flow becomes fully turbulent. When the cycle is at the start of its acceleration (denoted by its phase given by $\omega_{osc}t$) the Reynolds number at which transition occurs is higher and gets lower as the cycle progresses. Interesting to see is that the Reynolds number for the onset of turbulence is quite high when compared to a steady flow. A transient oscillatory flow starts at a value of around 45,000 (when only taking the maximum velocity and width of the channel into account), where the critical Reynolds number is only around 2040 for steady flow [17]. Due to the oscillating behavior, the flow is not able to develop turbulence. The sinusoidal change of momentum makes it possible to have stronger viscous damping.

Minor losses

A minor loss coefficient is used to find the losses created by the development of heat during the process of energy conversion inside the diffuser. The minor loss coefficient is given as a pressure coefficient:

$$K = \frac{\Delta p}{\frac{1}{2}\rho u^2} \tag{2.5}$$

Here K is the minor loss coefficient, p the pressure, ρ is the density and u is the channel velocity.

It will vary depending on the entering state of the diffuser and whether the flow is laminar or turbulent [27]. In literature there are approaches available to calculate these losses, but only the simplest geometries are available for oscillating flows. This includes flow through pipes, channels and simple cardiovascular models.

When minor losses in an oscillating flow are studied, there is made a difference between the blowing stroke and the suction stroke, defined as K_B and K_S. Where K_S compared to K_B is very small. Here t=0 is declared to be the start of the blowing section in positive direction. An expression was suggested by Swift et al. [46] to relate the difference in loss factors ($K_B - K_S$) to the time-averaged pressure drop.

The derivation starts with the standard Bernoulli equation with a loss factor incorporated. The unsteady term can be ignored, because its integral will be zero over the cycle.

$$p_1 + \frac{1}{2}\rho u_1^2 - \frac{1}{2}K\rho u_1^2 = p_2 + \frac{1}{2}\rho u_2^2 \tag{2.6}$$

Subscript 1 denotes the inlet and subscript 2 the outlet. The pressure and velocity will vary over time. The ratio of the lower channel width h and the upper channel width H will be used in the next equation, $\eta = h/H$, to scale the velocity. Averaging over both the blowing and suction section of the cycle gives:

$$\Delta P = \frac{\rho}{2}\left[\left(K_B - 1 + \eta^2\right)\alpha_B u_{1,max}^2 + \left(\eta^2 - 1 - K_S\right)\alpha_S u_{1,max}^2\right] \tag{2.7}$$

where

$$\alpha_B = \frac{1}{T u_{1,max}^2}\int_0^{T/2} u_1^2 dt, \quad \alpha_S = \frac{1}{T u_{1,max}^2}\int_{T/2}^{T} u_1^2 dt \tag{2.8}$$

The loss factors of the minor losses of the blowing stroke and the suction stroke are respectively given by α_B and α_S. The time-averaged pressure difference is given by ΔP, the period of a cycle is T, and $u_{1,max}$ is the maximal velocity of a cycle at location 1. When the oscillations are sinusoidal $\alpha_B = \alpha_S$ =1/4 [42], which results in the following equation:

$$\Delta p = \frac{\rho u_{1,max}^2}{8}\left(K_B - K_S - 2 + 2\eta^2\right) \tag{2.9}$$

From this equation it is seen that the time-averaged pressure drop can be related to the difference in minor loss coefficients.

Thermoacoustic engines make use of the same principle, where a sudden expansion is seen when the fluid exits the stack. The geometry of a thermoacoustic engine also makes use of area expansion, where minor losses will take place. The time-averaged pressure drop can make it possible to calculate these losses. It was found by Wakeland and Keolian [48] that a uniform flow will have less losses through a change in area compared to a fully developed flow.

Acoustic power

The quantity that enables to see how much power is available to drive an oscillating flow through a component is called the acoustic power. The acoustic power is expressed as a force that is driven by a velocity, comparable to electric power. The acoustic power is given by the following formula:

$$\dot{E} = \int_0^T p\dot{V} dt \tag{2.10}$$

Here $\dot{V}$ is the volume flow rate and p and $\dot{V}$ vary periodically. Inside a diffuser acoustic power dissipations takes place. The acoustic power dissipation for a fully developed flow is linear across the diffuser, due to

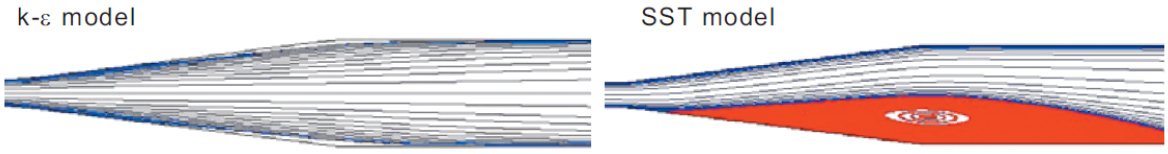

Figure 2.6: Stream lines produced by the $k-\epsilon$ and SST turbulence models

viscous dissipation. It was found by Backhaus and Swift [9] that pressure scales by u^2 inside a thermoacoustic-Stirling heat engine. Therefor it is assumed the acoustic power will scale by u^3

Smith and Swift [42] studied the normalized power dissipation ($\dot{E}/\rho A u^3$) through a sudden area change with a rounded exit. It was found the dissipation would increase with displacement amplitude and decrease with Reynolds number, especially when the transition from laminar to turbulent takes place. Afterwards a look was taken what would happen when the exit radius was increased. It was found it would have a positive effect on the adverse pressure gradient, which needs to be as small as possible. It was seen it would decrease and the core flow would have more space to expand, resulting in smaller losses.

Turbulence model

Turbulence is one of the phenomenon which is frequently encountered in fluid dynamics. In computational fluid dynamics this can be modelled by turbulence models. Over the years many of the turbulence models have been created. All of the models have their own strong and weak points. There are models which for example perform better in free shear flows, while other models perform better with boundary layers. There is also a variety in amount of transport equations that need to be solved for each iteration, which has its repercussions on computational time.

It is difficult to determine a correct turbulence model, because there is not a model that performs well in every situation. Although it possible to use earlier studies to make predictions. The main focus here is on separation and oscillating flow, both caused by an adverse pressure gradient. Turbulence models like transitional models are designed to simulate the onset of turbulence, so these turbulence models should perform better in the simulated cases. To our knowledge such models have not been used to simulate oscillating flow. Flow reversal can be compared to cases where adverse pressure gradients along a flat plate exist. Two equation based models have difficulty to predict the onset and amount of separation as well as under predicting the amount of separation later on [6].

Turbulent flow

The article published by Ansys.Inc [7] compares the $k-\epsilon$ model with the $k-\omega$ SST model in a diffuser. The $k-\omega$ SST uses the $k-\omega$ model at the wall and blends in the $k-\epsilon$ model for the bulk flow, which should result in better results. It is found for the $k-\epsilon$ that the separation from the wall as can be seen from figure 2.6 is not observed. Furthermore it is found that the axial velocity profiles when compared to experimental results, as found in fig. 2.7, are in good agreement with the $k-\omega$ SST model and differ quite a lot from the $k-\epsilon$ model especially when there is separation. The $k-\omega$ SST model has been studied for aerodynamic cases a lot. It was found that it was the most accurate model for aerodynamic cases [7]. Also worth noting is the better prediction of heat transfer, since this can be of importance in thermoacoustic heat engines.

The article by Bardina et al. [11] compares more turbulence model, the Spalart-Allmaras (S-A) one-equation model, the $k-\epsilon$ model, the $k-\omega$ model and the $k-\omega$ SST model. The models are compared using 8 flows, four fully-developed free-shear layer flows, an incompressible boundary layer, and three complex flows with separation. The free-shear layer flows are the following a mixing layer, a round jet, a plane jet and a plane wake flow. Where the complex flow consists of an adverse pressure gradient boundary layer, an axisymmetric shock-wave/boundary-layer interaction, and a transonic airfoil flow. Here the round jet and the adverse pressure gradient boundary layer show shows the most similarities with the current case, because of the adverse pressure gradient boundary layer.

Velocity profiles are obtained for the round jet flow. Here all the models aren't able to accurately reproduce the problem. The $k-\omega$ SST model and $k-\epsilon$ model perform well, this is because for free shear flows the $k-\omega$ SST model uses the $k-\epsilon$ model. The other models are way off. The adverse pressure gradient boundary layer in a circular duct was tested showing the skin friction, surface pressure, velocity profiles at two locations, as

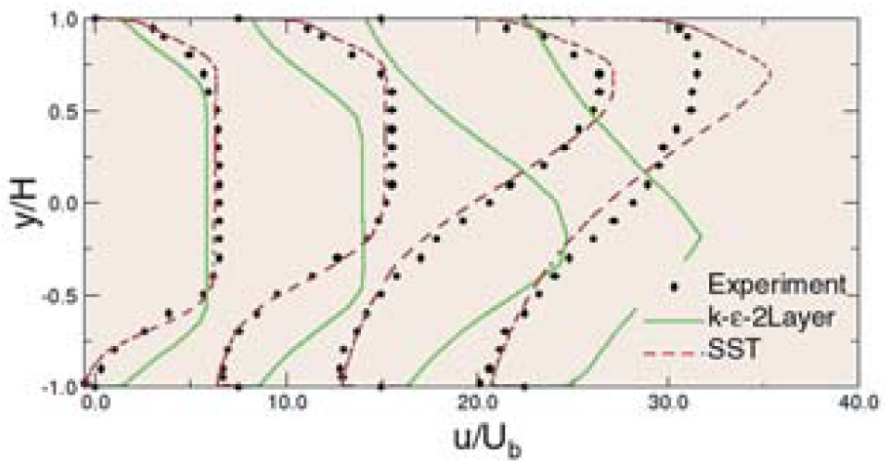

Figure 2.7: Comparison of axial velocity profiles normalized by the bulk velocity based on the $k-\epsilon$ model, the $k-\omega$ SST model and experimental data

Model	*k-ω*	*k-ε*	*S-A*	*SST*
Mixing layer	●	☆	☆	☆
Far wake	●	◗	☆	◗
Plane jet	●	☆	◗	☆
Round jet	●	✧	●	✧
ZPG BL	☆	☆	☆	☆
APG BL	◗	●	✧	☆
Trans. bump	◗	●	○	✧
RAE 2822	◗	●	○	✧
Scale: (Bad) ● ◗ ○ ✧ ☆ (Good)				

Table 2.1: Performance chart of the different turbulence models [11].

well as shear stress profiles at two locations. All of the turbulence models predict separation except the $k-\epsilon$ model. For the skin friction and surface pressure it was found that $k-\omega$ SST shows the best agreement with experimental results. The S-A model tends to over predict the surface pressure and under predict the skin friction. The $k-\omega$ model performs well for skin friction, but gives higher values for surface pressure. The $k-\epsilon$ model does the worst job, by giving much higher values for surface pressure and skin friction. For the mean velocity and shear stress again the $k-\omega$ SST model gives the best results, but it under predicts the shear stresses at reattachment. The $k-\epsilon$ model performs the worst and the other two models are in between.

An overview of all the flows is found in table 2.1. Concluding the $k-\omega$ SST model is the best choice except for far wake flows, which is not of importance for the present study.

Transitional flow

Transition models that can predict laminar to turbulent transition can show an improvement in the modelling of oscillatory flow, especially when they perform in the region of laminar flow, disturbed laminar flow and intermittently turbulent flow. The article by Bhushan et al. [12] investigates transitional flow. It is found that in a capillary tube the laminar model (no turbulence model activated) only shows good agreement for the frictional factor at low Re, while turbulence models tend to over predict it. The transitional $k-kl-\omega$ model on the other hand showed the same results when compared to experiments for the whole Re range from 625-

5100. When a nozzle with an inlet diameter of 0.012 m was tested, it was found that the axial velocity had deviations in the 0.012 m expanding area for the used turbulence models at Re=500. At Re=6500 the model performs much better. It must be noted that it is important to use the right turbulence intensity, otherwise results could deviate.

In the article by de Jesus et al. [14] research is done with an adverse pressure gradient in turbulent channel flow by using three different bumps. It was found that the standard turbulent models $k-\omega$ SST and RSM were unable to reproduce the skin friction coefficient near the rear of the bump as well as the peaks of turbulent kinetic energy in the adverse pressure gradient section. The models do not include streak instability mechanisms in their formulation and were therefor unable to reproduce the same results as DNS or LES. The transitional $k-kl-\omega$ model and the transitional SST model, which is based on the $k-\omega$ SST model, show an improvement in predicting these results, especially the $k-kl-\omega$ model is able to predict the recovery pattern and the skin friction coefficient. The decrease of the skin friction coefficient after the bump is sometimes larger and the recovery smaller compared to reference computations. In the adverse pressure gradient region both models are also able to represent the strong increase in Reynolds stresses, but the $k-\omega$ SST model is not far behind. Therefore it is chosen to use a transitional model for the diffuser model.

Some more investigations were done on the $k-kl-\omega$ model to see how it performs. Samala [39] compared the $k-\omega$ SST model with the $k-kl-\omega$ model using an airfoil in a wind tunnel. The airfoil shares the same characteristic as the diffuser by creating an adverse pressure gradient by having a sudden angle change, the flow shows separation in this case. At the airfoil the transition from laminar to turbulent takes place. It was found that the drag coefficient for different angles of attack of the airfoil was very much identical to experimental results for the $k-kl-\omega$ model. The $k-\omega$ SST model deviated between 100%-250% increasing further with a bigger angle of attack. For the lift coefficient the $k-\omega$ SST performed better than the $k-kl-\omega$ model, for an attack angle of 8° respectively 17% and 37%. For an attack angle of 0° both models almost performed identical to the experimental results, where the $k-kl-\omega$ performs a little worse.

From the results it follows that separation is modelled by the transitional models. For the oscillating flow the transitional $k-kl-\omega$ model will be used, as it seems to perform a little better when compared to the transitional SST model. How well it will perform for an oscillating flow in a diffuser must turn out by the simulations done. To our knowledge there are no other comparable cases which use the transitional $k-kl-\omega$ or transitional SST model, this is probably because the models are more recent turbulence models.

Thermoacoustic engines

A thermoacoustic engine is a device which produces acoustic power or can make use of it, it has two functional modes. In the prime mover mode the hot and cold heat exchanger function just like a heat exchanger and produce sound waves. In the heat pump mode it cools down and heats up a reservoir by the use of sound waves. A stack or regenerator is found in between the heat exchangers, these produce or absorb the sound waves. The difference between these parts is that a stack (thermoacoustic engine) functions by standing waves, while the regenerator (thermoacoustic-Stirling engine) functions by travelling waves [45]. In figure 2.8 an example of a simple thermoacoustic engine is given, which functions as a prime mover at a frequency of 500 Hz, a quarter of the wavelength fits the pipe length [45].

The stack or regenerator consist of thin plates that create small parallel channels, where the heat flows through. The stack needs a distance between the plates comparable to the thermal penetration depth of the gaseous medium, while the regenerator needs a distance which is smaller than the thermal penetration depth [45]. A certain temperature difference across the stack or regenerator will produce acoustic power, which is equal to work. The sound waves are created by heat, the heat is transferred to the solid wall of the stack or regenerator as it flows through, this introduces oscillations in the pressure and temperature [20]. The reverse is true when putting in acoustic power by a driver, where the heat transfer is forced. The geometry determines the resonance frequencies and boosts the amplitude of the acoustic pressure and acoustic velocity.

A diffuser is an integral part of thermoacoustic engines, where a flow expands from a small volume to a larger region. Also, as already was shown in section 1, in Fig. 1.1 a jet pump is installed inside a thermoacoustic engine. It are small diffusers to create an adverse pressure gradient and thereby introducing minor losses. Minor losses need to be as small as possible in normal diffusers, but in thermoacoustic engines these losses can be used to increase the efficiency of the device. The losses cancel out streaming. Streaming, or Gedeon streaming, is a steady flow from the hot heat exchanger to the cold heat exchanger. Heat will be convected, but without producing work. The streaming occurs due to a pressure loss in the stack, which is created when

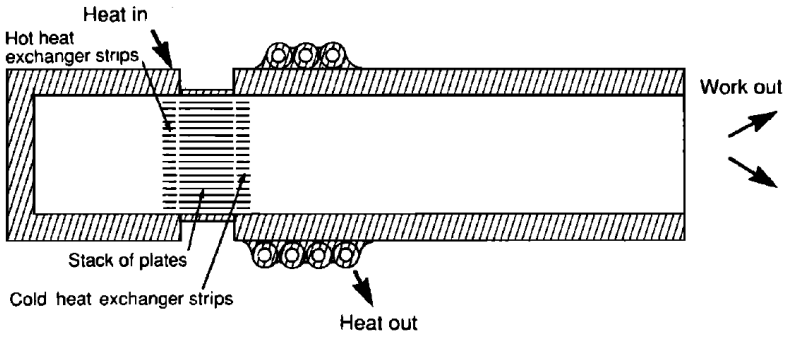

Figure 2.8: A thermoacoustic heat engine which produces acoustic power from heat [45].

the phase difference between velocity and density starts to deviate from its value of $\pi/2$ [10]. A non-zero net mass flux will be created. Ideally the flow would be purely oscillatory, where a zero mean mass flux is seen.

3

Simulation of steady flow in a diffuser

In this chapter a steady flow in a conical diffuser is studied. The geometry for the diffuser is given by Azad [8], where the diffuser has an opening angle of $2\theta = 8°$. The geometry will be modelled in 2D as being axisymmetric. The flow is incompressible and will be modelled at a Reynolds number of 15,000. The simulations are done with Ansys Fluent v16.0, where three different turbulence models are used, which are the $k-\epsilon$ model, the $k-\omega$ model and the RSM model. Results will be compared with experimental data and DNS results of Lee et al. [31].

Mesh setup

Geometry and grid size

Various meshes have been setup to model a $2\theta = 8°$ conical diffuser. The diffuser also known as the Azad diffuser is commonly used through experiments. The standard geometry is used in collecting the same experimental results at different locations throughout the world. The geometry can be found in the article by Azad [8]. It has an entrance diameter of 0.1016 m, outlet diameter of 0.202 m and a length of 0.7179 m (fig. 3.1). It is known that optimal efficiency of diffusers lies between 5°and 15° [51]. Separation is seen when the angle is bigger than 15°. The entrance and exit were extended by 3 m, for better numerical stability and development of the flow. The flow will be fully developed at the entrance of the diffuser, therefor no extra influences from inlet conditions will occur. There is a no-slip condition at the wall and inlet velocity is uniform. Meshes with distances between the cells of 3 mm, 2 mm, 1 mm and 0.5 mm in the pipe section in front of the diffuser were tested. The first two meshes gave non convergent results with the use of different turbulence models.

Boundary layer

A boundary layer mesh profile is placed near the wall. The mesh with a distance of 1 mm between its cells and 112 cells in total over the radius of the inlet, starts at the wall with a first cell of 0.2 mm and has a growth factor of 1.205 resulting in a boundary layer of 10 cells, seen in figure 3.2. The mesh with a cell distance of 0.5 m and 56 cells in total over the radius of the inlet, has a first row of 0.1 mm with a growth factor of 1.09 resulting in 20 cells, figure 3.3. This is chosen for better accuracy of the model, such that it stays within the limits of having one cell with a value of $y^+ = 1$ and two cells within the $y^+ = 5$ region, where $y^+ = y * u_\tau / \nu$,

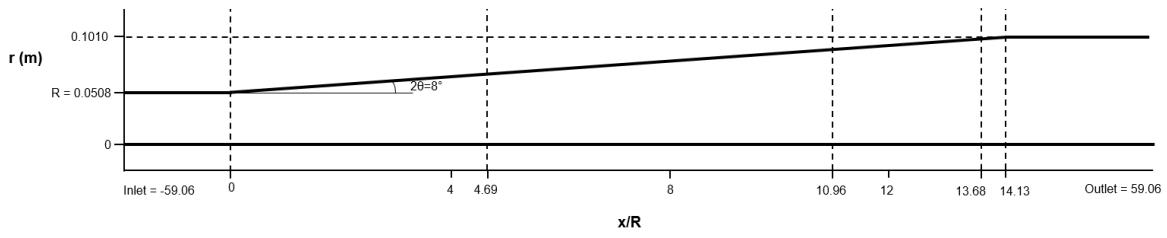

Figure 3.1: Overview of the geometry of the diffuser with the x-axis the distance normalized by the radius of the pipe

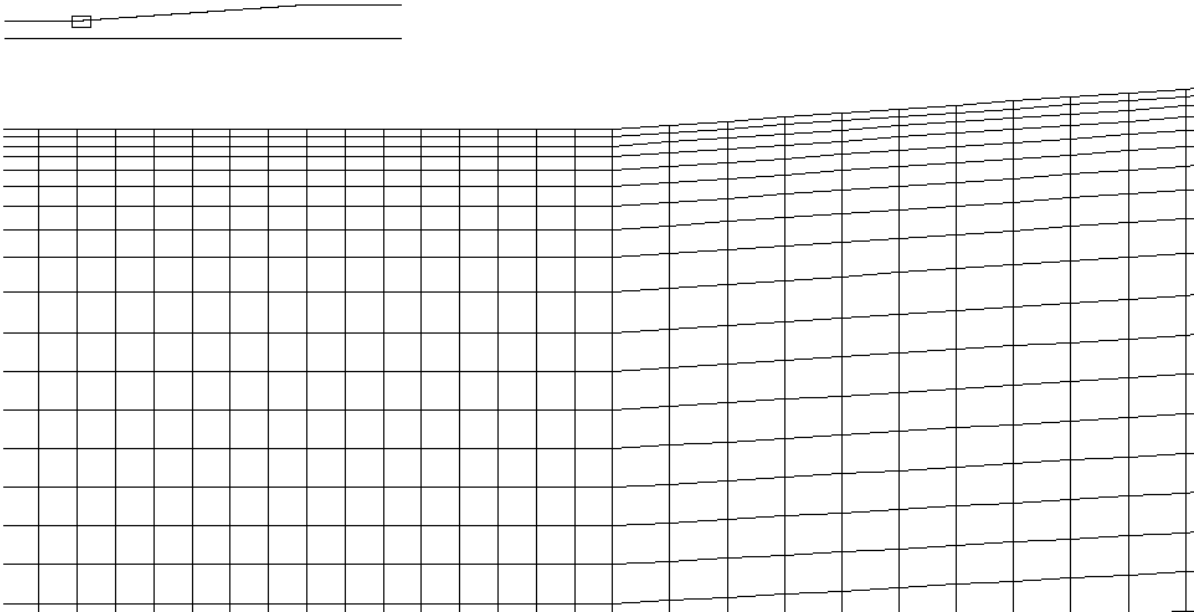

Figure 3.2: An overview of the mesh at the zoomed in section with cell distance 1 mm.

y^+ is a non-dimensional wall distance, y is the distance from the wall and $u_\tau = \sqrt{\tau_w/\rho}$ is the friction velocity. This region is also called the laminar region or viscous sub-layer according to the law of the wall [1]. There is no turbulence in this region. The buffer layer and the log-law region follow up the laminar region. The turbulence begins to start developing in the buffer layer before it enters a turbulent state. In the log-law region the flow is turbulent and the non-dimensional velocity ($u^+ = u/u_\tau$) is equal to a logarithmic function. The regions lie respectively in between $5 < y^+ < 30$ and $30 < y^+ < 300$. The three regions deviate from normal turbulence outside the boundary layer and turbulence models are not accurate in that region [1]. Therefore the turbulence models make use of near-wall treatment functions, where the boundary layer is modelled by the use of certain equations. A certain precision for the boundary layer mesh is required for obtaining good results.

There are different near-wall treatment functions, but some of them require a different mesh setup in the boundary layer. When the model uses the standard near-wall treatment function it is desired to have the first cell at a distance of $30 < y^+ < 300$ [1]. Smaller is possible, but the turbulence models are possibly not able to account for the low-Reynolds number effects. The standard near-wall treatment function will try to approach the flow in the boundary layer by making an estimation of the effects near the wall, but it does not simulate the flow in detail near the wall. For the enhanced wall treatment the value is not preferred to lay in one region and can be as small as the value of $y^+ = 1$ to model the laminar sub-layer. The enhanced wall treatment method is optimized for small cell distances near the wall, but can also operate with coarser meshes. It determines by itself whether the grid lays in the viscous sub-layer or the log-law region. When the grid is fine enough it is will use the two-layer zonal mode, here the flow is subdivided into a viscosity-affected region and a fully turbulent region. The viscosity-affected region depends on the one-equation model by Wolfstein [55] and the fully turbulent region by its own turbulence model. To have a smooth transition between these two, a blending function approach is used.

All the turbulence models tested in this section support enhanced near-wall treatment function or make use of a build in near-wall treatment function ($k-\omega$ model), which support meshes with a first cell at $y^+ = 1$.

Simulation settings

Turbulence model

For the simulation of steady flow it was chosen to test three different turbulence models, the $k-\epsilon$ model, the $k-\omega$ model and the Reynolds stress model. The first two models were chosen based on the variation of performance between each other (section 2.6). The RSM model was chosen, because it is a more complex model

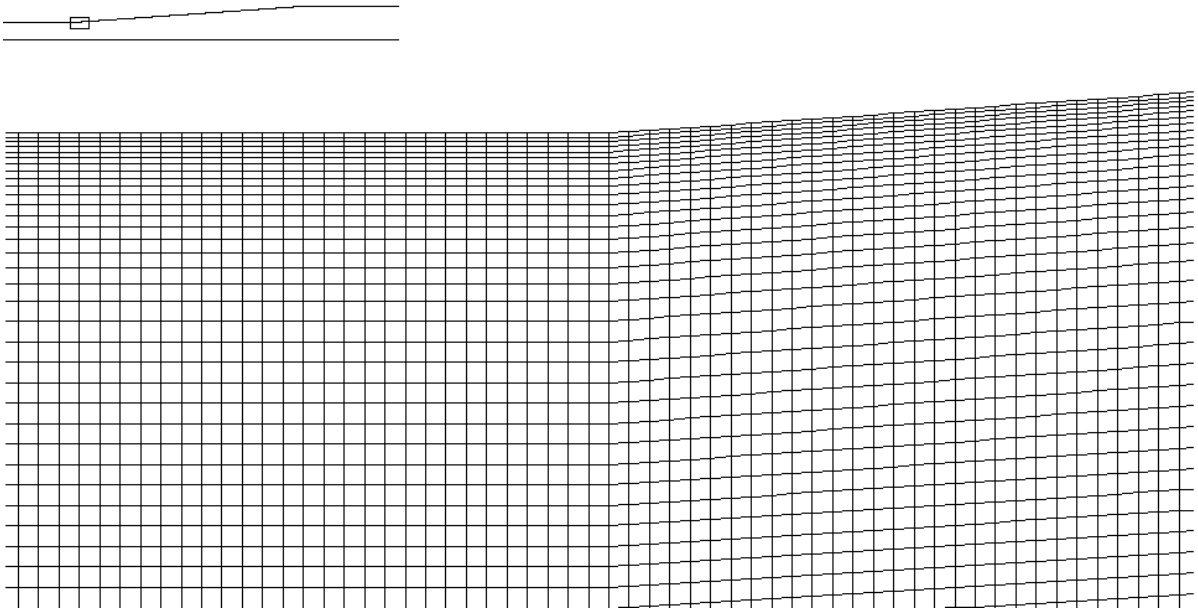

Figure 3.3: An overview of the mesh at the zoomed in section with cell distance 0.5 mm.

as will turn out in this section. The transitional SST and transitional $k-kl-\omega$ models were also considered, but were not able to resolve under steady state circumstances. One possible explanation is unsteady behavior. Another could be that transitional models are sensitive for numerical errors under these circumstances, where the steady state option uses pressure and velocity corrections to calculate the next step.

$k-\epsilon$ model
The first turbulence model that will be discussed is the $k-\epsilon$ model. It is one of the simplest two equation models [1]. The turbulent kinetic energy (k) and turbulent dissipation rate (ϵ) are solved in this model. Which is used for calculating turbulent velocity and length scales. It was proposed by Launder and Spalding [30] and thanks to its robustness, efficiency and reasonable accuracy in for example industrial flows and heat transfer simulations it is used a lot. Over the years enhancements have been proposed, resulting in the RNG $k-\epsilon$ model and the Realizable $k-\epsilon$ model. The main differences between the three models are, (1) how the turbulent viscosity is calculated, (2) the turbulent diffusion of the turbulent kinetic energy and the turbulent dissipation rate and (3) the generation and destruction terms in the turbulent dissipation rate equation. Though it was seen that no big deviations in velocity profiles were produced, independent of whether the Standard, the RNG or the Realizable model was chosen. The turbulent viscosity however would show small differences in profiles at different locations, which will produce different Reynolds shear stresses for example. The $k-\epsilon$ model uses empirical constants which influence the used transport equation and algebraic models. Empirical constants are used for all turbulence models and were left standard.

$k-\omega$ model
The Wilcox $k-\omega$ model [53], which calculates the turbulent kinetic energy (k) and the specific dissipation rate (ω). It has modifications for low-Reynolds-number effects, compressibility, and shear flow spreading [1]. The model performs well for free shear flow spreading inside far wakes, mixing layers, and plane, round and radial jets. Also separation and adverse pressure gradient behavior are modelled better [11]. It therefore can be used for wall-bounded flows and free shear flows.

Reynolds Stress model
The Reynolds stress model (RSM) is a more extensive model. The eddy-viscosity (turbulent viscosity) is replaced by solving transport equations for the Reynolds stresses [1]. The turbulent dissipation rate (ϵ) is used for closing the Reynolds-averaged Navier-Stokes equation. A total of seven additional equations are used to solve the calculations. The RSM model performs better in simulating streamline curvature, swirl, rotation and rapid changes in strain rate than two equation models. This is due to the replacement of the eddy-viscosity, it

therefore has the ability of accounting for directional effects of Reynolds shear stresses (anisotropy). The RSM model is not always superior to models with less transport equations, but when the flow shows anisotropy in the Reynolds stresses it is recommended [1]. For example when stress-induced secondary flow exists in ducts, which is possible in diffusers. As a side note the turbulence can prevent the forming of secondary flow.

Solver settings

The Solver type is chosen to be pressure-based. It is applicable to a wide range of flows ranging from low-speed incompressible flow to high-speed compressible flow [2]. It is chosen to use the segregated algorithm of the solver. It saves memory, but the convergence is slower. The procedure of this solver is as follows:

(1) It will first update the fluid properties, such as density, viscosity, specific heat based on the current solution.
(2) Solving the momentum equations, using values of pressure and mass fluxes.
(3) Solve the pressure correction equation, using the velocity and mass flux.
(4) With the pressure correction the face mass fluxes, pressure and velocity field can be recalculated.
(5) Calculate the additional scalars, such as turbulent quantities, energy, species and radiation intensity.
(6) Check for convergence.

The discretization methods used are given in appendix A, they are also used for the final simulation.

Boundary conditions

The next step is to choose the boundary conditions, which can be found in appendixe A. The boundary at the inlet was set as velocity-inlet and at the outlet as outflow. The turbulence inlet conditions were chosen to be the turbulence intensity and the length scale. The turbulence intensity was chosen based on conditions, where the turbulence intensity is between 1-5% [1] for simple pipe flow. From the article by Alfredsson et al. [5] a value of around 3% was found in the core. The length scale is around 1/10 of the hydraulic diameter [1].

Mesh and residual dependent simulation results

For testing the error induced by the mesh resolution, two meshes as described in section 3.1 with cell distances of 1 mm and 0.5 mm were set up. The simulation settings were set as described in section 3.2.2 and the turbulence model used was the $k-\epsilon$ model with enhanced wall treatment enabled.

Figures 3.4, 3.5, 3.6 show the difference between the obtained results. Residuals of mass, velocity and turbulence variables of $0(10^{-3})$ showed behavior that was not expected when compared to experimental data. Separation appeared and the results were not uniform along the diffuser. Converging the residuals to $0(10^{-6})$ solved the problem. Fig. 3.4 shows almost no difference between the velocity profiles normalized by the mean inlet velocity ($u_{m,in}$) at different locations in the diffuser given by y/R, where R is the radius of the pipe. The mean velocity profile normalized by the friction velocity is shown in 3.5, where $u^+ = \frac{u}{u_\tau}$. The results show a small difference, which is due to the cell size used to determine the wall shear stress at the wall. Since the wall shear stress is equal to $\mu \frac{\partial u}{\partial y_{(y=0)}}$, it is the part $\frac{\partial u}{\partial y}$ which is determined differently. The pressure coefficient along the diffuser axis also shows only a negligible difference, found in fig. 3.6. Therefore it is chosen to use the 1 mm mesh to save computational time. There was also no change seen when letting the residuals of the continuity, velocity or variables dependent on the turbulence model converge to $0(10^{-9})$. Therefore the limit of error for the residuals was set to a number of $0(10^{-6})$.

Validation of simulation results

A comparison is made with the article of Lee et al. [31]. In this article a comprehensive study is done at an incompressible turbulent flow in a conical diffuser with three different opening angles $2\theta = 2°, 4°$ and $8°$. It is done by comparing direct numerical simulation (DNS) data with experimental data. In diffusers it is seen that the flow is wall-bounded and being influenced by an adverse pressure gradient. The diffuser performance can strongly be affected by separation of the boundary layer close to the wall. The boundary layer near the wall, i.e. an organized motion, has a big influence on production and dissipation of wall turbulence. The article investigates this behavior with the goal to improve predictions of turbulent flow in conical diffusers. So that in the future it is possible to use more accurate tools that will help with improving the design of diffusers.

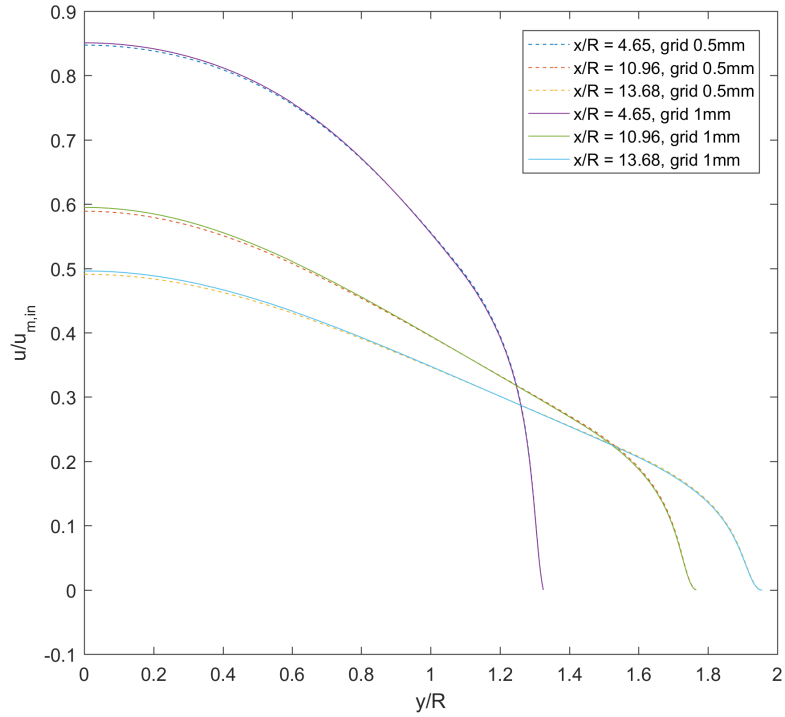

Figure 3.4: Comparison of grid size for the axial velocity distribution at three locations in the conical diffuser

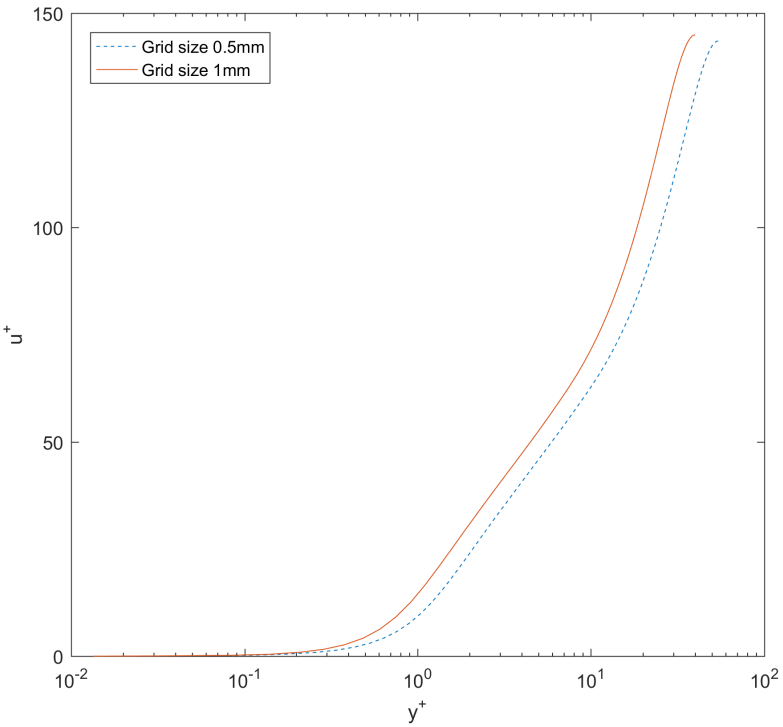

Figure 3.5: Comparison of grid size for the mean velocity profile normalized by the friction velocity at location x/R = 10.96

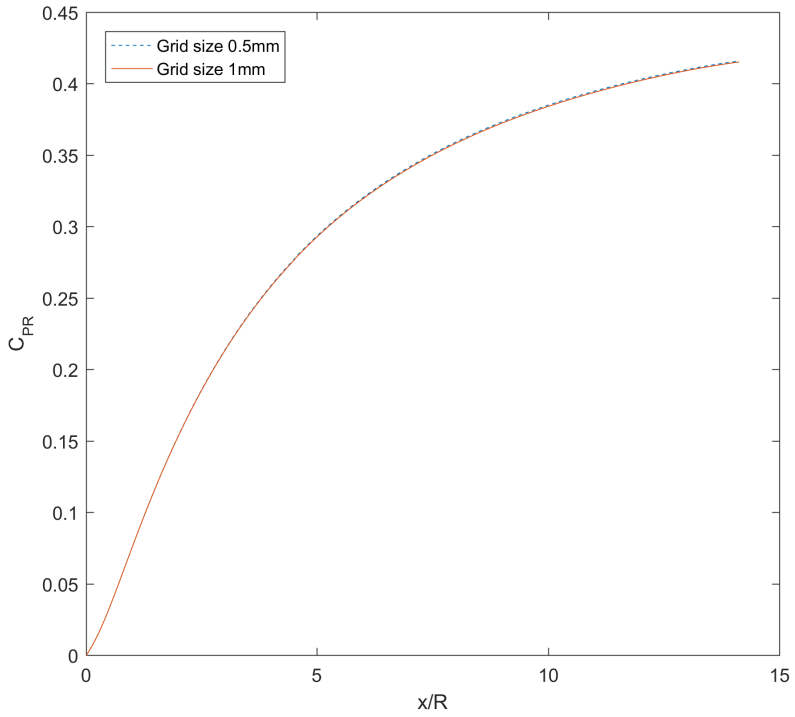

Figure 3.6: Comparison of grid size for the pressure coefficient along the axis of the conical diffuser

Velocity contour plots

The velocity contour plots seen in figs. 3.7 to 3.9 are obtained by the different turbulence models. It can be seen that they all show different patterns. Where the $k-\epsilon$ and the RSM model show almost the same behavior in front of the diffuser as well as inside the diffuser. The $k-\omega$ model shows results that are in better agreement with the results of Lee et al. [31] Compared to the $k-\epsilon$ model it is especially seen that it has a high centerline velocity and as a result tends to go more slowly to a more uniform like velocity field. It also shows a bigger boundary layer in the pipe section. The velocity development in front of the diffuser and all the way to the end of the diffusing part varies in value at different heights, there is a specific big low speed region seen at the corner of the exit of the diffuser. After the diffuser the $k-\epsilon$ and the $k-\omega$ model do not manage to develop as quickly as the RSM model, while the $k-\epsilon$ model shows almost the same contour plot as the RSM model in the expanding area.

The differences between the models can be explained by how the different models approach the problem. Different transport equations and algebraic models are used for finding the solutions. For example both two equation models use simplified algebraic models for calculating influences from for example generation or dissipation of turbulent kinetic energy, where both the $k-\epsilon$ and $k-\omega$ model use different influences. The RSM-model almost uses the same approach as the $k-\epsilon$ model to find the turbulent kinetic energy and turbulent dissipation rate at the boundaries, but uses additional Reynolds stresses to find a far more complete transport equation model outside the boundaries. It incorporates more influences caused by the flow, although some influences need to be modelled and it is seen that for example the generation of turbulent kinetic energy is modelled using the same approach for all three models. Furthermore the same accounts for the $k-\epsilon$ and the RSM model when buoyancy, dilatation dissipation and turbulent viscosity are calculated. It is difficult to predict which equations or models are giving the right values.

Velocity profiles

The comparison of the axial mean velocity profiles divided by the mean inlet velocity, which is denoted as $u_{m,in}$, found in figure 3.10 shows that all simulations show small deviation from the experiments. The DNS and experimental results show a small difference, because a higher Reynolds number is used by the experiments [31]. The DNS results, especially further downstream in the diffuser, are very close to the experimental

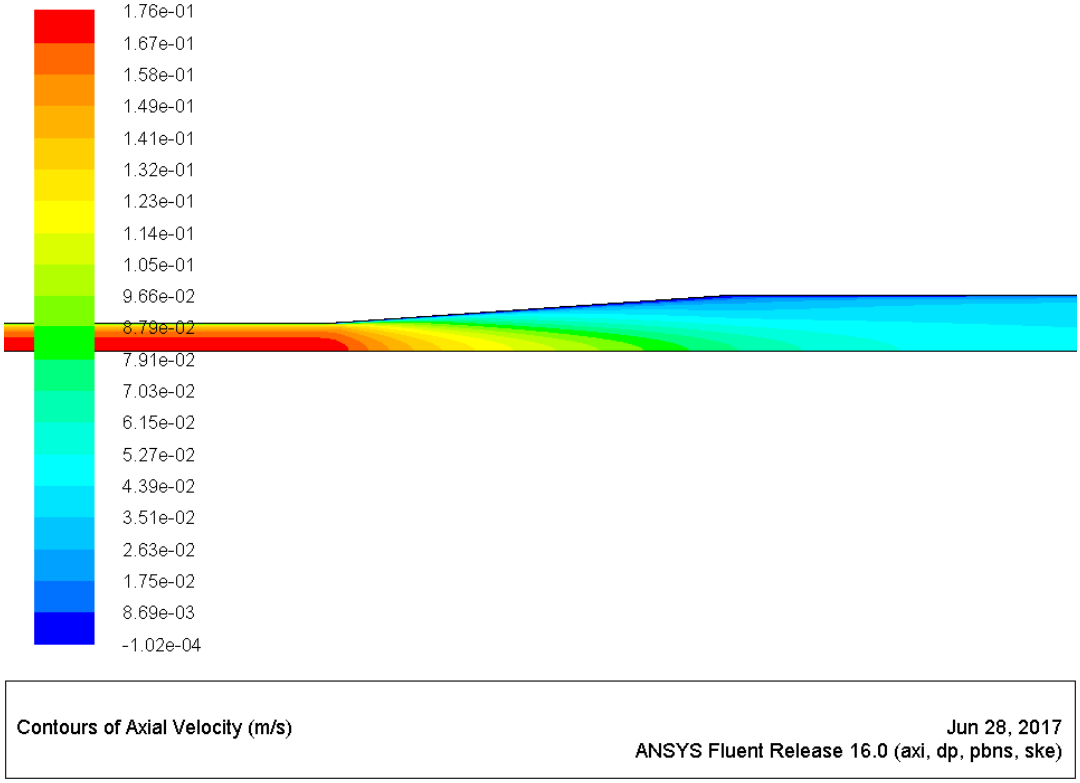

Figure 3.7: Velocity contour plot inside the diffuser for the $k-\epsilon$ model

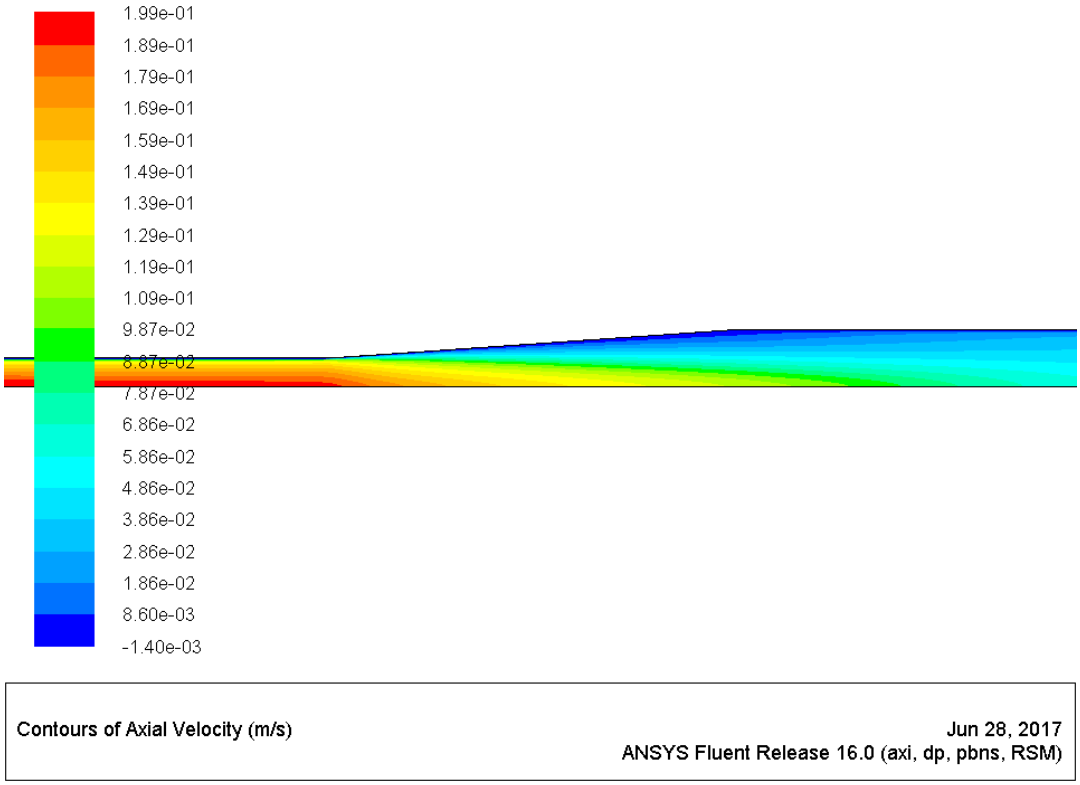

Figure 3.8: Velocity contour plot inside the diffuser for the $k-\omega$ model

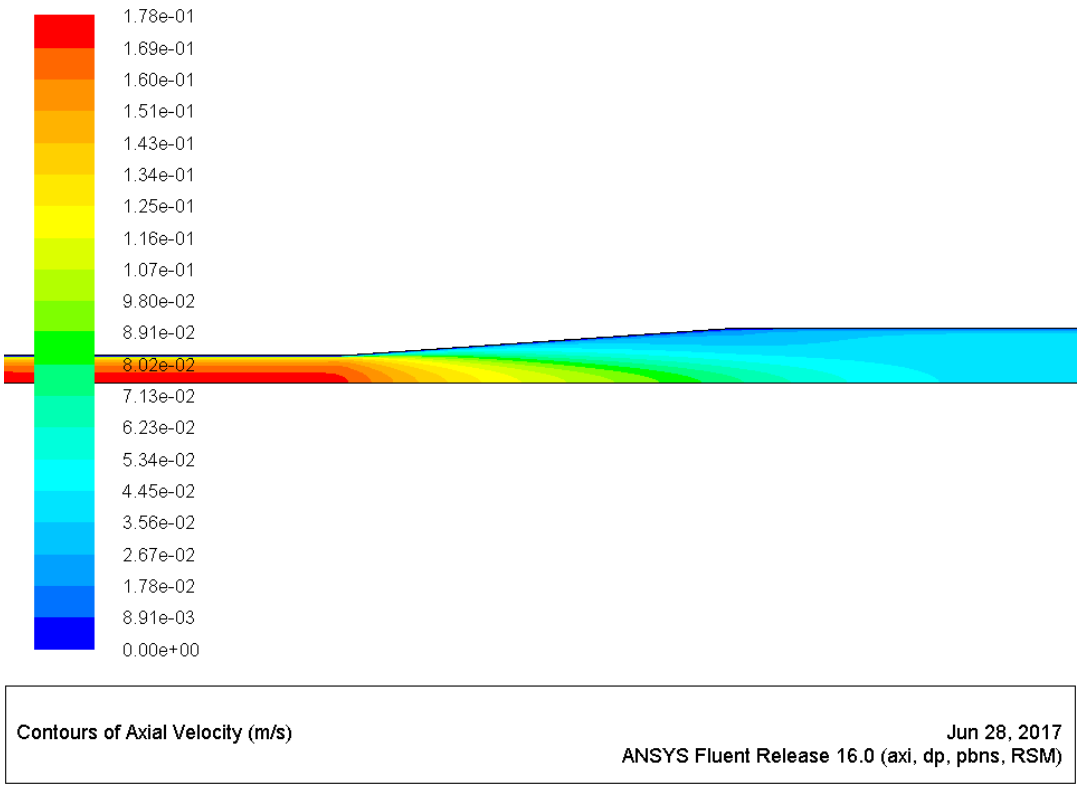

Figure 3.9: Velocity contour plot inside the diffuser for the RSM model

results. The $k-\omega$ is very close to the DNS results, but shows flow reversal close to the wall at $x/R = 10.96$ and $x/R = 13.68$. This behavior is also shown by the $k-\epsilon$ model at $x/R = 13.68$. The RSM model seems to be the most reliable at that aspect, but is deviating quite a lot from the mean velocity profile at all three locations. The $k-\epsilon$ model shows almost the same results as the RSM model. The boundary layer is a complicated region to calculate, because of high gradients, viscous damping in the laminar region and shear forces starting to take over in the buffer region. When this is not modelled correctly it is possible that the flow is also affected further on. The $k-\omega$ model shows that it overestimates the viscous damping, while the other two models are quite accurate. The turbulence near the wall is simulated too weak for the $k-\omega$ model, while it is too strong near the core for the $k-\epsilon$ and RSM model. An increase in turbulence can be seen by velocity profiles, where the profiles will be more flat in the middle and will show smaller boundary layers, this is due to turbulent mixing. The $k-\omega$ model becomes more flat when moving away from the core. The turbulent kinetic energy should be higher, as a result so will be the Reynolds stresses.

In figure 3.11 the mean velocity profiles divided by the friction velocity at three streamwise locations are shown. Here $y^+ = (R(x) - r)\cos\theta u_\tau(x)/\nu$, where $R(x)$ is the local radius of the diffuser and r is the distance from the axis. The profile of the DNS results shows a reduction of the thickness of the log-layer, due to the strong adverse pressure gradient. For a straight pipe the profile maintains the log-law behavior to the center. Near the core the log-layer was enlarged [31]. This was also confirmed by Singh and Azad [41], who noted that the standard law of the wall does not hold for the defined diffuser geometry. The viscous sub-layer, where the linear law holds, is reduced in the downstream direction. When comparing the results of the different turbulence models to the DNS it is seen that due to varying velocity profiles or wall shear stress, the results are not consistent.

Skin frictin coefficient

The skin friction coefficient C_f is shown in fig. 3.12 together with DNS and experimental results, where $C_f = \tau_w/(\rho u_{m,in}^2/2)$. The DNS results are not that accurate in this case. At around $x/R = 1$ the skin friction coefficient shows a drop and a peak afterwards, while this is not seen in the experiment. This can be explained by a separation bubble at the inlet of the diffuser [31]. The $k-\epsilon$ model seems to perform the best,

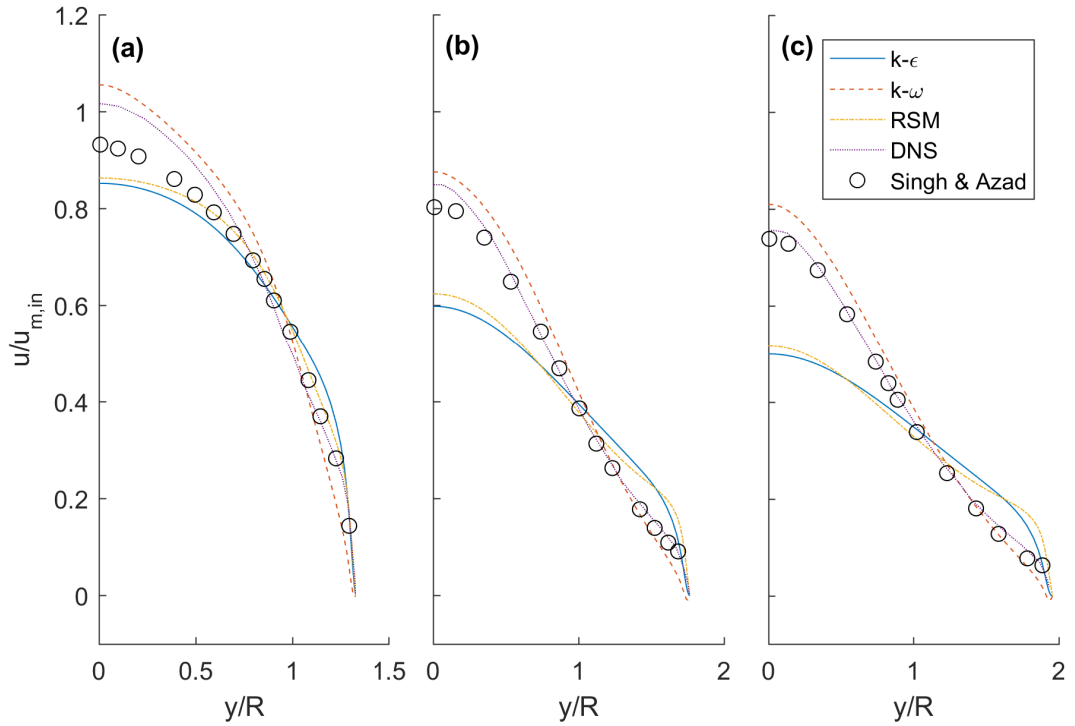

Figure 3.10: Mean velocity profiles for the $k-\epsilon$ model, the $k-\omega$ model, the Reynolds stress model, the DNS [31] and the experimental results of Singh and Azad [41] (a) at $x/R = 4.69$, (b) at $x/R = 10.96$ and (c) at $x/R = 13.68$.

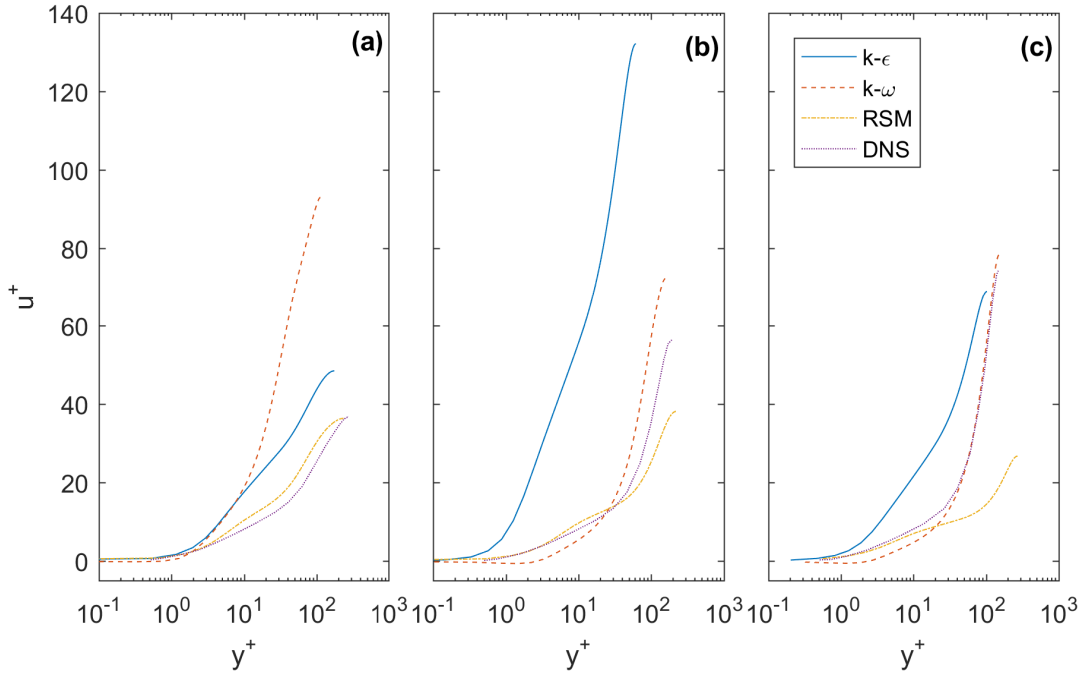

Figure 3.11: The mean velocity profiles normalized by the friction velocity along y^+ for the $k-\epsilon$ model, the $k-\omega$ model, the Reynolds stress model and the DNS [31] (a) at $x/R = 4.65$ and (b) at $x/R = 10.96$ and at (c) $x/R = 13.68$.

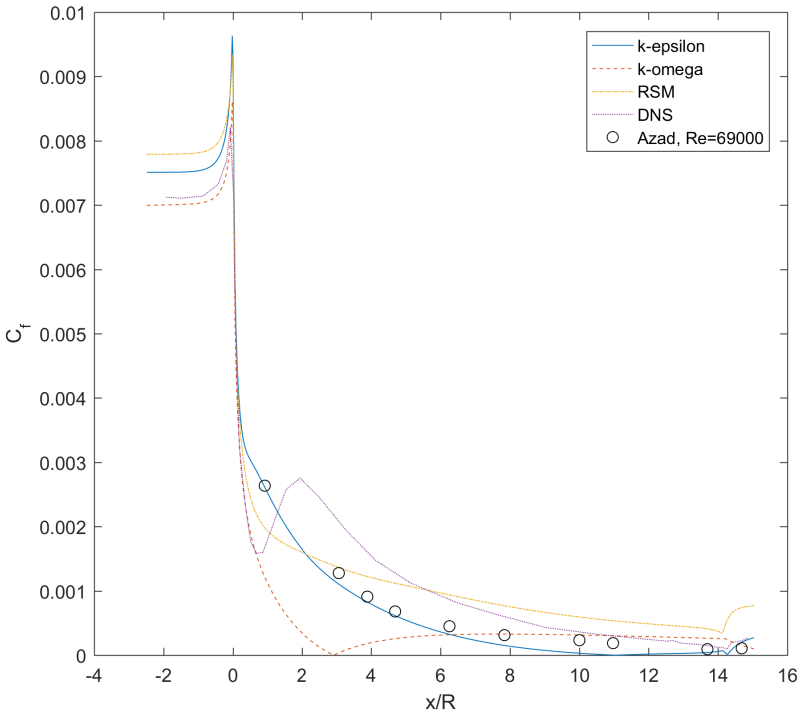

Figure 3.12: Skin friction coefficient for the $k-\epsilon$ model, the $k-\omega$ model, the Reynolds stress model, the DNS [31] and the experimental results of Singh and Azad [41].

but at $x/R \approx 11$ the value goes to zero, indicating flow reversal. This also happens for the $k-\omega$ model, but at $x/R \approx 3$. The RSM model shows values, which are after $x/R = 5$ around a factor 2 higher when compared to the experimental results. For all models the results are deviating, but the flow reversal of the $k-\epsilon$ and the $k-\omega$ model causes problems.

Pressure coefficient

As can be seen from figure 3.13 the C_p values predicted by the turbulence model are a good representation of the expected values, where $C_p = (p_{w(x)} - p_{w,in})/(\rho u_{m,in}^2/2)$, $p_{w(x)}$ gives the local wall pressure at coordinate x and $p_{w,in}$ is the wall pressure at the inlet of the diffuser. The quick increase of C_p at the beginning of the diffuser implies a strong adverse pressure gradient, where it gets weaker along the x-axis. The results of the DNS model are almost corresponding to the experimental results of Azad [8]. The $k-\omega$ shows almost the same values as the DNS model, whereas the $k-\epsilon$ model and the RSM model under predict the pressure losses.

Turbulence intensity

The turbulence intensity is a measure for the amount of turbulence that exists in the stream and is plotted in figure 3.14. The figure shows the fluctuating velocity normalized by the mean inlet velocity versus the local radial distance (1 - y/R(x)) for the different turbulence models and the DNS. The turbulence intensity is given by $TI = \frac{u'}{u_{m,in}}$, where u' is the fluctuating velocity. The fluctuating velocity can be converted into turbulent kinetic energy by $k = \frac{1}{2}\left(u_x'^2 + u_y'^2 + u_z'^2\right)$, the subscripts x,y and z stand for their corresponding directions. The turbulence intensities reach a maximum value in the outer region of the adverse pressure gradient turbulent boundary layer. For straight pipe flow the maximum value is found in the buffer layer [31]. As the flow progresses through the diffuser, the maximum value advances to the diffuser's axis. The decrease near the wall can be explained by damping by viscous effects near the wall. As already was expected the $k-\omega$ model shows low turbulence near the centerline. What is unexpected is that the DNS begins to show higher amounts of turbulence in this region as the stream progresses downstream through the diffuser. The difference has smaller influence on the flow development as the gradients are smaller in this region. The $k-\epsilon$ and the RSM model

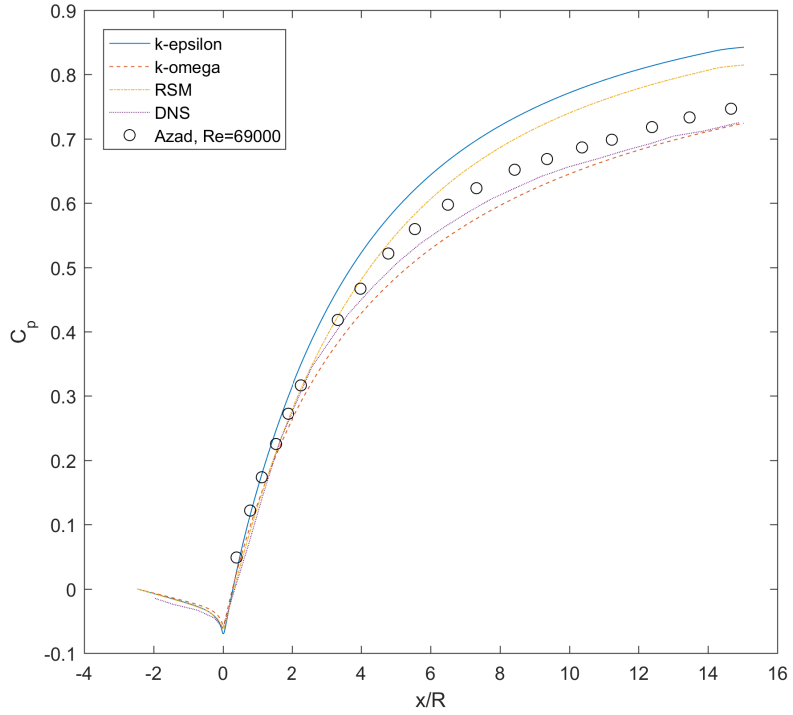

Figure 3.13: Comparison of the pressure coefficient between the $k-\epsilon$ model, the $k-\omega$ model, the Reynolds stress model, the DNS [31] and the experimental results of Azad [8]

show relative high turbulence near the center of the diffuser until around the end of the diffuser, at that moment the DNS transcends below the turbulence models. Both the $k-\epsilon$ and the RSM model show a decreasing amount of turbulence between the center and the wall, while the $k-\omega$ model and DNS show an increase. Probably because the $k-\omega$ model constantly lies closer to the DNS values and behavior, therefor the development of the flow is better modelled. It is also an effect of continuity, since the flow was already developed in the right direction.

Reynolds shear stresses

The Reynolds shear stresses give a good impression of how much turbulent energy or momentum is distributed. In figure 3.15 of the Reynolds shear stresses normalized by the mean inlet velocity at three locations throughout the diffuser are shown. For the two-equation models in Fluent, the equation used to compute the Reynolds shear stresses is the Boussinesq approximation:

$$-\rho\overline{u_i' u_j'} = \nu_t\left(\frac{\partial u_i}{\partial x_j}+\frac{\partial u_j}{\partial x_i}\right)-\frac{2}{3}\rho k\delta_{ij} \tag{3.1}$$

Where k is the turbulent kinetic energy, ν_t is the turbulent viscosity and δ_{ij} is the Kronecker delta. From the equation it follows that only the turbulent viscosity and velocity gradients are important. The turbulent viscosity is dependent on the amount of turbulent kinetic energy. The RSM-model uses a transport equation to compute the Reynolds shear stresses. From the figure it can be seen that the profiles show the same behavior as for the turbulence intensity profiles. The $k-\omega$ model now shows values which are close to the DNS results. It gives a good explanation why the velocity profiles are in good agreement, since the Reynolds-averaged Navier-Stokes (RANS) equations only use the turbulent variables $u_i' u_j'$ for completing its equations. The RSM model shows values which in the beginning of the diffuser are too high and at the end of the diffuser are too low. The $k-\epsilon$ model is in the first section correct, but afterwards it predicts the values too low. The spread of momentum of the turbulence is therefor too low. This can be coupled to the turbulent kinetic energy, since the turbulent dissipation rate is negligible.

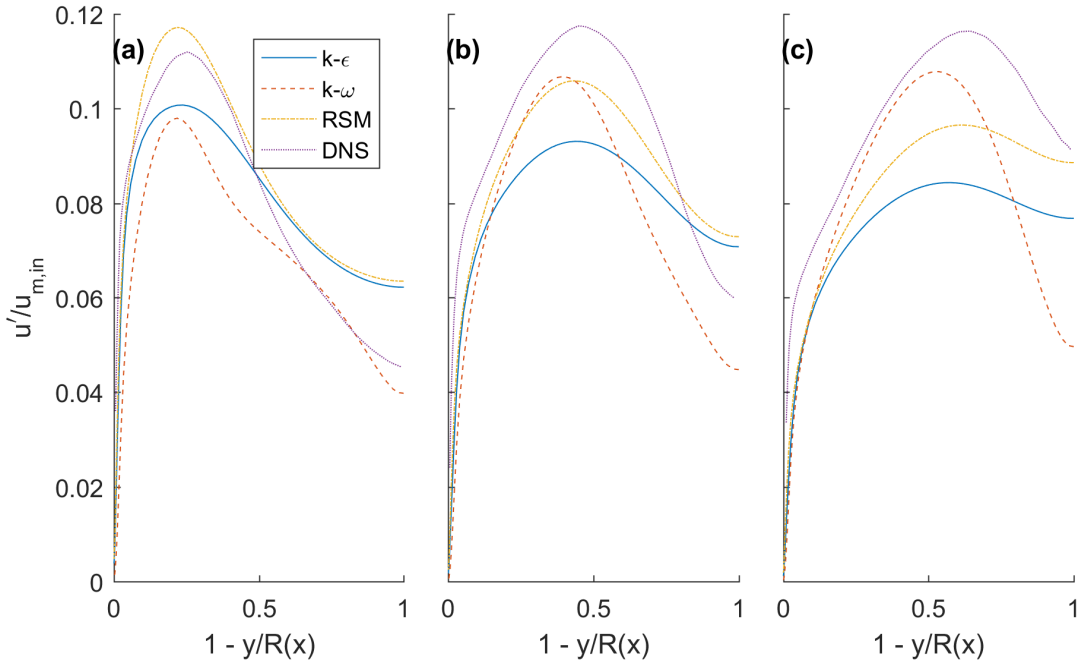

Figure 3.14: The turbulence intensity profiles of the different models at three streamwise locations (a) at $x/R = 4.69$, (b) at $x/R = 9.54$ and (c) at $x/R = 14.41$

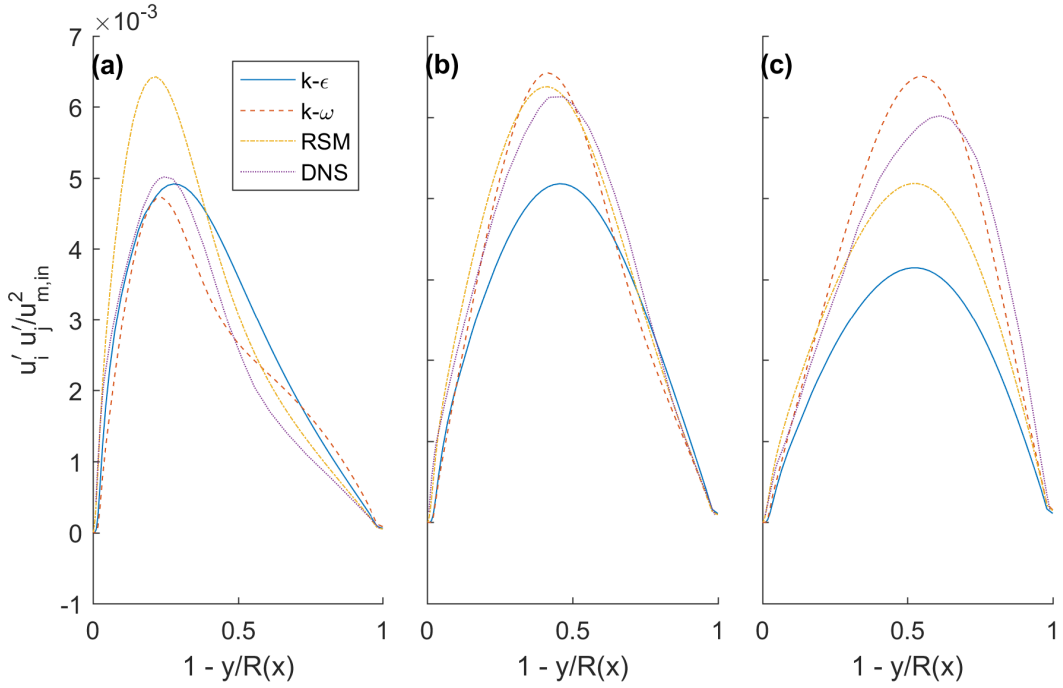

Figure 3.15: The Reynolds shear stress profiles of the different models and DNS [31] at three streamwise locations (a) at $x/R = 4.69$, (b) at $x/R = 9.54$ and (c) at $x/R = 14.41$

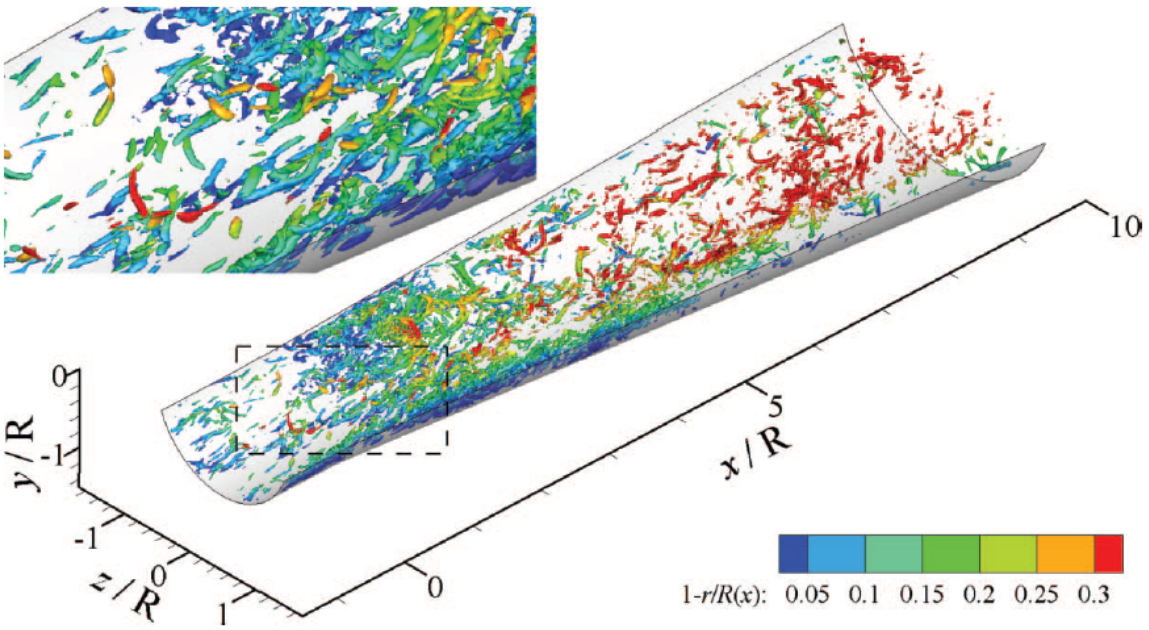

Figure 3.16: Vortical structures of the DNS [31] with 20% of the maximum swirl length. The colors indicate the distance from the wall.

Vorticity

When comparing vorticity structures produced by the DNS and the $k-\omega$ model (fig. 3.16, 3.17) it is observed that Fluent models the problem, while the DNS calculates it directly. The structures are not seen in the velocity vector field of Fluent, which indicates it is based on an algebraic model. The same is found for velocity fluctuations, which is caused by the use of average velocities introduced by the RANS equations used by Ansys Fluent. When comparing the figures, the $k-\omega$ model seems to predicts the magnitude of vorticity, which is high at the inlet and gets lower throughout the diffuser.

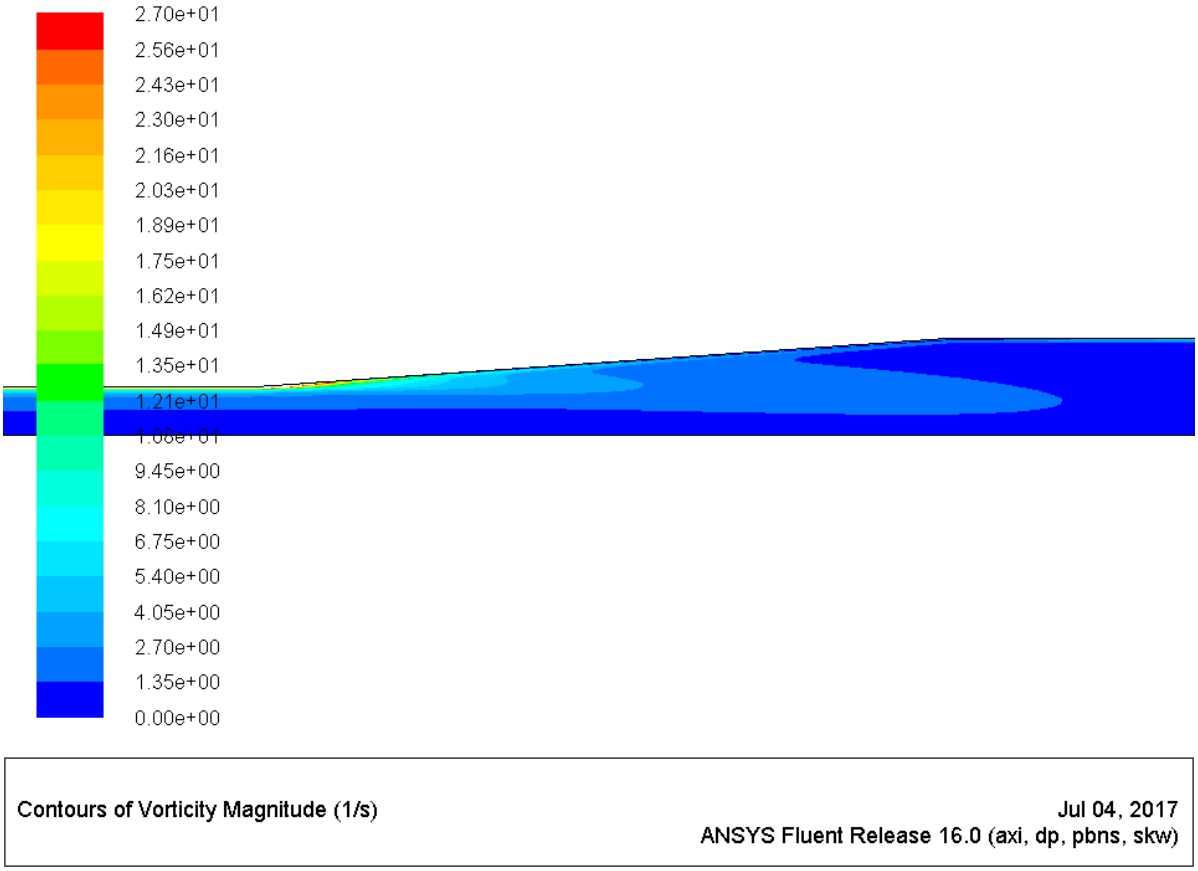

Figure 3.17: Vorticity magnitude (1/s) produced by the $k-\omega$ model

4

Simulation of oscillating flow in a diffuser

In this chapter an oscillating flow in a diffuser is studied. For oscillating flow a difference is seen between laminar flow, disturbed laminar flow, intermittently turbulent flow and turbulent flow. All conditions will start at a certain Re_δ number, the Re_δ numbers that will be investigated in this chapter are 380, 580 and 740 with varying displacement amplitudes. The simulations in this chapter will be compared to the results of King and Smith [27]. The geometry that is used is a $2\theta = 30°$ rectangular diffuser. In Ansys Fluent v16.0 it will be modelled as a symmetric 2D plane flow. The turbulence models investigated are the $k-kl-\omega$ and $k-\omega$ SST model.

Oscillating flow can be quite complex as flow in the experiments by King and Smith [27] oscillate with a frequency of 8-28 Hz, this will create a fluid which moves quickly. A difference can be made between turbulence and separation. Where separation is expected to only exist in the diffusing part and already starts at a diffuser angle of 12° [27]. The turbulence is expected to be dependent on flow characteristics in the accelerating phase, decelerating phase or both phases of the cycle [35]. The displacement amplitude will have influence on the point of separation, where a bigger amplitude causes earlier separation [27]. The flow will also never be fully developed and can create different shapes of velocity profiles, because of difference in Wombersley number and turbulence.

A difference in results of simulation and experiment will be expected as was seen in previous chapter. Probably it will deviate more, because of the more complex flow. It should be taken into account that depending on the position of the cycle laminar flow is simulated, care should be taken with choosing the right turbulence model as they are not designed for laminar flow. Strong curvatures will also have an important role. The results of previous chapter were for a steady flow, so the conclusion made in that chapter concerning the turbulence model may not correspond to the performance of oscillating flows. A new choice was made regarding the turbulence model.

Mesh setup

Geometry and grid size

The geometry of the mesh is based on the geometry used in the thesis and article by King [26], King and Smith [27] respectively. The geometry used is seen in figure 4.1 and the enclosed section gives the part of the geometry which is used for the mesh. In figure 4.2 the diffuser itself is shown with accompanying location coordinates.

It is a rectangular diffuser with a depth of 15.4 cm and at the start of the diffuser a width of 1.66 cm and at the end 6.67 cm. In the enclosed section of the figure it can be seen that the removable test section consists of the diffuser, which is placed inside a bigger channel. This will force the flow to go from a big surface area to a smaller one, when entering the channel in front of the diffuser. This should not have effect on the development of the flow [27]. The corners of the entrances are rounded so that a negligible pressure loss will occur [51], additionally it will reduce entrance effects as much as possible. The mesh based on the geometry is started from the middle of the first speaker from the inlet, which is seen as reference point for the inlet. From that point the development of the flow will not be influenced from external additions. It was chosen not to extend the diffuser at both entrances as was done in previous chapter, this in accordance with literature. The

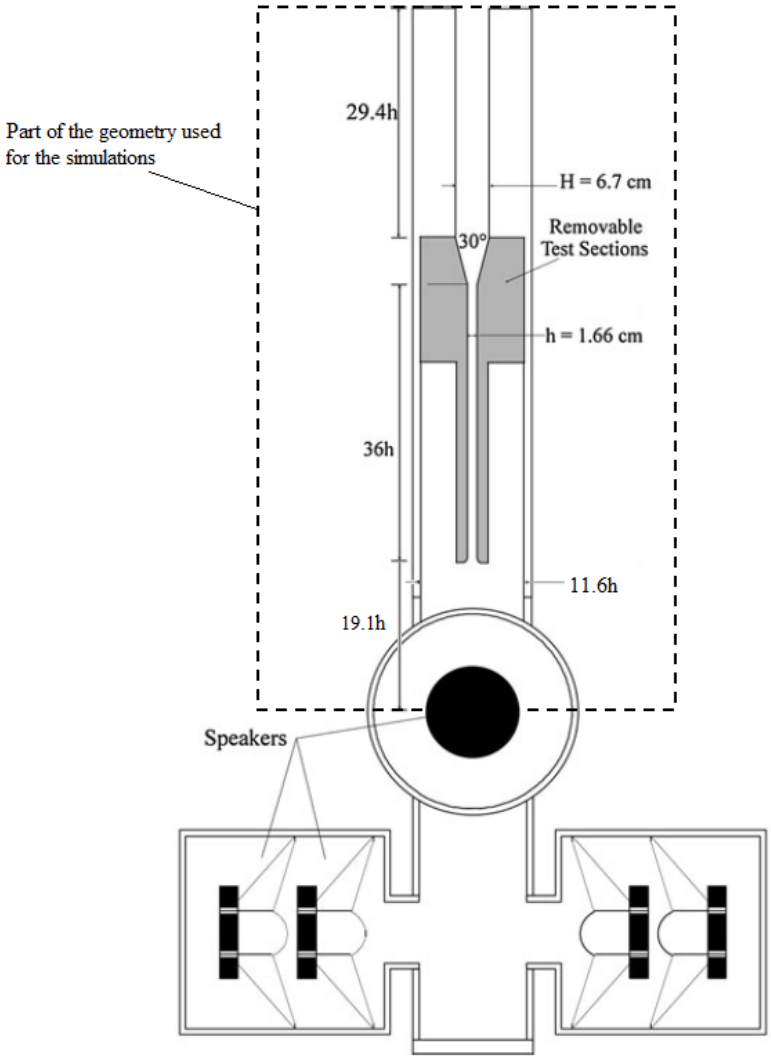

Figure 4.1: Diffuser geometry used for simulating an oscillating flow. The enclosed part of the geometry focusses on the geometry which will be used in the simulations.

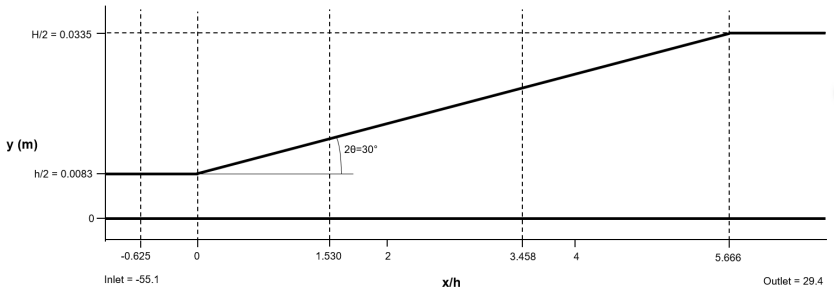

Figure 4.2: Diffuser geometry in detail used for simulating an oscillating flow with on the x-axis the distance normalized by its channel width.

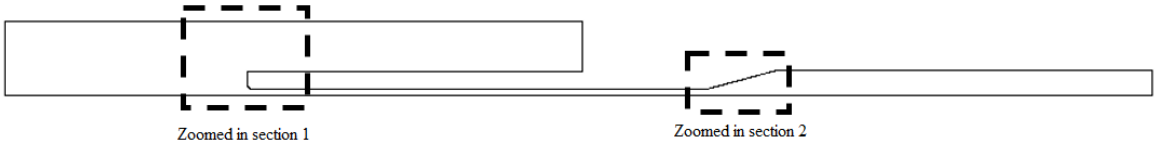

Figure 4.3: The geometry used in Ansys Fluent and build with Gambit, zoomed in sections are found in figures 4.4,4.5

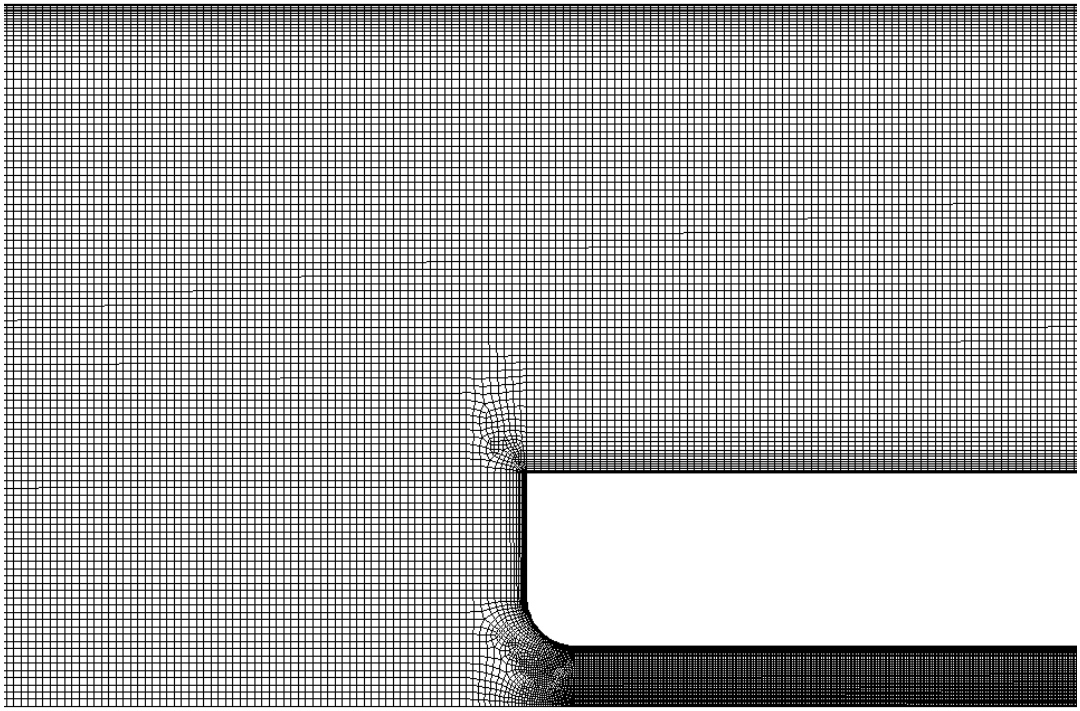

Figure 4.4: The mesh at the transition from the wide channel to the entrance of the channel in front of the diffuser

results should point out whether this has influence. It could be more realistic since the flow has the same length to develop as the experiment.

The diffuser with an angle of 30° was chosen as the preferred geometry. Compared to angles of 20° and 12°, the flow will separate earlier. Counter rotating vortex pairs can occur, which causes reattachment. The flow than remains attached for the rest of the blowing cycle. Effects of separation for the 30° angle are bigger and will therefore show more interesting results.

The grid for the final simulations consists of 105 cells over the width of the inlet and 47 cells over the width of the channel in front of and after the diffuser. In chapter 3 it was found this should give accurate results. Skin friction coefficients to determine the wall shear stress are not available for this range of stroke length and kinetic Reynolds number [56]. The smallest first row of the boundary layer is set at $7.7(10^{-6})$ m in the channel in front of the diffusing section to maintain a $y^+ = 1$ at the maximum velocity of the cycle, this was also maintained for the other sections. The boundary layers consist of 20 rows with a growth factor chosen such that the last row fits well to the entire mesh. An overview of the geometry and zoomed in at sections of the mesh can be found in figures 4.3, 4.4,4.5.

Convergence

All the turbulence models have difficulty to simulate an oscillating flow at $Re_\delta = 740$ and $L0/h = 31$. It was not possible to converge with residuals for mass, velocity, turbulent kinetic energy and turbulent dissipation set at $0(10^{-4})$. For the turbulence models it wasn't enough to reduce the time step to $\frac{T}{1000}$, T is the time of one cycle, or lower to solve the problem. Different cell distances were tested with the idea of finding better convergence.

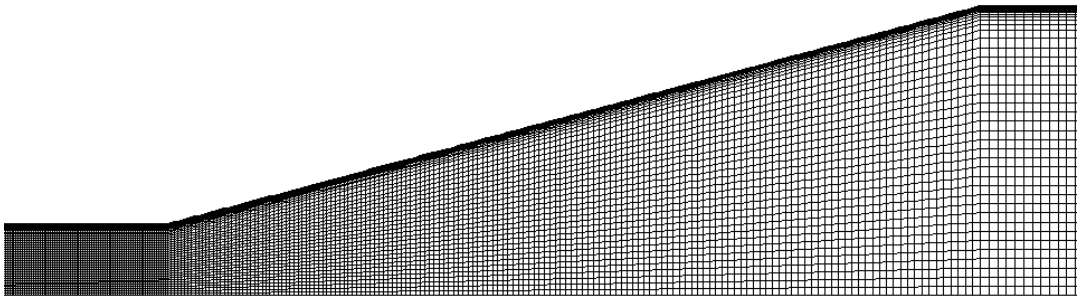

Figure 4.5: The mesh of the diffuser

It was thought a finer mesh would create less difficulty in calculating flow characteristics, such as eddies, which will create smaller steps for differentials and creating smaller errors. This enables the possibility to capture the change in motion more accurately. A coarser mesh could also improve the calculations, because the calculations of phenomena in the flow will not have to be calculated in detail. It was chosen to model the mesh with different cell distances found in appendix A. All models didn't show improvement in convergence.

When the residuals were set higher it was found that it causes a divergence error of momentum in the second cycle for all turbulence models. Therefore it was chosen to only model the diffuser itself, using the same lengths as in the experimental setup from the speaker to the end. The small inlet channel in front of the diffuser was extended to meet the same length, so the flow is not directly influenced by the flat pressure profile, the geometry is shown in fig. 4.6. The point where the flow is forced to go from a wide area to a smaller area will cause certain effects in the more complex model, like compression and mixing. The flow flows in from a different angle and will mix to a certain degree. Because of the length of the pipe in front of the diffuser this effect will not be seen in the diffuser. Also compressibility seems negligible. Both cases were validated and found to be true. The velocity profiles in front of the diffuser for both geometries were identical. It was found that the pressure needed at the inlet to reach certain speeds was for the simple model higher, this is caused by friction losses due to the increased length of the smaller channel. The friction losses are higher, because of the higher velocity and smaller surface area.

The convergence problems were still present using the simple geometry. The problem of convergence disappeared when pressure and velocity waves had settled in their behavior. Where the velocity reaches a higher amplitude in the first cycles and is around $0.25 \cdot T$ behind the pressure when settled. The result was that the $k-kl-\omega$ model was able to converge to residuals of continuity, velocity, energy and turbulence parameters of $0(10^{-6})$, which is accurate enough as seen in section 3.

Simulation settings

Turbulence model

For the oscillating flow the $k-kl-\omega$ model was used as turbulence model, as it seemed the most favourable found in section 2.6. The $k-\omega$ SST model was also add to the comparison afterwards. Both models are based

Figure 4.6: The final more simple geometry used in Ansys Fluent and build with Gambit

on the $k-\omega$ model, but have their own adjustments. The $k-\omega$ SST model still uses two transport equations, while the $k-kl-\omega$ model adds a third transport equation. The laminar kinetic energy k_l is added, which are small oscillations in the flow.

Solver settings

Again the solver type was set to Pressure-Based. This time the coupled solver was chosen, because it should have superior performance over the segregated solver [2]. For the coupled solver mass and momentum are solved simultaneously. The Density-Based solver could give an improvement, because it can have beneficial effects on compressible high speed flow. The density is used to solve the continuity and momentum equations and the pressure is calculated from an equation of state. Because the density is an important variable for compressible effects it can be more accurate. It is stated that the Density-Based solver especially outperforms the Pressure-Based solver on cases with high speed compressible flow combustion, hypersonic flows and shock interactions, which are not the case. As a side note the Density-Based solver wasn't able to converge. The used solution methods can be found in appendix A.2.

Boundary conditions

The used boundary conditions will be discussed and can be found in appendix A.2. However influences from the boundary conditions are dampened in all cases, since the displacement amplitudes will be smaller than the entrance length of the pipe. The inlet was set to pressure-outlet, because it also functions as an outlet for the oscillating flow. Here only the static pressure is needed. When choosing pressure-inlet as boundary condition the dynamic pressure is needed. This is a lot harder to define, since it is dependent on the velocity. As was the case for the steady flow in previous chapter, the turbulence intensity and length scale were chosen as the turbulent boundary conditions. Due to the turbulence model chosen ($k-kl-\omega$) also the laminar kinetic energy needs to be defined at the boundaries. In the article of Furst [19] it is found that the laminar kinetic energy is the amount of large-scale turbulence, it is given by $k_l = k - k_s$, where k_s is the amount of small scale kinetic energy. In this model small-scale turbulence is expected instead of large-scale turbulence, it therefore was set to 0 m^2/s^2.

When comparing the turbulence intensity at the center line of a pipe flow between time-averaged oscillating flow and steady flow it was found to have almost identical values, it would only be smaller for the oscillating flow in the Stokes layer [37]. For turbulent flow the turbulence intensity was therefore chosen to be 3%. Transitional flow tends to have a higher turbulence intensity ranging from 0.2%-12% [15], for this case it was assumed to be 6%. The turbulence intensity of the laminar flow was set to 0.2%.

The turbulence length scale used for turbulent cases will be based on parameters provided by the Fluent manual [2]. The turbulent length scale is 7% of the width of the hydraulic diameter. For the transitional case it was calculated with the following formulas [3]. The turbulence length scale is based on the turbulent dissipation and turbulent kinetic energy.

$$l = \frac{k^{\frac{2}{3}}}{\epsilon} \tag{4.1}$$

Here l is the turbulence length scale. The turbulent kinetic energy is calculated with the turbulence intensity and maximal velocity, assuming isotropic turbulence.

$$k = \frac{3}{2}(TI \cdot u_{max})^2 \tag{4.2}$$

The turbulence intensity is given by TI. Finally the turbulent dissipation is calculated from the Reynolds number and turbulent kinetic energy.

$$\epsilon = \frac{1}{Re_{max}} \frac{k^2}{\nu} \tag{4.3}$$

The maximum Reynolds number is calculated from the maximum velocity during a cycle. From the calculations it followed that, under transitional circumstances, the turbulent length scale would be around 12.4% of the width. For laminar flow it was chosen to use the viscosity ratio instead of the turbulent length scale for the boundary conditions. The viscosity ratio was set to 0.01, to create a laminar flow.

Validation of simulation results

The results of the simulations were compared to the experimental results by King [26]. A good comparison can be made between the experiments and the simulation results. Different cases are studied to find patterns in performance behavior when doing simulations.

Velocity profiles

In fig. 4.7 the phase-averaged velocity profiles over 5 cycles are shown in front of the diffuser ($x/h = -0.625$) for different Re_δ numbers and dimensionless displacement amplitudes during the acceleration of the blowing part of the cycle. Only the blowing part was studied, since separation will occur in this part of the cycle. The results show good similarity, but there is almost no change in momentum noticed near the wall when turbulence is introduced. This can be seen in the experiments resulting in an overall flatter line. The mixing properties of turbulence causes the low momentum boundary layer to keep more in pace with the high momentum bulk flow, as is the case for $Re_\delta = 580$ and 740 at $t/T = 0.97$, the viscous damping is less prominent. For the acceleration part of the cycle the results are in good correspondence. Also for $t/T = 0.97$, where the flow is still decelerating.

A simulation was done with the same higher speed and frequency as used by King and Smith [27], resulting in $Re_\delta = 856$ and $L0/h = 31$ to see how the results would compare. It showed at $t/T = 0.03$ the velocity profile is a little bit more flat in the middle, as would be expected when comparing it with the experimental case.

The phase-averaged velocity profiles are shown in fig. 4.8 for the deceleration part of the blowing part of the cycle. The boundary layers of the experiments and the simulation show good similarity for all three cases. For $Re_\delta = 740$ and $L0/h = 31$ and $Re_\delta = 580$ and $L0/h = 30$. The bulk flow of the simulation starts to lag behind the experiments from $t/T = 0.31$. It shows viscous damping is more prominent than the turbulence caused by the turbulent viscosity. At $Re_\delta = 380$ and $L0/h = 20$ the velocity also lags behind the experimental results, but the difference is smaller. The low momentum boundary layer leads the high momentum bulk flow when getting closer to the point of zero velocity. In section 2 it was mentioned that the profile shape is also dependent on Wombersley number, a dimensionless number which gives a relation between frequency and viscous effects. The Wombersley numbers for the first case is 26.5, the second case is 27.0 and for the third case it is 33.3. The difference in Wombersley number between the cases shouldn't have big consequences.

Under the circumstances of $Re_\delta = 856$ and $L0/h = 31$ it shows the simulation still does not simulate the turbulence well, there is almost no difference compared to $Re_\delta = 740$ and $L0/h = 31$. Comparing the boundary layers between the experiment and the simulation at the same velocity and frequency shows a steeper profile for the simulation results, which is caused by higher inertial forces compared to viscous forces. The Reynolds shear stresses will be bigger in this case.

The decision was made to run a few cases with the $k-\omega$ SST mode, to see if similar results are found. The velocity profile (fig. 4.9) shows a steeper boundary layer, which indicates viscous damping is smaller. Also more turbulent mixing is simulated. However the change in velocity during the cycle still lags behind the experiments, though it is smaller. It is possible that this is caused by a difference in influence of the pressure gradient on the velocity gradients, which can be caused by viscous forces and Reynolds stresses not modelled correctly. For example it can be caused by the effects of separation or the amount of turbulence, due to the amount of turbulent kinetic energy and value of turbulent viscosity.

From the phase-averaged velocity profiles in the expanding area of the diffuser obtained from both turbulence models and shown in figure 4.10, it can be observed that the amount of separation influences the core velocity. The $k-\omega$ SST model constantly has a higher core velocity when compared to the $k-kl-\omega$ model, at $x/h = 3.458$ the speed is even higher than at the entrance of the diffuser. When the separation is not present, at $t/T = 0.97$ and $t/T = 0.08$, the flow profiles are almost identical.

Velocity vector field

The velocity vector field at different phases of the cycle are found in figure 4.11, 4.13, 4.13 for $Re_\delta = 580$ and $L0/h = 26$. The two turbulence models differ in the amount and behavior of separation showing up. Where the $k-kl-\omega$ model performs a better job in simulating the distance of the center of the vortex from the wall.

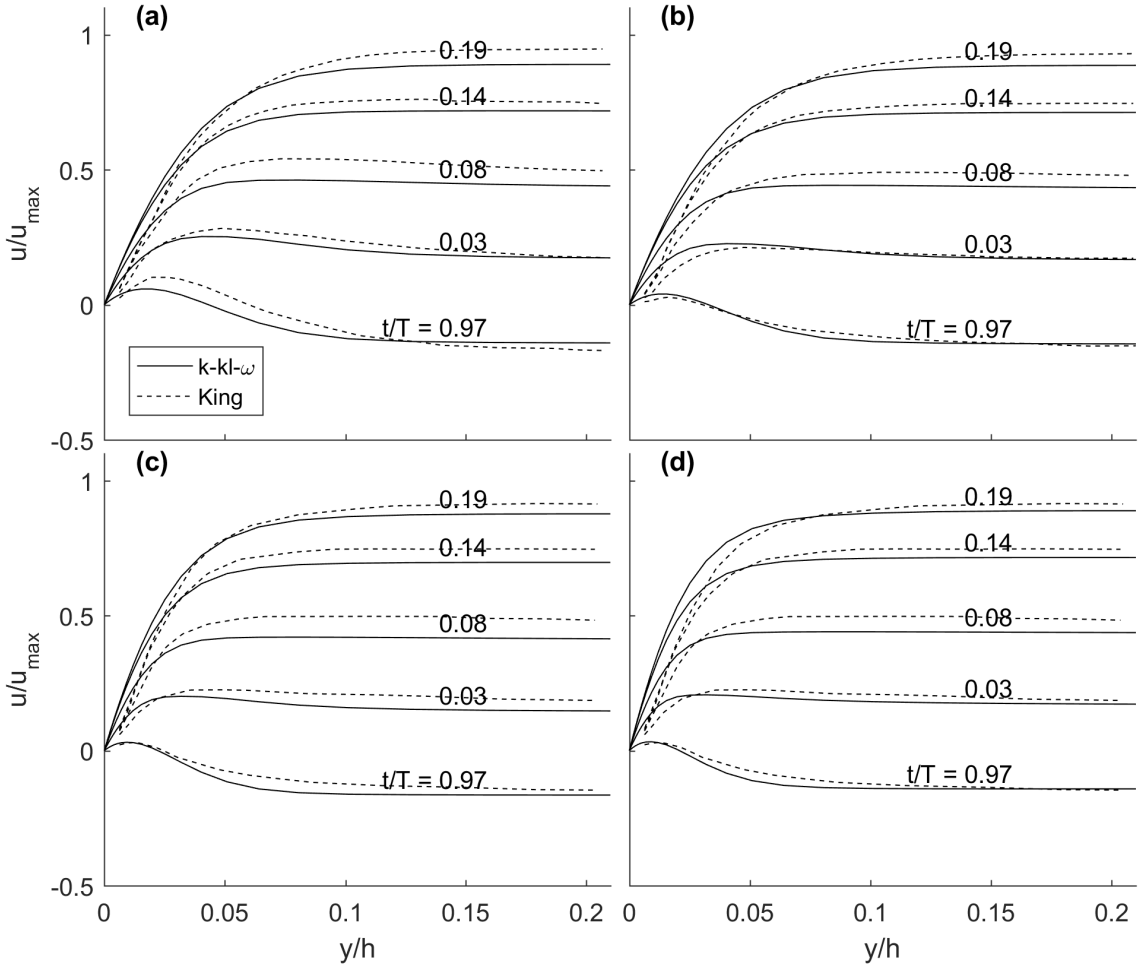

Figure 4.7: Phase-averaged streamwise velocity profiles at $x/h = -0.625$ of the $k-kl-\omega$ model compared with experiments by King and Smith [27] for (a) $Re_\delta = 380$ and $L0/h = 20$, (b) $Re_\delta = 580$ and $L0/h = 30$, (c) $Re_\delta = 740$ and $L0/h = 31$ and (d)$Re_\delta = 856$ and $L0/h = 31$ compared with $Re_\delta = 740$ and $L0/h = 31$

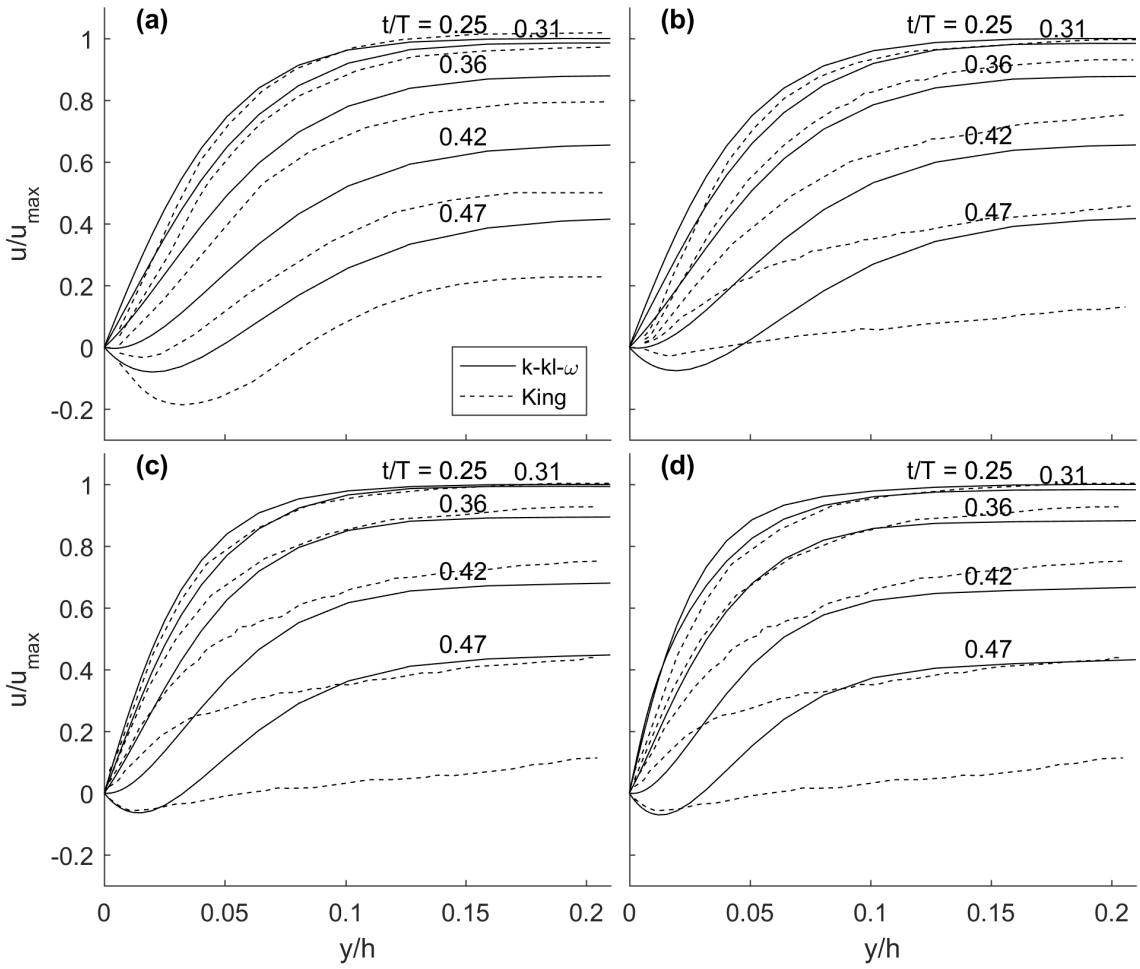

Figure 4.8: Phase-averaged streamwise velocity profiles at $x/h = -0.625$ of the $k-kl-\omega$ model compared with experiments by King and Smith [27] for (a) acceleration at $Re_\delta = 580$ and $L0/h = 30$, (b) acceleration at $Re_\delta = 740$ and $L0/h = 31$, (c) deceleration at $Re_\delta = 580$ and $L0/h = 30$ and (d) deceleration at $Re_\delta = 740$ and $L0/h = 31$

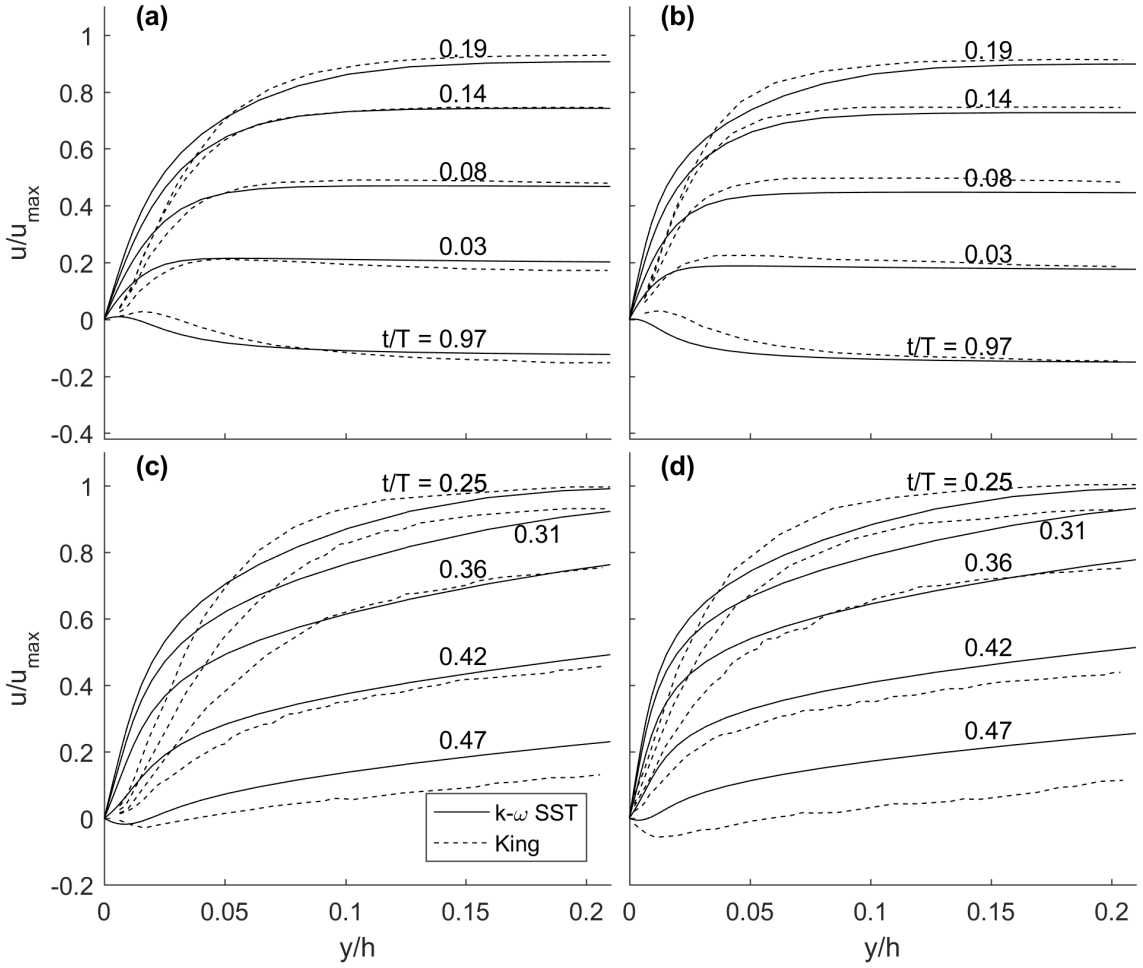

Figure 4.9: Phase-averaged streamwise velocity profiles at $x/h = -0.625$ of the $k-\omega$ SST model compared with experiments by King and Smith [27] for (a) $Re_\delta = 580$ and $L0/h = 30$, (b) $Re_\delta = 740$ and $L0/h = 31$

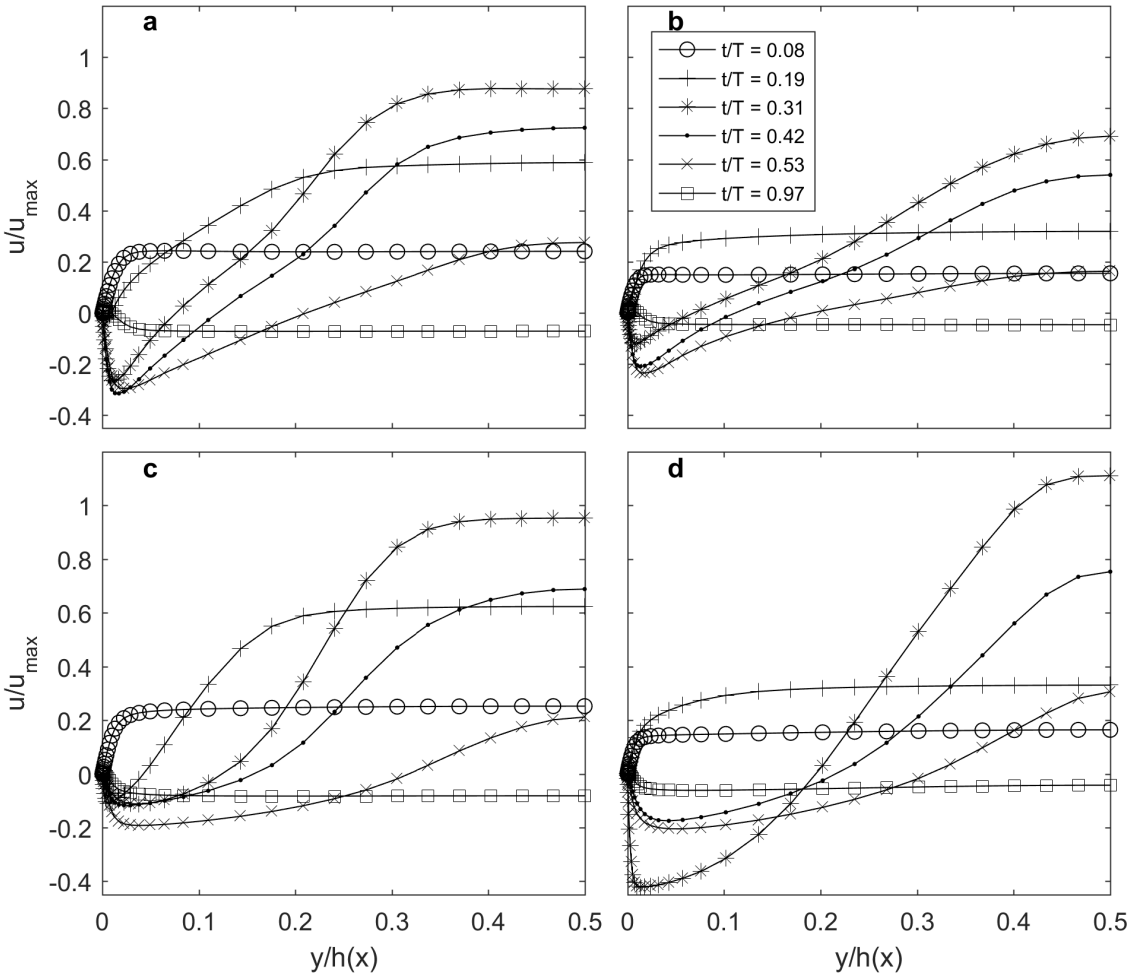

Figure 4.10: Phase-averaged velocity profiles normalized by the maximum velocity, which are produced by the two turbulence models during the cycle at different locations of the diffuser for $Re_\delta = 740$ and $L0/h = 31$. The figures are (a) the $k-kl-\omega$ model at $x/h = 1.530$, (b) the $k-kl-\omega$ model at $x/h = 3.458$, (c) the $k-\omega$ SST model at $x/h = 1.530$ and (d) the $k-\omega$ SST model at $x/h = 3.458$.

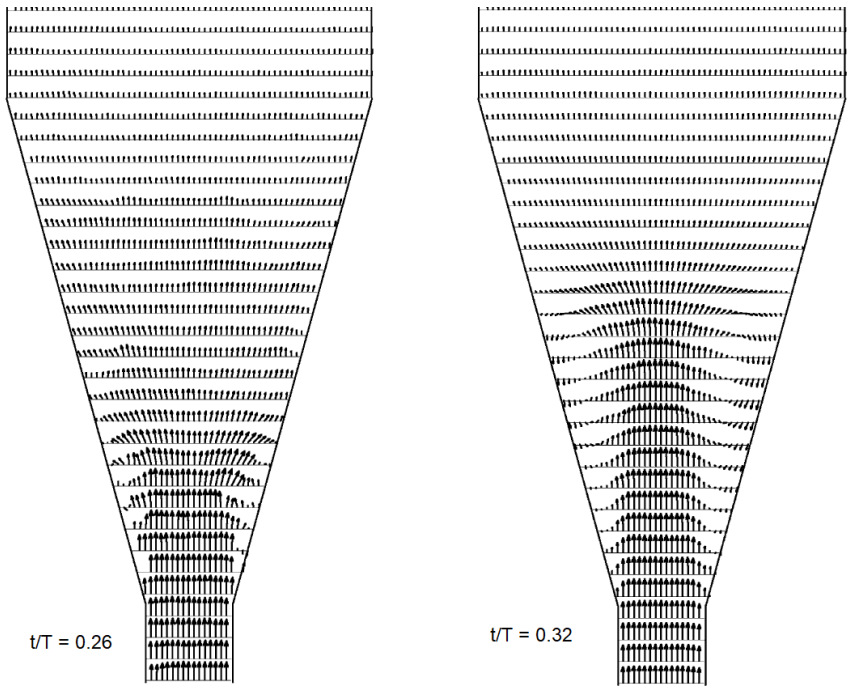

Figure 4.11: Velocity vector field from the experiments by King and Smith [27] at two different phases of the cycle for Re_δ = 580 and L_0/h = 26.

The $k-\omega$ SST model is better in simulating the velocity near the wall as the vortex progresses along the diffuser wall. The $k-kl-\omega$ computes the reversal of the velocity from the beginning of the diffuser till the center of the progressing vortex to be increasing as the cycle passes, instead of locating the highest velocity near the center of the expanding vortex. This results in a higher velocity at the beginning of the diffuser as the cycle progresses. The $k-\omega$ SST model has the center of the vortex too far away from the wall, therefor the predicted velocity of rotation is too high. For both models the separation already seems to be settled at $t/T = 0.26$ while it is just starting for the experimental results. As a result the separation is earlier in both simulations. The turbulence intensity could influence these results. Separation starts later with a higher value of turbulence intensity, as well as reattachment occurs earlier [49].

In figures 4.14, 4.15 the cases for both turbulence models for Re_δ = 740 and $L0/h$ = 31 are shown (no experimental results were available). The only difference seen between the transitional case and this turbulent case is the faster development of separation for both turbulence models. Which is especially caused by the higher Reynolds number. The overall behavior of both models stays the same.

Pressure profiles

The difference in phase between the phase-averaged centerline velocity at x/h = -0625 normalized by its maximum velocity and the pressure difference between inlet (x/h = -55.1) and outlet (x/h = 29.4) normalized by the maximum inlet pressure is shown in figure 4.16 for the $k-\omega$ SST model at Re_δ = 740 and $L0/h$ = 31. At the start of the cycle the difference in phase is $0.22T$. The velocity in the suction part of the cycle reaches a lower peak value compared to the blowing part, this is because of the higher minor losses during the blowing part.

In figure 4.17 the pressure profiles of the transitional $k-kl-\omega$ model and the experiment by [26] are shown for Re_δ = 740 and $L0/h$ = 31, where the cycle starts at the point where the centerline velocity is 0 m/s at x/h = -0.625. In figure 4.18 the $k-\omega$ SST model is compared. When comparing the pressure profiles it is seen that the simulation computes a much lower pressure drop across the channel. Where the experimental results show a maximal pressure drop of 162 Pa, the simulation for both models only show a pressure drop of 82 Pa. It is caused by the lower velocity gradients and lower viscosity used in the simulations. The pressure drop for Re_δ = 856 and $L0/h$ = 31 is closer with 140 Pa. It seems the simulation in this scenario is quite accurate in predicting the pressure drop although it is uncertain. It could be possible the simulation is limited by 2D conditions, where the flow is showing 3D effects such as vortex shedding [34]. Also the thickness of the boundary layer effects the pressure drop, when thicker lower losses will occur. The boundary layer for the

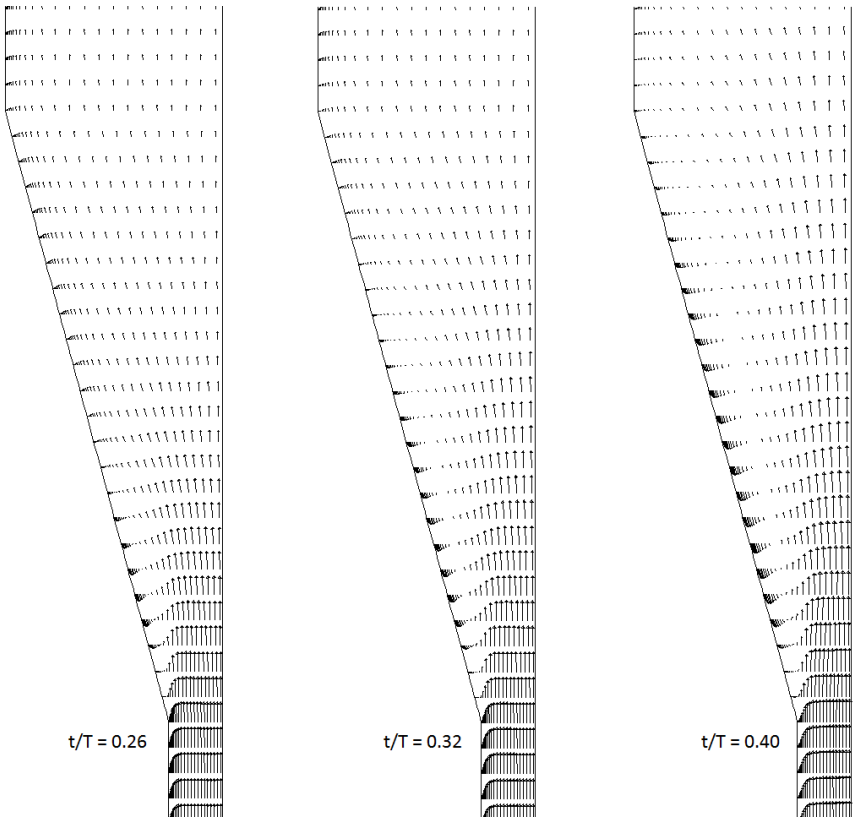

Figure 4.12: Velocity vector field from the $k-kl-\omega$ model at three different phases of the cycle for $Re_\delta = 580$ and $L_0/h = 26$.

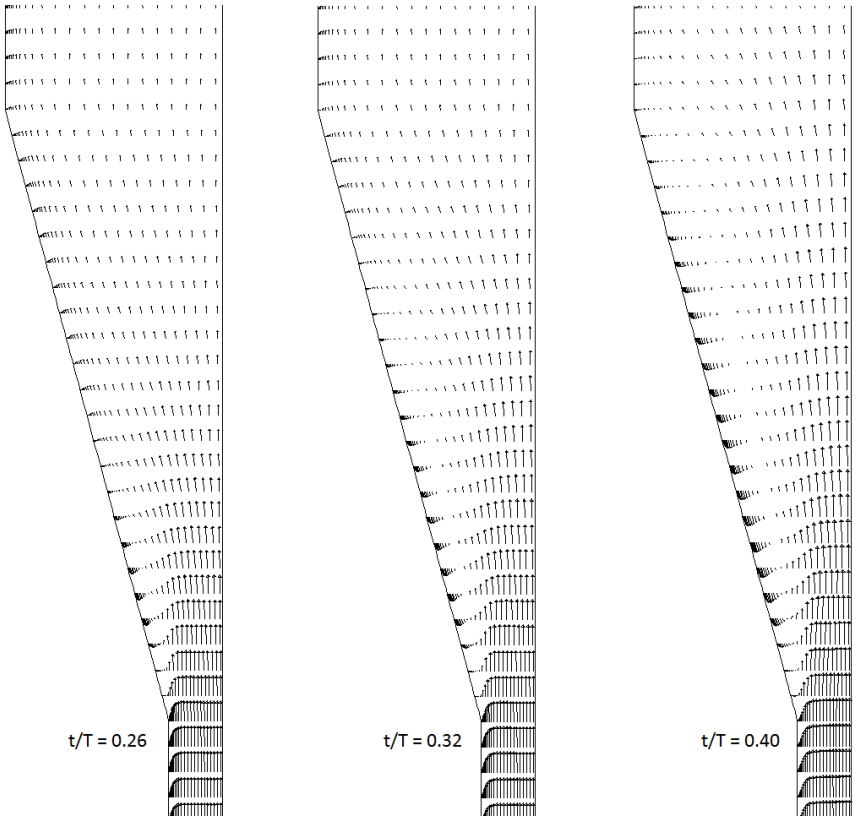

Figure 4.13: Velocity vector field from the $k-\omega$ SST model at three different phases of the cycle for $Re_\delta = 580$ and $L_0/h = 26$.

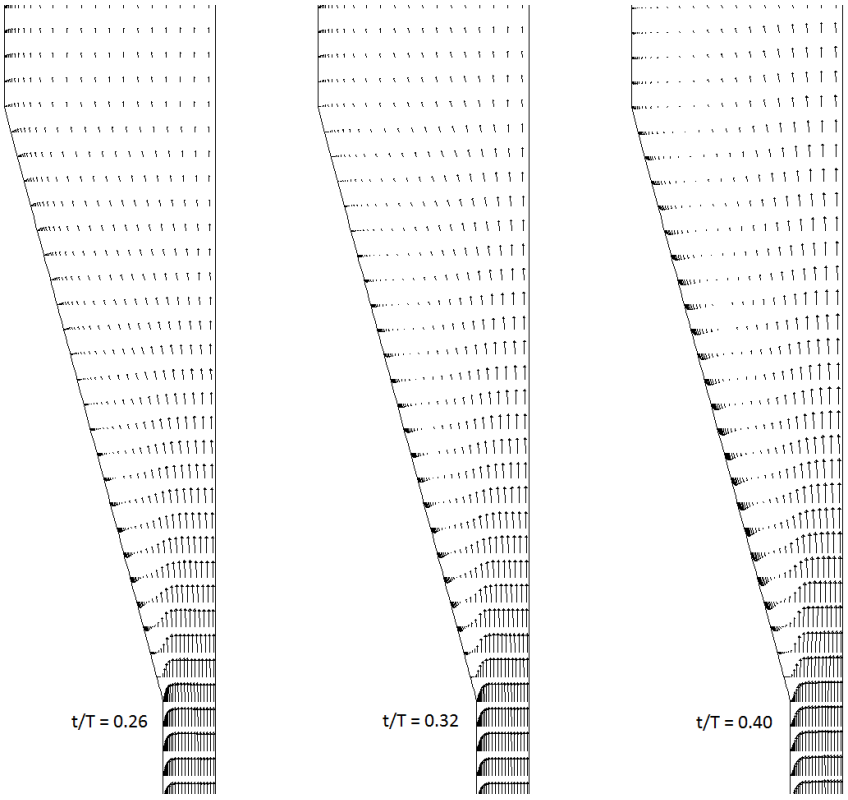

Figure 4.14: Velocity vector field from the $k-kl-\omega$ model at three different phases of the cycle for $Re_\delta = 740$ and $L_0/h = 31$.

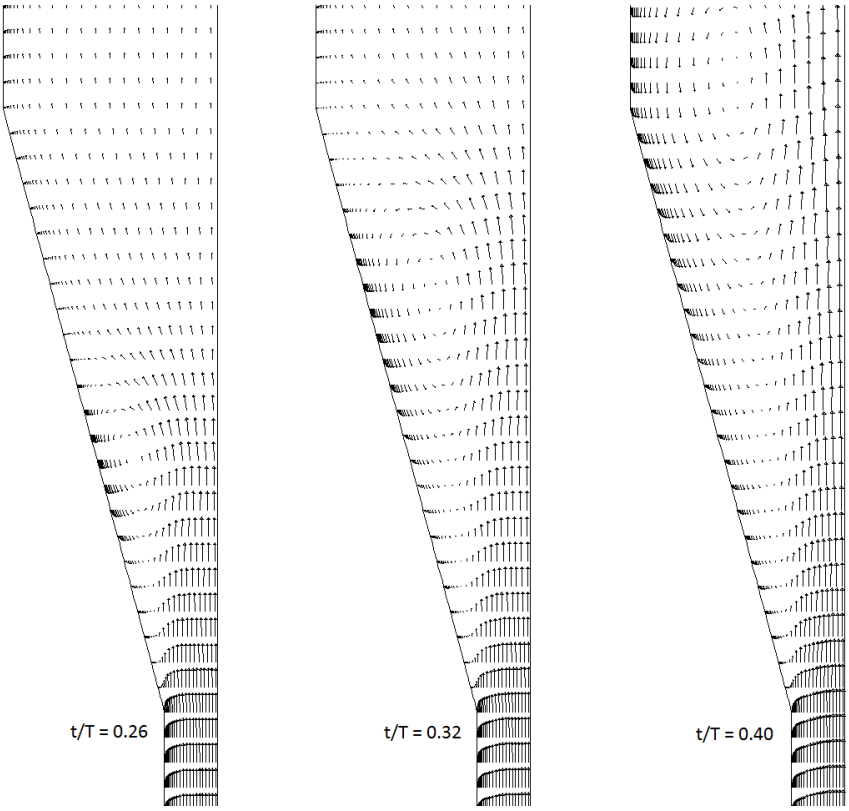

Figure 4.15: Velocity vector field from the $k-\omega$ SST model at three different phases of the cycle for $Re_\delta = 740$ and $L_0/h = 31$.

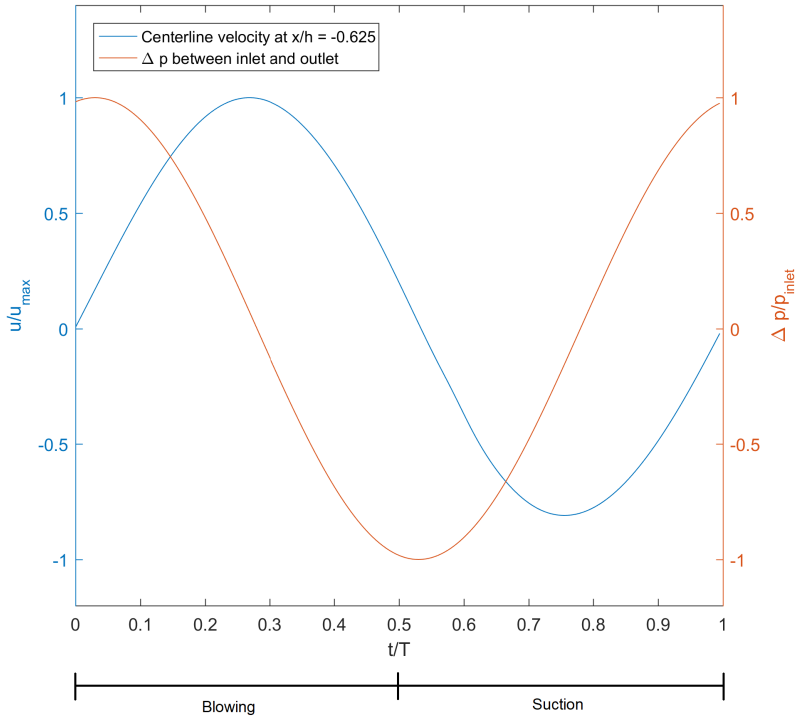

Figure 4.16: Pressure difference between inlet (x/h = -55.1) and outlet (x/h = 29.4) normalized by the maximum inlet pressure and the phase-averaged centerline velocity normalized by its maximum velocity at $x/h = -0.625$ for the $k-\omega$ SST model at $Re_\delta = 740$ and $L0/h = 31$

$k-kl-\omega$ model is modelled correctly and for the $k-\omega$ SST model it is only a little under predicted. The phase difference between the pressure and velocity is equal for both models and experiment.

When separation arrives at the plotted locations a downward shift in pressure will be seen. It can be found that at location $x/h = 1.43$ both the experiment and the models show a steeper line at $t/T = 0.2$ compared to the other locations, which is the cause of the inducing separation. The separation starts around this location and moves further along the diffuser as time passes. For the experiment the separation arrives at $t/T = 0.28$ at $x/h = 3.35$. However for the $k-kl-\omega$ model this drop is not seen. The $k-\omega$ SST shows a more accurate profile. However it over predicts the drop at $x/h = 5.27$. The boundary layer will increase during development of separation resulting in a lower local pressure.

The effect that the diffuser has on the pressure can be seen with the experimental results. It results in a downward shift of pressure. At turbulent state the Bernoulli equation does not hold and a loss is created instead of a gain [9]. The $k-\omega$ SST model performs better at this aspect than the $k-kl-\omega$ model.

As can be seen in figure 4.19 the pressure profiles at laminar conditions are more steady. The simulation shows good similarities.

Turbulence intensity

The phase-averaged turbulence intensity at three different locations of the diffusser at $Re_\delta = 740$ and $L0/h = 31$ extracted from the results obtained from both turbulence models (fig. 4.20) show profiles which can be related to the Reynolds shear stress profiles. At $x/h = -0.625$ it can be seen that for the $k-kl-\omega$ model the peaks of the turbulence intensity are high near the wall, but decrease rather fast afterwards when compared to the $k-\omega$ SST model. The turbulent dissipation rate is also high in this region and this results in a low eddy-viscosity as the distance from the wall increases. The $k-\omega$ SST model maintains the turbulence intensity for a higher distance from the wall, resulting in a higher eddy-viscosity. Therefore the Reynolds shear stresses at this location are higher for the $k-\omega$ SST model as was found in section 4.3.5.

The highest peak value of the turbulence intensity is for both turbulence models found at $t/T = 0.31$ with the exception of $t/T = 0.42$ at $x/h = 3.458$ for the $k-kl-\omega$ model. The velocity inside the separation area is higher at that moment of the cycle and at that location, but this is also the case for the $k-\omega$ SST model where

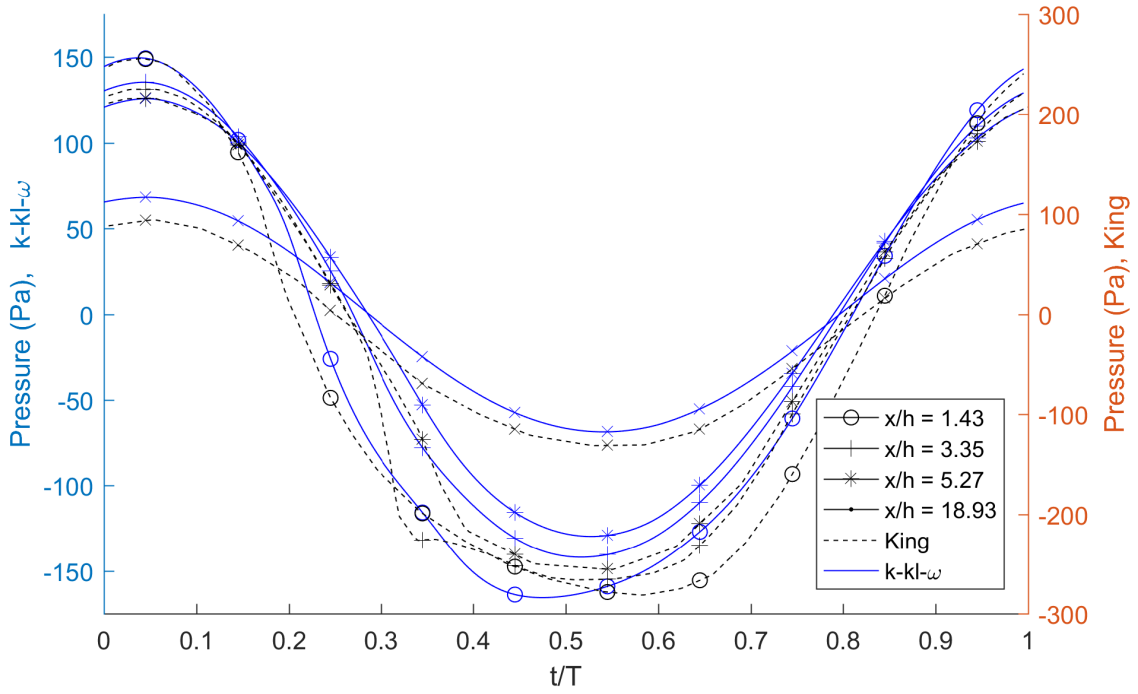

Figure 4.17: Phase-averaged pressure profile of the $k-kl-\omega$ model compared to experimental results of King [26] at $Re_\delta = 740$ and $L0/h = 31$, the profiles start at the moment that the centerline velocity is 0 m/s at x/h = 0.625

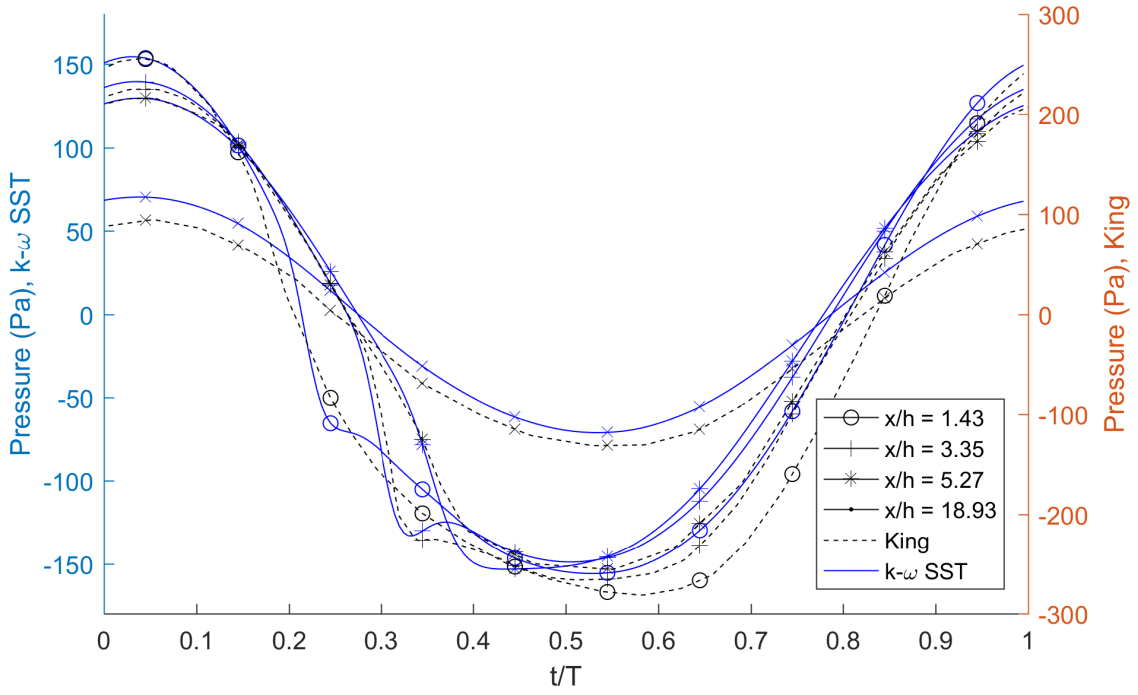

Figure 4.18: Phase-averaged pressure profile of the $k-\omega$ SST model compared to experimental results of King [26] at $Re_\delta = 740$ and $L0/h = 31$, the profiles start at the moment that the centerline velocity is 0 m/s at x/h = 0.625

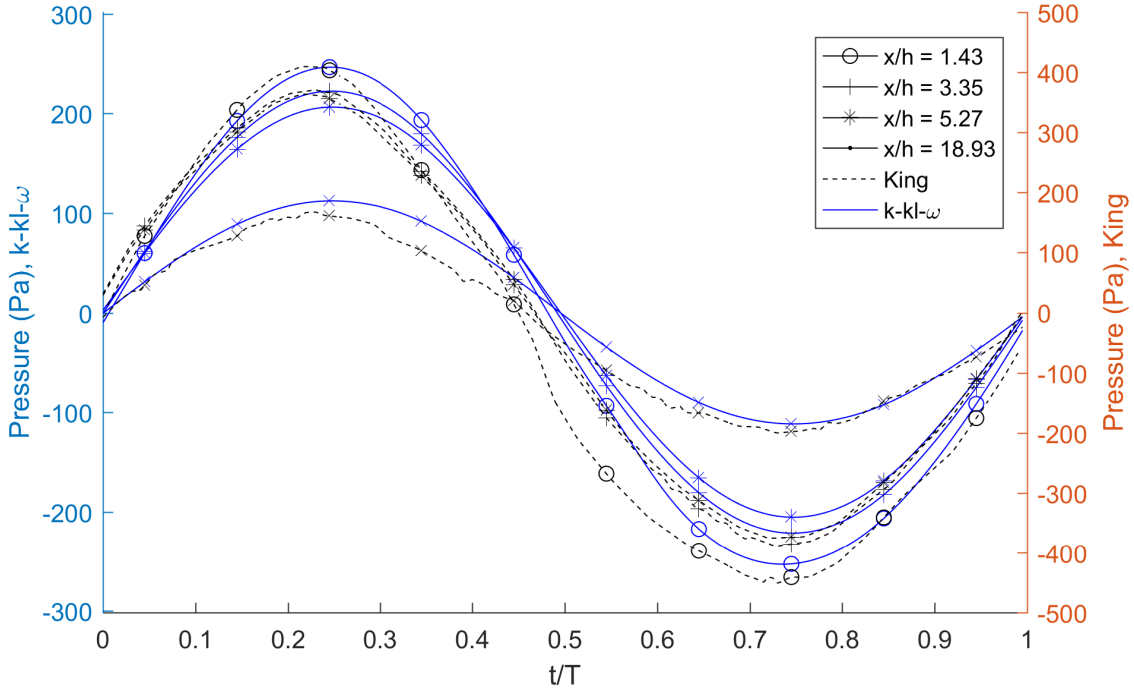

Figure 4.19: Phase-averaged pressure profile of the $k-kl-\omega$ model compared to experimental results of King [26] at $Re_\delta = 380$ and $L0/h = 20$

the turbulence intensity is not higher. The higher turbulent dissipation rate is likely to cause this behavior.

The deceleration of the phase is characterized by high peak values near the wall, but values decrease as the core of the channel is approached. When comparing the locations $x/h = 1.530$ and $x/h = 3.458$ at $t/T = 0.19$ it can be concluded this is caused by the separation region, since at $x/h = 3.458$ the separation is not present. From the turbulence intensity profiles between $0.97 < t/T < 0.19$ at $x/h = -0.625$ it can be seen that the turbulence intensity decreases as the cycle progresses during the acceleration phase. During deceleration the turbulence created will be the highest near the wall and through advection this spreads to the core. There are seen differences between the $k-kl-\omega$ and $k-\omega$ SST model. The main difference is found in how the turbulence intensity develops throughout the diffuser. The values at the end of the deceleration phase at the beginning of the diffuser are quite low for the $k-kl-\omega$ model, while the values are high at $x/h = 3.458$. The $k-\omega$ SST model shows a more gradual development.

The turbulence instensity of the flow in the channel in front of the diffuser increased fast as the flow approached the diffuser. It should however have around the same value as at the beginning of the diffuser of the $k-\omega SST$ model, showing that also in the channel the amount of turbulence is not modelled well for both models.

Reynolds shear stresses

The Reynolds shear stresses for the $k-kl-\omega$ model at different Re_δ numbers and displacement amplitude normalized by u^2_{max} at $x/h = -0.625$ are shown in fig. 4.21. From equation 3.1 it follows the behavior is formed by the amount of turbulent viscosity and velocity gradients. The velocity gradients will be higher with increasing Reynolds numbers and with decreasing displacement amplitude.

From figure 4.21 it follows that for $Re_\delta = 740$ and $L0/h = 31$ and also for $Re_\delta = 580$ and $L0/h = 30$ the Reynolds shear stresses tend to show large turbulent mixing when the flow decelerates for the experimental data, which coincides with the prediction of the first turbulence showing up when the flow decelerates. The largest Reynolds shear stresses take place at the middle of the deceleration part of the cycle. In all the three cases it is seen that at $t/T = 0.97$ the Reynolds shear stresses tend to show relatively large positive values, but smaller when compared to the blowing section of the cycle. It is being caused by the separation, which does not occur in any part of the geometry when the flow is in counter-direction.

The results of $Re_\delta = 380$ and $L0/h = 20$ show good agreements with the experimental results, as was the

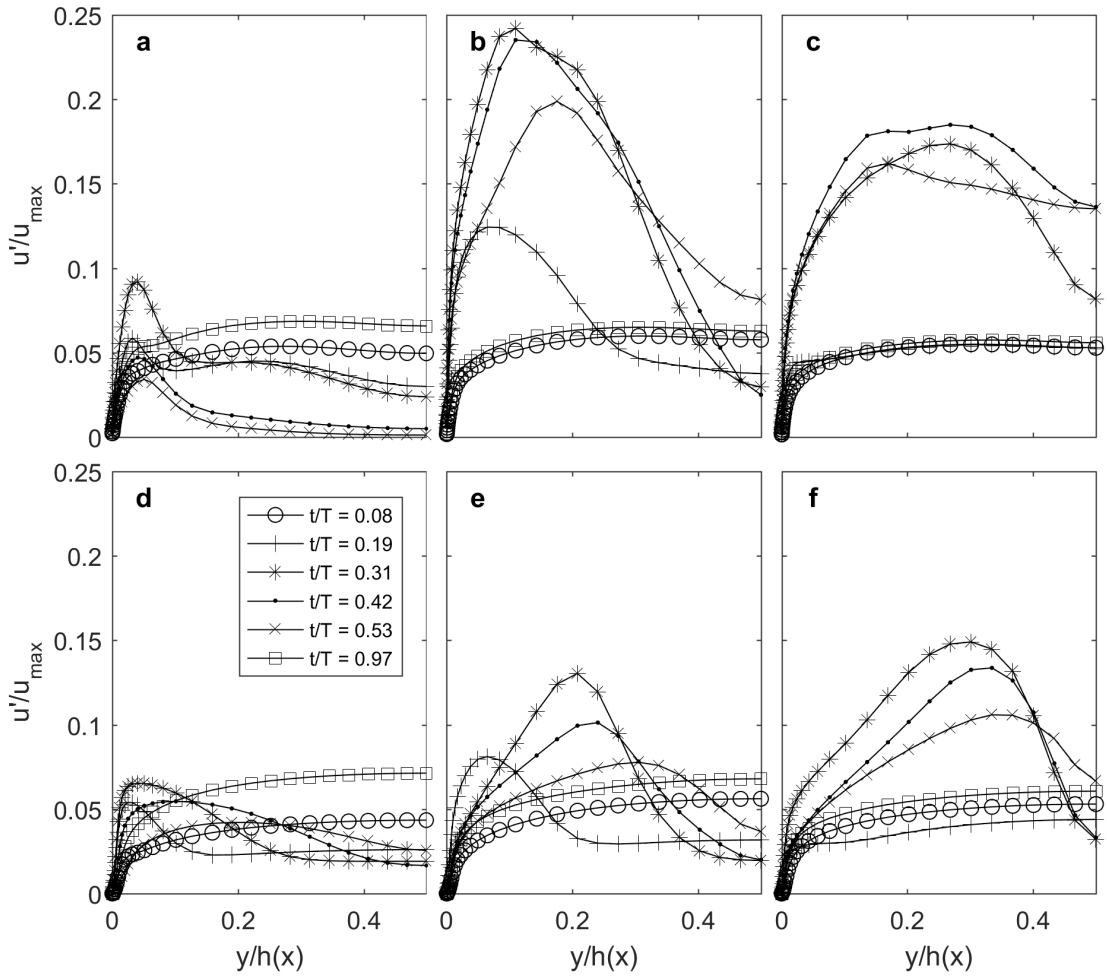

Figure 4.20: Phase-averaged turbulence intensity profiles normalized by the maximum velocity, which are produced by the two turbulence models during the cycle at different locations of the diffuser for $Re_\delta = 740$ and $L0/h = 31$. The figures are (a) the $k-kl-\omega$ model at $x/h = -0.625$ (b) the $k-kl-\omega$ model at $x/h = 1.530$, (c) the $k-kl-\omega$ model at $x/h = 3.458$, (d) the $k-\omega$ SST model at $x/h = -0.625$, (e) the $k-\omega$ SST model at $x/h = 1.530$ and (f) the $k-\omega$ SST model at $x/h = 3.458$.

case for the velocity profiles. A pattern is seen for Reynolds stresses reaching relatively high values in the accelerating part of the cycle. It could be due to separation inducing earlier. At $t/T = 0.08$ and $y/h = 0.06$ a bigger decrease is found in Reynolds shear stresses, which is also seen for other Reynolds numbers. The turbulent viscosity is not modelled correctly, which is dependent on solid boundaries, turbulence intensity and flow history effects [54].

The transitional region (i.e. intermittently turbulent flow), where $Re_\delta = 580$ and $L0/h = 30$, shows, even though the turbulence intensity is higher, a profile which is comparable to the laminar case. The turbulent bursts and thus the higher turbulent viscosity in the decelerating part of the cycle are not noticeable.

When comparing the simulation for the $k-kl-\omega$ model with the experimental results for $Re_\delta = 740$ and $L0/h = 31$, it still shows relatively small normalized values. Also the shear stress profile at $t/T = 0.31$ is only slightly higher than that at $t/T = 0.19$ and weakens quickly afterwards, which is not seen for the experimental data. It can be seen that the turbulent viscosity also tends to be higher at an earlier point of the cycle. The Reynolds shear stresses are higher at $t/T = 0.31$ than at $t/T = 0.42$. Also it is already much lower near the point of the cycle where the flow changes direction. The turbulence tends to damp quicker. Furthermore the profile tends to go to zero more early as the distance from the wall increases for the simulations. Somehow the turbulence model predicts the existence of turbulence outside the boundary layer too small, although it is correct that the Reynolds shear stresses become smaller in the bulk flow. It coincides with the behavior seen for the velocity profiles. As expected even at $Re_\delta = 856$ and $L0/h = 31$ the results are showing small Reynolds shear stresses. An exception must be made for $t/T = 0.31$ where the maximal value is much higher. The deceleration in this case is causing a higher amount of turbulence.

The Reynolds shear stresses produced by the $k-\omega$ SST turbulence model at $Re_\delta = 580$ and $L0/h = 30$ and at $Re_\delta = 740$ and $L0/h = 31$ is viewed in fig. 4.22. In both cases the model over predicts the stresses at $t/T = 0.19$ and $t/T = 0.31$, probably due to effects of arising separation. For the $Re_\delta = 740$ case it can be seen that most of the profiles at different points of the cycle are quite accurate. The $Re_\delta = 580$ case shows different profiles, but the amount of normalized shear stress although at a different point of the cycle seems quite accurate.

In figure 4.23 the phase-averaged Reynolds shear stress profiles normalized by u^2_{max} are found, modelled by the turbulence models at different locations in the diffuser during the cycle at $Re_\delta = 740$ and $L0/h = 31$. It can be seen that the $k-kl-\omega$ now starts to develop more turbulent behavior, this is also found in the amount of turbulent kinetic energy. The separation influences the amount of turbulence as can be seen in 4.23(b), where at $t/T = 0.19$ the separation has not yet arrived and as a result the Reynolds shear stresses are zero. The $k-\omega$ SST model seen in figure 4.23(c) and (d) show smaller values of the Reynolds shear stresses. The separation area is stronger, which causes a higher turbulent dissipation rate. Therefore the turbulent kinetic energy is smaller and as a consequence the eddy-viscosity is also smaller. For both turbulence models it is seen that the highest peak of Reynolds shear stresses is now at $t/T = 0.31$ and it does not weaken as quickly during the cycle as it does in the channel section. This behavior can be declared by the location of the separation area. As the flow progresses through the diffuser the peak of the Reynolds shear stresses progress to the axis for both models, this was also seen for a steady flow.

Separation

As already discovered separation starts early for all the cases when reviewing the simulation results. Also it starts at a shorter distance from the beginning of the diffuser. In figure 4.24 the results can be found. The beginning of the diffuser is denoted as $x = 0$. In Fluent a line was drawn from the beginning of the diffuser to the end of the diffuser at a distance of 0.05 mm from the wall, across this line the velocity vectors along the x-axis were plotted. The location and time of the first negative vector from the beginning of the diffuser was plotted in the figure. From the experiments and simulations it is found that the point of separation induces earlier in the cycle with increasing Reynolds number and increasing displacement amplitude. The early onset of separation by the simulations does not seem to be caused by the amount of turbulence, since the laminar cases are also affected and the Reynolds shear stresses are relatively low for most of the cases. However the turbulence could affect the results by adding extra variables. To be sure a simulation should be done without a turbulence model. It is also seen that at the beginning of the diffuser the flow will not separate till almost the point of flow reversal. By increasing the turbulence intensity it could influence this behavior in the correct direction.

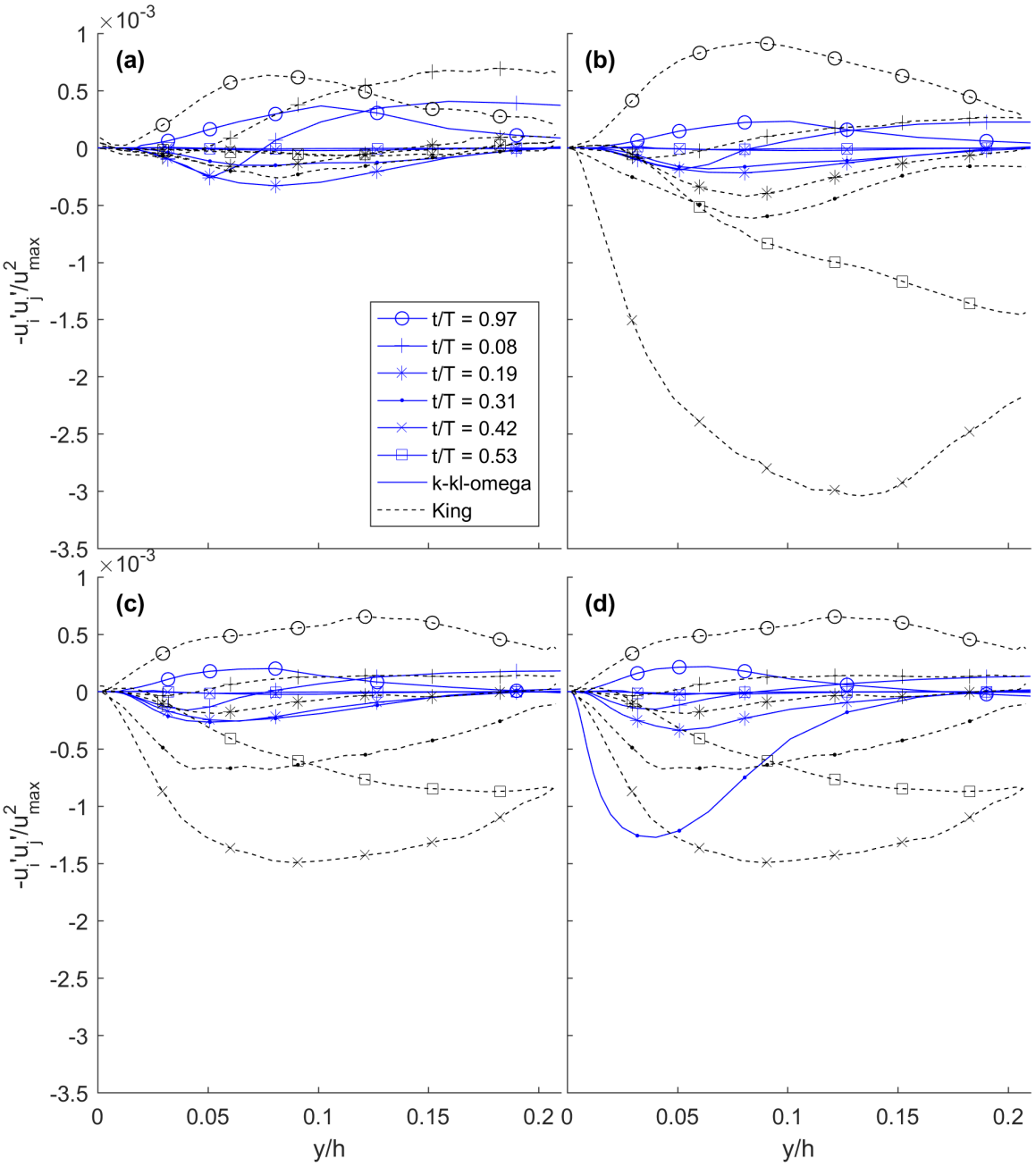

Figure 4.21: Reynolds shear stress profiles at $x/h = -0.625$ for the $k-kl-\omega$ model compared with experiments by King and Smith [27] for (a) $Re_\delta = 380$ and $L0/h = 20$, (b) $Re_\delta = 580$ and $L0/h = 30$, (c) $Re_\delta = 740$ and $L0/h = 31$ and (d) $Re_\delta = 856$ and $L0/h = 31$ compared with the experimental case $Re_delta = 740$ and $L0/h = 31$

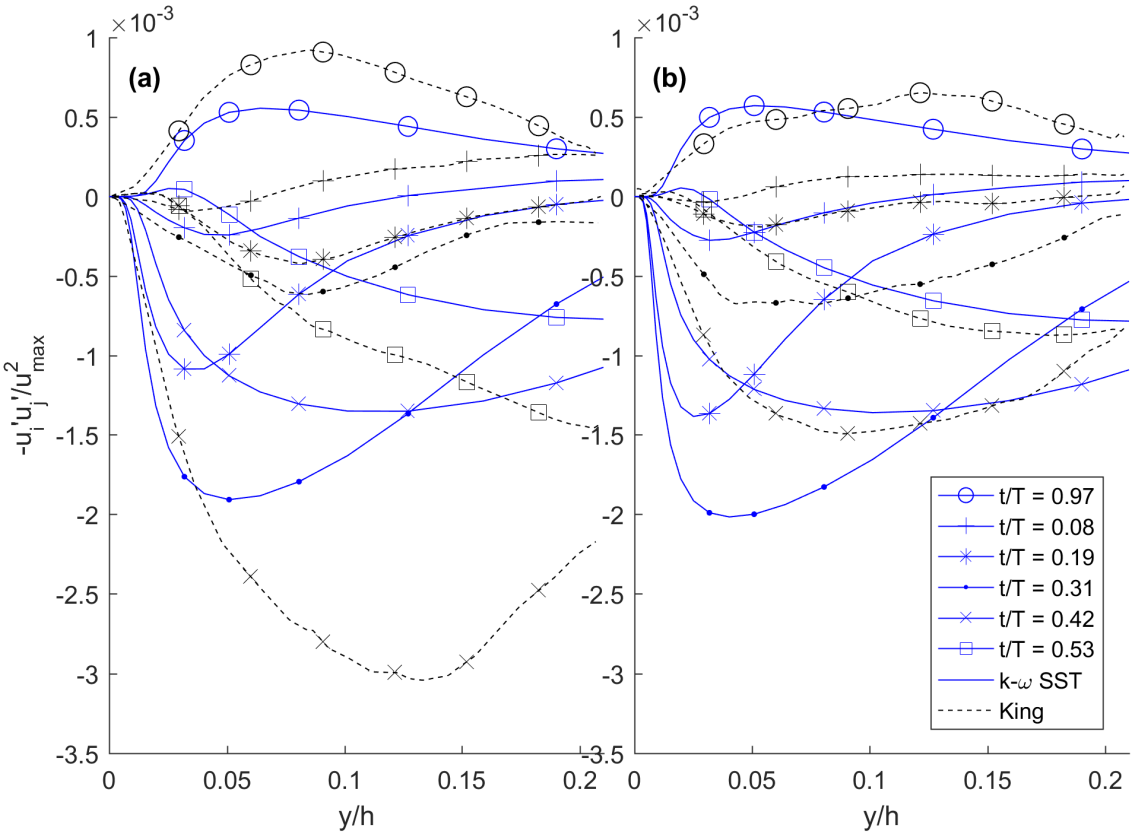

Figure 4.22: Phase-averaged normalized Reynolds stresses at $x/h = -0.625$ compared with experimental data by King and Smith [27], results are shown for (a) $Re_\delta = 580$ and $L0/h = 30$ and (b) $Re_\delta = 740$ and $L0/h = 31$.

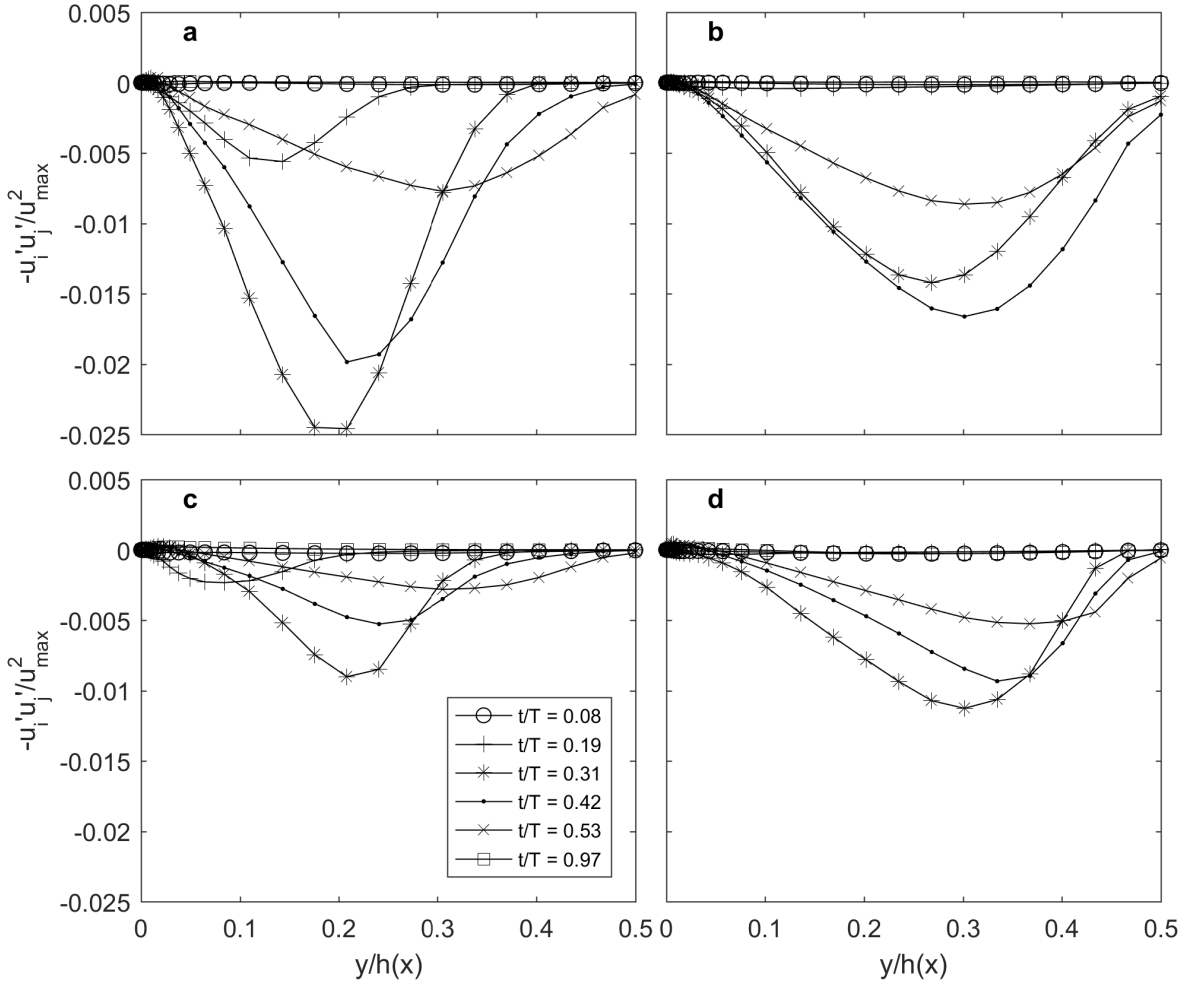

Figure 4.23: Phase-averaged Reynolds shear stress profiles normalized by the maximum velocity, which are produced by the two turbulence models during the cycle at different locations of the diffuser for $Re_\delta = 740$ and $L0/h = 31$. The figures are (a) the $k-kl-\omega$ model at $x/h = 1.530$, (b) the $k-kl-\omega$ model at $x/h = 3.458$, (c) the $k-\omega$ SST model at $x/h = 1.530$ and (d) the $k-\omega$ SST model at $x/h = 3.458$.

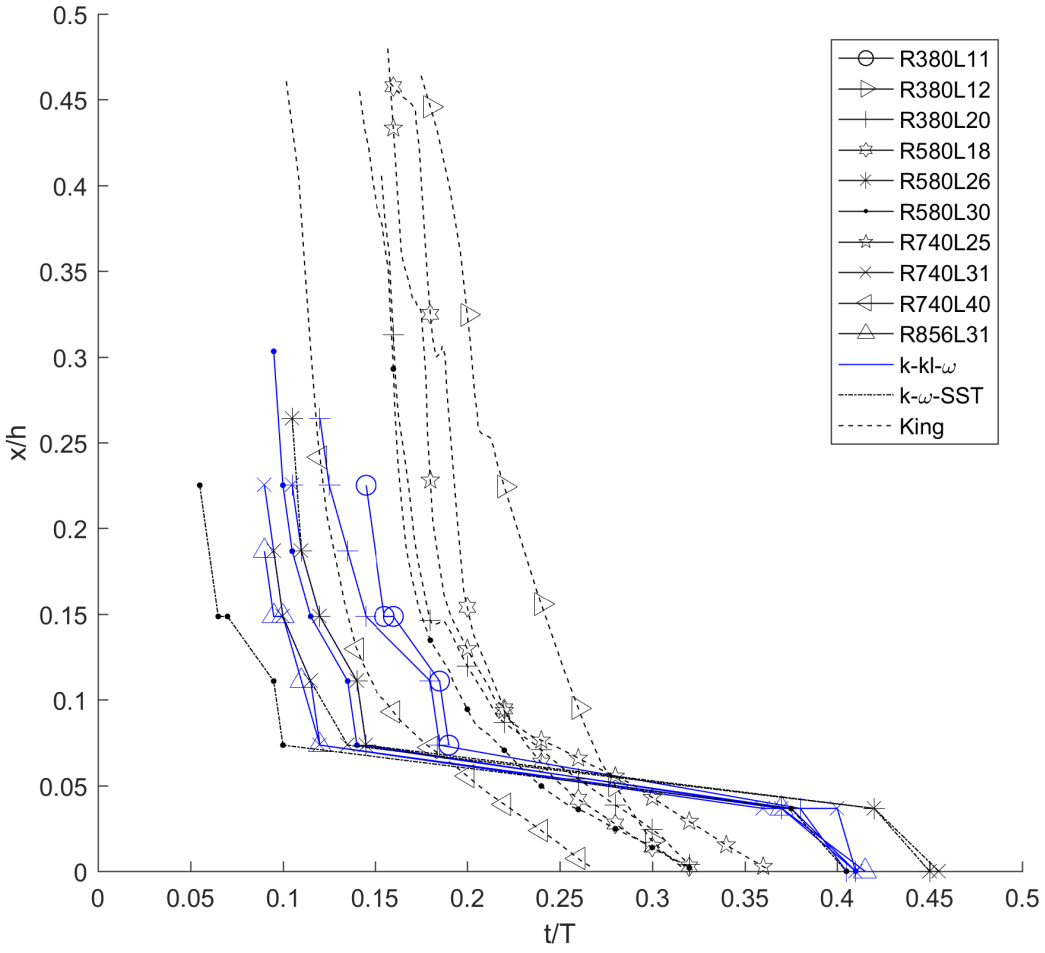

Figure 4.24: Point of inducing separation for different Reynolds numbers and displacement amplitudes, experimental results by King and Smith [27]

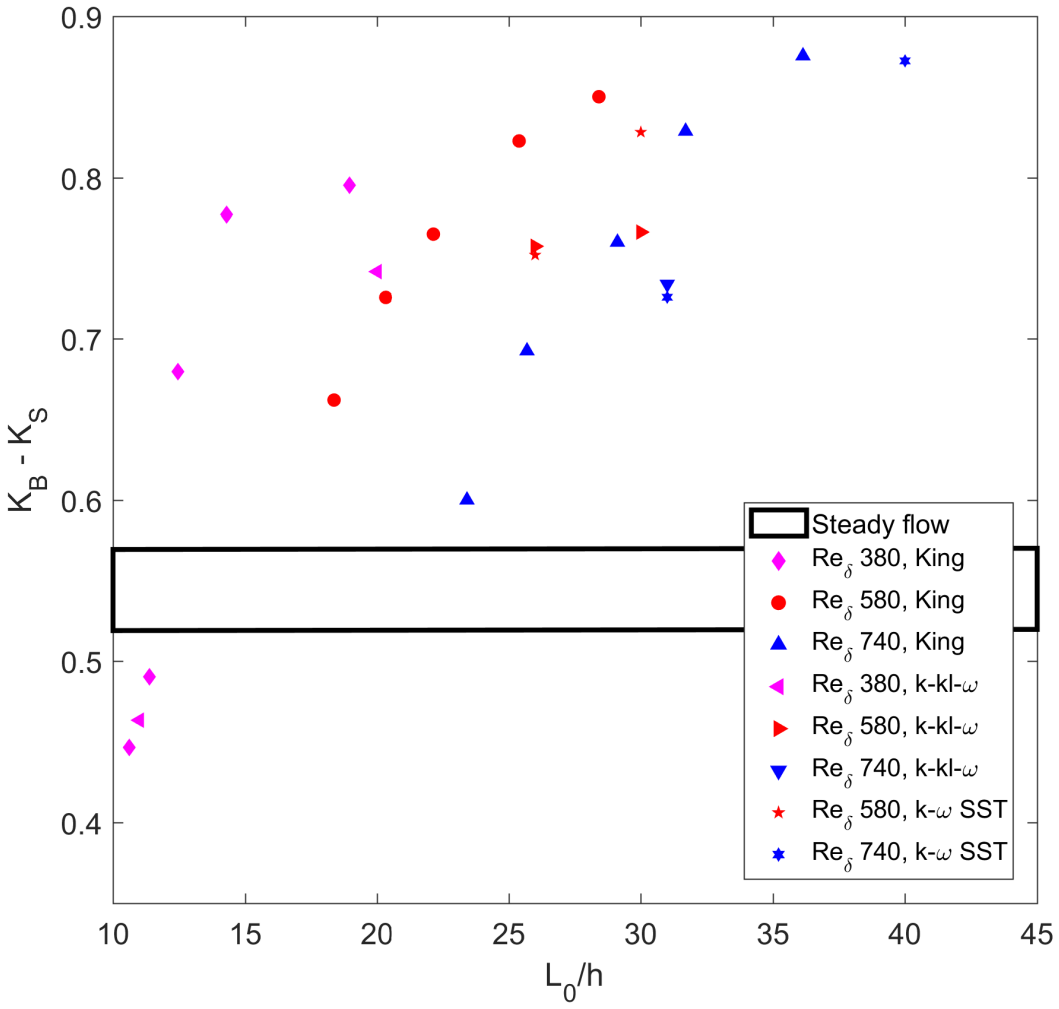

Figure 4.25: Sum of the minor losses computed from the time-averaged pressure. The grey area represents the minor losses for steady flow. [27]

Minor losses

The minor losses were calculated using equation 2.9 between $x/h = -1.54$ and $x/h = 18.93$, seen in fig. 4.25. From the experimental data it was found separation would induce earlier for bigger displacement amplitudes. The simulations are giving the same results. A bigger displacement amplitude causes bigger irreversibilities and therefor greater minor losses. When the stroke length is shorter the flow travels a smaller length and is able to relatively reattach earlier after separation, thereby reducing the losses. When compared to steady flow this could account for smaller losses. The results show that this is the case for small stroke lengths and at a Re_δ number of 380. The flow reattaches during the blowing part of the cycle due to the counter-rotating vortices, while for steady flow the separation is across the whole diffuser. The minor losses in this case will become bigger. Larger stroke lengths reattaches later to the diffuser wall, which instead can cause bigger losses than steady flow. It also follows that the minor losses decrease with Reynolds number when maintaining the same displacement amplitude, because separation is reduced due to turbulent mixing. When comparing the results the laminar case at $Re_\delta = 380$ is quite accurate, but when turbulence starts to form the results start to deviate. The increase in minor losses due to increased displacement amplitude is for the $k-kl-\omega$ model smaller for $Re_\delta = 580$ compared to the $k-\omega$ SST model. At $Re_\delta = 380$ the $k-kl-\omega$ model scales well. At $Re_\delta = 580$ and $L0/h = 26$ and at $Re_\delta = 740$ and $L0/h = 31$ it is interesting to see that both models lie very close to each other. The results show that minor losses increase with decreasing Re_δ number and increasing displacement amplitude as is seen for the experimental data.

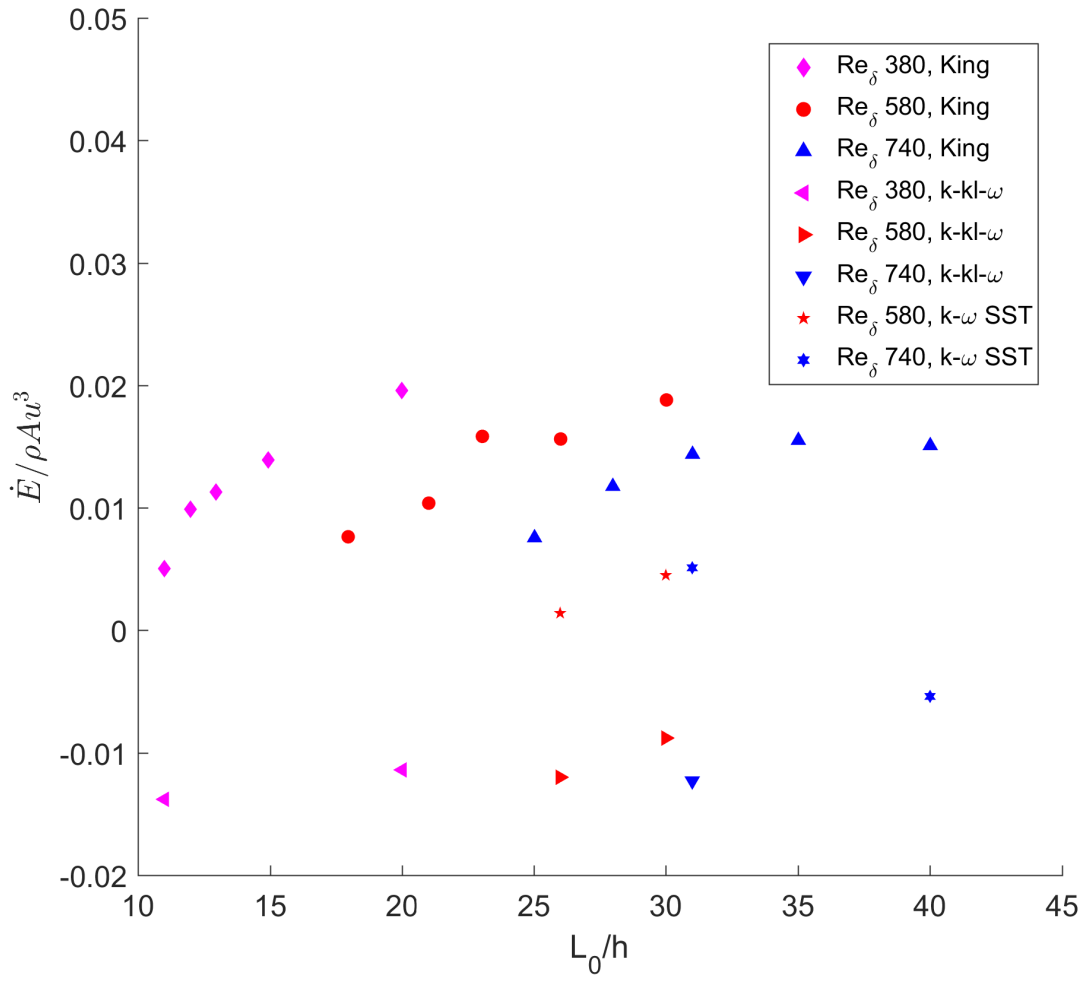

Figure 4.26: Normalized acoustic power dissipation over the diffuser for different Reynolds numbers and displacement amplitudes [27].

Acoustic power dissipation

The acoustic power dissipation is calculated over the length of the diffuser. The normalized acoustic power dissiaption (fig. 4.26) for given Reynolds numbers and dimensionless displacement amplitudes shows deviating results. The $k-kl-\omega$ and $k-\omega$ SST model show negative values, which indicates that work is needed for the flow through the diffuser. This would cause the fluid to flow back. The lagging velocity influences the results for the $k-kl-\omega$ model, since the pressure magnitude is for both models almost the same. The time-averaged pressure influences the results further. The $k-\omega$ SST model is able to achieve positive values, although the acoustic power is rather small. If the magnitude of the pressure would be higher and scale better for the different cases, the results would probably be in better agreement with the behavior of the results from the experiments. For the $k-kl-\omega$ model it can be seen that the acoustic power scales with increasing displacement amplitude and decreasing Reynolds number. It can be concluded that both models do not perform well in simulating the correct pressure and the scaling of the pressure with speed, this results in deviating normalized acoustic power dissipation.

5

Conclusion

Steady flow

When setting up the simulation it was found that convergence of the variables, such as velocity, continuity, turbulent kinetic energy and turbulent dissipation rate, used by the RANS-equations and the turbulence models is dependent on mesh accuracy. A cell distance of 1 mm at inlet and 2 mm at outlet turned out to give accurate results. No difference in velocity profile and pressure were found when reducing this distance further.

The turbulence models $k-\epsilon$, $k-\omega$ and RSM were able to converge without any problem, with the exception of the transitional turbulence models. The possible cause lies in how the steady state solution is calculated, since transient calculations didn't form a problem.

The three turbulence models used all show different behavior. The mean velocity profiles seem to be the most characteristic. The $k-\omega$ model shows profiles which are in good agreement with the DNS results. The results of the $k-\epsilon$ and the RSM model already deviate at the start of the diffuser, especially the centerline velocity is quite low for both models. As the flow progresses through the diffuser the centerline velocity starts to deviate even further. The boundary layer was simulated quite accurate, except for the $k-\omega$ model. It also showed flow reversal, but so did the $k-\epsilon$ model. Therefore the wall shear stress is not that reliable for both models. The DNS also showed a separation bubble, which shows the calculations are very sensitive for this behavior.

The deviations for the turbulence models arise from the amount of turbulence, which is being predicted too low or too high. The $k-\epsilon$ and the RSM model tend to over predict the amount of turbulent kinetic energy in the core until the end of the diffuser, while the $k-\omega$ model has low values near the wall. The $k-\omega$ model also shows relative low values near the core at the end when compared to the DNS, but by continuity the velocity profile stays correct at that point. The amount of turbulence can be viewed by the Reynolds stresses, where the same behavior is seen for the various turbulence models. The $k-\omega$ is the most accurate for the Reynolds shear stresses, which indicate the spread of momentum will be correct. Inside the expanding area the adverse pressure gradient is in good agreement for the $k-\omega$ model. Both the $k-\epsilon$ and the RSM model predict the pressure losses to be too low, caused by the deviating Reynolds stresses.

The $k-\omega$ model turns out to perform the best, but also has its limitations. When Reynolds stresses and as a result velocity profiles are deviating, it can be expected that other aspects of the flow also will deviate.

Oscillating flow

For the oscillating flow it was chosen to use one turbulence model instead of multiple. The transition $k-kl-\omega$ seemed the most promising. It turned out it was also necessary to use another turbulence model, because of disappointing results. It was chosen to use the $k-\omega$ SST model, because this model should perform better than the $k-\epsilon$, the $k-\omega$ and the Spalart-Allmaras model on all-round tasks.

It turned out that complex geometries can give problems with oscillating flows. Therefore only the diffuser itself was modelled as geometry. Also it is for all turbulence models necessary, when starting up the simulation, to let the velocity, which arises from the exerted pressure, settle in its average and phase difference with the pressure, before setting the residuals of continuity, velocity and turbulence variables lower.

The simulations do not perform as well as the steady flow simulations. The $k-kl-\omega$ model performed the worst. It shows laminar-like behavior independent of the Re_δ number. The phase-averaged velocity profiles show a laminar boundary layer as the cycle progresses, which can be explained by the Reynolds shear stresses being very small. The momentum of the turbulence is too low near the wall, meaning the eddy-viscosity is also modelled too small. The flow also tends to lag behind on the experimental results in the deceleration phase, while the difference in phase between the pressure and velocity is correct. The balance between Reynolds stresses and viscous damping is not correct. The amount of turbulence intensity on the other hand seems to be a right estimation. The transition from laminar to turbulent, where in the transitional state the turbulence intensity is higher, was not observed.

The $k-\omega$ SST model performs better. It shows the turbulent mixing is simulated better. The phase-averaged velocity profiles are in better agreement with the experiments, where the low-momentum boundary layer is now following the high-momentum bulk flow more closely. Also the flow does not lag behind the velocity profile in the decelerating phase as much as the $k-kl-\omega$ model does, but the boundary layer is too small. The Reynolds shear stresses show stronger profiles, but the strongest amount introduces earlier when compared to the experiments. The separation also shows up earlier, which declares this behavior.

The separation starts at the acceleration phase for both models, this is also seen with the experimental results. For both models it starts at around the same phase of the cycle and around $t/T = 0.075$ earlier than with the experiments. The location of point of separation is about half the distance from the start of the diffuser when compared to the experimental results for both models. Also the turbulence models both show a much stronger separation region, which expands over the whole diffuser as the cycle progresses. It gives rise to dissipation, which affects the amount of turbulence produced. The $k-\omega$ SST model produces the biggest area of separation, where the biggest negative velocity vector is found near the wall at the center of the separation region. Whereas the $k-kl-\omega$ model produces a separation area which lies closer to the wall. The highest negative velocity vector is found near the start of the diffuser and as the separation progresses it increases relative to the velocity in the diffuser. A trend can be seen of separation starting earlier with increasing Re_δ number or increasing displacement amplitude, the same is true for the experiments. It can be concluded both turbulence models have difficulty with simulating the effects of the adverse pressure gradient in oscillating flow.

The phase-averaged pressure profile throughout the diffuser is for the $k-kl-\omega$ model rather mild with turbulent flow. The $k-\omega$ SST model performs better and is good agreement with the experiments, by reflecting the drop in pressure when separation arrives. The relative pressure losses for both models seem to be quite correct.

The minor losses showed deviating values, which were often lower. But did show the trend of increasing minor losses with increased displacement amplitude or decreased Re_δ number. The acoustic power however was not very realistic and even showed negative values for both models and very low positive values for the $k-\omega$ SST model, which is caused by deviating magnitude of pressure profiles. The $k-kl-\omega$ model showed the trend of increasing acoustic power with increasing displacement amplitude and decreasing Re_δ number. No trends were found for the $k-\omega$ SST model.

From the results it can be concluded that both turbulence models do not simulate oscillating flow in a wall-bounded adverse pressure gradient geometry very well. For finding the basics in how the flow will behave and finding parameters like the turbulent viscosity and pressure the $k-\omega$ SST model could be used, but when accuracy is important this will not be a good approach.

Recommendations

The steady flow is simulated quite accurate by the $k-\omega$ model, may be it is possible to tune the turbulence model a little more by adjusting the empirical constants. To further validate the model it would be interesting to simulate a steady flow inside a diffuser where separation arises.

By stretching the cells of the mesh it could be possible that flow reversal is prevented in the diffuser area of the steady flow. The problem is that the accuracy of flow development will be disrupted (or numerical accuracy), because the gradients in x-direction will get higher.

The laminar region and buffer region in the boundary layer could also cause problems, because the region is not turbulent. By using a value of $y^+ > 30$ for the first cell next to the wall this could possibly deliver more realistic results.

The simulations are done in 2D, but it is expected that a 3D simulation will not give any benefits. It is expected that there are no big 3D effects, like for example vortex shedding. The problem lies in how the

turbulence models estimate the problem. In case of the oscillating flow a DNS would probably give better results, where every aspect of the flow is simulated and is not being modelled. Otherwise experiments are still necessary and keep in mind a DNS is very time consuming. It could be possible that this is a better way, because you have no uncertainties and for most cases with oscillating flow it can be a small setup.

The boundary layer may be needs more cells for the turbulence models to be more accurate for the oscillating flow.

Adjusting a turbulence model which will be specialized in oscillating flow and adverse pressure gradient geometries could also be an option. Probably it would also be better in predicting pulsating flows, which can be beneficial for cardiovascular cases.

Interesting will be and that will be the next step is how the regenerator, cold and hot heat exchanger are simulated. It is however unlikely that Ansys Fluent, based on the conclusions of this thesis, is able to produce the waves correctly. Another question is what will happen when in detail as the flow passes from the regenerator to the diffuser, which is also unclear. No research articles are dedicated to that subject. If somehow the results of Ansys Fluent could be enhanced, this would mean a leap into the right direction. The transport of sound waves could be mapped more precisely.

A

Steady flows

Incompressible turbulent flow

Boundary conditions	*Inlet*	*Outlet*
Type	Velocity-inlet	Outflow
Variable	0.148 m/s	-
Temperature	273.15 K	-
Turbulence intensity	3%	-
Turbulent Length Scale	0,01016 m	-

Table A.1: Boundary conditions

Solution Methods	
Pressure-Velocity Coupling	
Scheme	Simple
Spatial Discretization	
Gradient	Green-Gauss Cell Based
Pressure	Second Order
Momentum	Second Order Upwind
Turbulent Kinetic Energy	Second Order Upwind
Turbulent Dissipation Rate	Second Order Upwind
Specific Dissipation Rate	First Order Upwind
Reynolds Stresses	First Order Upwind

Table A.2: Solution methods

Oscillating flow

Grid specifications (mm and no. of cells)		
Wide channel	*In front of diffuser*	*After diffuser*
0.25/~1052	0.125/~2104	0.5/~526
0.75/~351	0.5/~526	2.0/~131
1.0/~263	1.0/~263	1.0/~263
1.0/~263	0.5/~526	2.0/~263
2.0/~131	2.0/~131	2.0/~131

Table A.3: Distance between cells of the mesh and number of cells along the y-axis at different regions of the complex mesh.

Boundary conditions		
Turbulent cases		
Passageway	Inlet	Outlet
Type	Pressure-Outlet	Pressure-Outlet
Variable	Case dependent	0
Temperature	293.15 K	293.15 K
Turbulence intensity	3%	3%
Turbulent Length Scale	0.01162 m	0.0469 m
Laminar Kinetic Energy	0 m2/s2	0 m2/s2
Transitional cases		
Passageway	Inlet	Outlet
Type	Pressure-Outlet	Pressure-Outlet
Variable	Case dependent	0
Temperature	293.15 K	293.15 K
Turbulence intensity	6%	6%
Turbulent Length Scale	0.01162 m	0.0469 m
Laminar Kinetic Energy	0 m2/s2	0 m2/s2
Laminar cases		
Passageway	Inlet	Outlet
Type	Pressure-Outlet	Pressure-Outlet
Variable	Case dependent	0
Temperature	293.15 K	293.15 K
Turbulence intensity	0.2%	0.2%
Turbulent viscosity ratio	0.01	0.01
Laminar Kinetic Energy	0 m2/s2	0 m2/s2

Table A.4: Boundary conditions

Solution Methods	
Pressure-Velocity Coupling	
Scheme	Coupled
Spatial Discretization	
Gradient	Green-Gauss Cell Based
Pressure	Second Order
Momentum	Second Order Upwind
Turbulent Kinetic Energy	First Order Upwind
Laminar Kinetic Energy	First Order Upwind
Specific Dissipation Rate	First Order Upwind
Energy	Second Order Upwind

Table A.5: Solution methods

Cases						
Re_δ (-)	L0/h (-)	u_{max} (m/s)	Frequency (Hz)	Wo (-)	P_{in} (Pa), $k-kl-\omega$	P_{in} (Pa), $k-\omega$ SST
380	11	11.94898138	20.82956683	48.23611	1780	-
380	20	6.571939759	6.300943966	26.52986	285	-
580	26	11.7771177	8.685757635	31.14842	699	731
580	30	10.20683534	6.523969068	26.9953	463	463
740	31	16.07896619	9.945771273	33.33124	1101	1160
740	40	12.4611988	5.973678871	25.83171	-	512
856	31	21.51504267	13.30829923	38.55613	1959	-

Table A.6: Variables of the Reynolds numbers with corresponding dimensionless displacement amplitudes

Bibliography

[1] *Ansys Fluent manual.* .

[2] *Introductory Fluent Notes Fluent v6.3*, .

[3] K. H. Ahn and M. B. Ibrahim. Laminar/turbulent oscillating flow in circular pipes. *International Journal of Heat and Fluid Flow*, 1992.

[4] R. Akhavan, R.D. Kamm, and A.H. Shapiro. An investigation of transition to turbulence in bounded oscillatory stokes flow. *J Fluid Mech*, 1991.

[5] P. H. Alfredsson, R. Örlü, and A. Segalini. A new formulation for the streamwise turbulence intensity distribution in wall-bounded turbulent flows. *European Journal of Mechanics B/Fluids*, 2012.

[6] Ansys. *CFX Modeling Guide 16.2.3.* 2015.

[7] Ansys.Inc. Innovative turbulence modeling: Sst model in ansys cfx. 2004.

[8] Ram S. Azad. Turbulent flow in a conical diffuser: A review. *Elsevier Science Inc.*, 1996.

[9] S. Backhaus and G.W. Swift. A thermoacoustic-stirling heat engine: detailed study. *J Acoust Soc Am*, 107, 2000.

[10] H. Bailliet, V. Gusev, R. Raspet, and R.A. Hiller. Acoustic streaming in closed thermoacoustic devices. *The Journal of the Acoustical Society of America 110*, 2001.

[11] J.E. Bardina, P.G. Huang, and T.J. Coakley. Turbulence modeling validation. 1997.

[12] S. Bhushan, D. Keith Walters, and G. W. Burgreen. Laminar, turbulent, and trtransition simulations in benchmark cases with cardiovascular device features. *Cardiovascular Engineering and Technology*, 2013.

[13] R.D. Blevins. *Applied Fluid Dynamics Handbook.* 1984.

[14] A.B. de Jesus, L.A.C.A. Schiavo, J.L.F. Azevedo, and J.-P. Laval. Further studies of adverse pressure gradient effects in turbulent channel flows. *American Institute of Aeronautics and Astronautics*, 2015.

[15] F. Durst and B. Ünsal. Forced laminar-to-turbulent transition of pipe flows. *J. Fluid Mech*, 2006.

[16] G. Eiffel. *Nouvelles recherches sur la résistance de l'air et l'aviation faites au laboratoire d'Auteuil.* Paris, E. Chiron, 1919.

[17] D. Feldmann and C. Wagner. Direct numerical simulation of fully developed turbulent and oscillatory pipe flows at $re_\tau = 1440$. *Journal of Turbulence*, 2012.

[18] R.W. Fox and S.J. Kline. Flow regimes in curved subsonic diffusers. *J. Basic Eng*, 1972.

[19] J. Furst. Numerical simulation of transitional flows with laminar kinetic energy. *Engineering Mechanics 2012*, 2012.

[20] N.M. Hariharan, P. Sivashanmugam, and S. Kasthurirengan. Influence of stack geometry and resonator length on the performance of thermoacoustic engine. *Applied Acoustics*, 2012.

[21] S.M. Hino, M. Sawamoto, and S. Takasu. Experiments on transition to turbulence in an oscillatory pipe flow. *J. Fluid Mech*, 75, 1976.

[22] I.E. Idelchik. *Handbook of Hydraulic Resistance.* Jaico Publishing House, 2008.

[23] D. Japikse. Turbomachinery diffuser design technology. *The Design Technology Series*, 1984.

[24] B.L. Jensen, B.M. Sumer, and J. Fredsoe. Turbulent oscillatory boundary layers at high reynolds numbers. *J. Fluid Mech*, 1988.

[25] Igor J. Karassik. *Centrifugal Pumps.* Chapman & Hall, second edition, 1998.

[26] C.V. King. Time-resolved piv and pressure measurements of oscillating and pulsating flow in a diffuser. 2008.

[27] C.V. King and B.L. Smith. Oscillating flow in a 2-d diffuser. *Exp Fluids*, 51, 2011. doi: 10.1007/s00348-011-1170-7.

[28] U.H. Kurzweg, E.R. Lindgren, and B. Lothdrop. Onset of turbulence in oscillating flow at low womersley number. *Phys. Fluids A. 1*, 1989.

[29] A.H.M. Kwong and A.P. Dowling. Unsteady flow in diffusers. *J. Fluids Eng 116*, 1994.

[30] B. E. Launder and D. B. Spalding. Lectures in mathematical models of turbulence. *Academic Press*, 1972.

[31] Jin Lee, Seong Jae Jang, and Hyung Jin Sung. Direct numerical simulations of turbulent flow in a conical diffuser. *Journal of Turbulence*, 2012. doi: 10.1080/14685248.2012.706368.

[32] A.T. McDonald and R.W. Fox. An experimental investigation of incompressible flow in conical diffusers. *Int. J. Mech. Sci. Pergamon Press Ltd.*, 1965. doi: 10.1016/0020-7403(66)90071-3.

[33] P.J. Morris, S. Boluriaan, and C.M. Shieh. Computational thermoacoustic simulation of minor losses through a sudden contraction and expansion. *7th AIAA/CEAS aeroacoustics conference*, 2001.

[34] S. Murakami and A. Mochida. On turbulent vortex shedding flow past 2d square cylinder predicted by cfd. *Journal of Wind Engineering and Industrial Aerodynamics*, 1995.

[35] M. Ohmi, M. Iguchi, K. Kakehashi, and M. Tetsuya. Transition to turbulence and velocity distribution in an oscillating pipe flow. *Bull JSME*, 1982.

[36] S.V. Poroseva and S.S. Girimaji. Analytical study of the oscillating channel flow solution with application to the turbulent case. *Proceedings of FEDSM2003 ASME fluids engineering summer conference*, (2003-45616), 2003.

[37] B. R. Ramaprian and S.W. TU. An experimental study of oscillatory pipe flow at transitional reynolds numbers. *J. Fluid Mech*, 1979.

[38] L.R. Reneau, J.P. Johnston, and S.J. Kline. Performance and design of straight, two-dimensional diffusers. *J. Basis Eng*, 89(1):141, 1967.

[39] B.P.R. Samala. Computational investigation of active flow control parameters on the aerodynamic performance of naca 2412 airfoil. Master's thesis, Universitat Politècnica de Catalunya, 2015.

[40] A. A. Schachenmann and D.O. Rockwell. Oscillating turbulent flow in a conical diffuser. *Journal of Fluids Engineering*, 1976.

[41] R.K. Singh and R.S. Azad. Measurements of instantaneous flow reversals and velocity field in a conical diffuser. *Exp. Therm. Fluid. Sci.*, 10:397–413, 1995.

[42] B.L. Smith and G.W. Swift. Power dissipation and time-averaged pressure in oscillating flow through a sudden area change. *J Acoust Soc Am*, 113, 2003.

[43] S. Spoelstra and M.E.H. Tijani. A high performance thermoacoustic engine. *Joural of Applied Physics 110*, 2011.

[44] Joseph H. Spruk and Nuri Aksel. *Fluid Mechanics.* Springer, second edition, 2008.

[45] G.W. Swift. Thermoacoustic engines. *J. Acoust Soc Am., Vol.84*, 1988.

[46] G.W. Swift, D.L. Gardner, and S. Backhaus. Acoustic recovery of lost power in pulse tube refrigerators. *J. Acoust Soc Am*, 105, 1999.

[47] P.S. Tromans. *Stability and transition of periodic pipe flow.* PhD thesis, 1978.

[48] R.S. Wakeland and R.M. Keolian. Influence of velocity profile nonuniformity on minor losses for flow exiting thermoacoustic heat exchangers. *J Acoust Soc Am*, 112, 2002.

[49] S. Wang, Y. Zhou, Md. Mahbub Alam, and H. Yang. Turbulent intensity and reynolds number effects on an airfoil at low reynolds numbers. *Physics of Fluids*, 2014.

[50] John Wheatley, T. Hofler, G.W. Swift, and A. Migliori. An intrinsically irreversible thermoacoustic heat engine. *J. Acoust Soc. Am. 74*, 1983.

[51] Frank M. White. *Fluid Mechanics.* Mc Graw Hill, sixth edition, 2008.

[52] Frank M. White. *Fluid Mechanics*, chapter 6.9, page 389. Mc Graw Hill, sixth edition, 2008.

[53] David C. Wilcox. *Turbulence Modeling for CFD.* DCW Industries, Inc., 1993.

[54] M. Woelke. Eddy viscosity turbulence models employed by computational fluid dynamic. *Transactions of the institute of aviation.*

[55] M. Wolfstein. The velocity and temperature distribution of one-dimensional flow with turbulence augmentation and pressure gradient. *Int. J. Heat Mass Transfer*, 1969.

[56] T. S. Zhao and P. Cheng. Experimental studies on the onset of turbulence and frictional losses in an oscillatory turbulent pipe flow. *Int. J. Heat and Fluid flow*, 1995.